Preparation of Janus nanosheets

using layered hexaniobate $K_4Nb_6O_{17}\cdot 3H_2O$

and their applications to functional materials

層状六ニオブ酸塩$K_4Nb_6O_{17}\cdot 3H_2O$を用いた
Janus型ナノシートの作製と
機能性材料への応用

July, 2020

Ryoko SUZUKI
鈴木　涼子

Preparation of Janus nanosheets

using layered hexaniobate $K_4Nb_6O_{17}\cdot 3H_2O$

and their applications to functional materials

層状六ニオブ酸塩$K_4Nb_6O_{17}\cdot 3H_2O$を用いた
Janus型ナノシートの作製と
機能性材料への応用

July, 2020

Waseda University

Graduate School of Advanced Science and Engineering
Department of Applied Chemistry
Research on Inorganic Synthetic Chemistry

Ryoko SUZUKI
鈴木　涼子

The thesis was reviewed and approved by the following

Dr. Yoshiyuki Sugahara
Professor
Waseda University
Thesis supervisor

Dr. Kazuyuki Kuroda
Professor
Waseda University

Dr. Hiroaki Wada
Professor(without tenure)
Waseda University

Dr. Toshiyuki Momma
Professor
Waseda University

Dr. Atsushi Shimojima
Professor
Waseda University

Preface

Janus materials are anisotropic materials that have two surfaces with different properties. Janus materials with various shapes have been prepared, such as Janus particles, Janus cylinders and Janus sheets, and applied as various materials, including optical materials and catalysts. Among these Janus materials, Janus nanosheets have the highest anisotropy due to their shape. It is an issue for Janus nanosheets that they swell in organic solvents, however, because most of them are made of polymers. Preparation of inorganic Janus nanosheets is therefore an important issue for applying Janus nanosheets in various solvents. There are several drawbacks to the previous methods of inorganic Janus nanosheet preparation, however: low versatility in terms of functional group selection or limitations on their use in water.

Ion-exchangeable layered metal oxides have been used to achieve ion-exchange reactions between interlayer ions and other ions. The surfaces of some of these layered materials can be modified, moreover, by organic molecules *via* grafting reactions. Also, since nanosheets are obtained by exfoliation of layered materials, layered materials could be used as starting materials for preparation of highly

anisotropic materials, or nanosheets, *via* exfoliation. Leveraging these features, ion-exchangeable layered materials have been applied as host materials for ion-exchange, raw materials for thin films and nanofillers for polymer-based hybrids.

This thesis describes preparation methods for Janus nanosheets using the layered hexaniobate $K_4Nb_6O_{17}\cdot 3H_2O$ and phosphorus coupling agents and functionalization of $K_4Nb_6O_{17}\cdot 3H_2O$-based Janus nanosheets. These preparation methods are important for application of functional inorganic Janus nanosheets.

The layered hexaniobate $K_4Nb_6O_{17}\cdot 3H_2O$ has a unique structure in which interlayer I with high reactivity and interlayer II with low reactivity appear alternately. In the first approach, interlayer I was modified using one phosphorus coupling agent at first, and interlayer II was modified subsequently using the other phosphorus coupling agent. Finally, the product was exfoliated into single-layered nanosheets. Thus, preparation of Janus nanosheets from $K_4Nb_6O_{17}\cdot 3H_2O$ could be achieved by regioselective surface modification and subsequent exfoliation. Since $K_4Nb_6O_{17}\cdot 3H_2O$-based Janus nanosheets have stable bonds between the niobate layer surface and surface modifiers, they could be functionalized by changing

phosphorus coupling agents. In the second approach, Janus nanosheets were prepared by exfoliation of products where only interlayer I was modified with a phosphorus coupling agent. Thus, two types of functional Janus nanosheets applicable to aqueous dispersions were prepared. One of these was Janus nanosheets prepared using orgonophosphonic acid with high hydrophilicity and phosphoric acid that could work as two-dimensional surfactants. The other was Janus nanosheets exhibiting Dual-functions comprising cation adsorption and thermo-responsiveness causing aggregation in water. Combination of these two functions leads to cation-adsorbent Janus nanosheets.

Contents

Chapter 1

Introduction

1.1 Layered metal oxides

Layered metal oxides consist of stacked single-crystalline metal oxide nanosheets. The thickness of nanosheets corresponds to several atoms, and the lateral size is in the micrometer range. Thus, nanosheets are considered to be materials with significantly high aspect ratios. Clay minerals,[1-3] layered silicates[4-6] and layered transition metal oxides[7-9], in particular, contain negatively charged nanosheets and interlayer metal cations. These cations can be exchanged with other cations, such as metal cations or alkylammonium ions, and these ion exchange reactions are categorized as intercalation.[10-12] The surfaces of nanosheets can be modified with alcohols, carboxylic acids, silylating agents or phosphorous coupling agents such as organophosphonic acids.[13-14] Metal oxide nanosheets can be obtained by exfoliation from layered compounds consisting of stacked nanosheets.[8, 15-16] Thus, layered metal oxides are considered to be useful host materials for intercalation and starting compounds for preparing nanosheets.

1.1.1 Surface modification of layered metal oxides

Interlayer surface modification of inorganic layered materials is classified into two types: that forming weak bonds, such as ionic bonds, and that forming stable bonds by grafting organic molecules onto interlayer surfaces. Ionic bonds are formed between charged nanosheets and ions that have a charge opposite to that of the nanosheets. In previous studies, organic ions, such as alkylammonium ions, cationic

dyes and heavy metal ions, were intercalated in the interlayers of clay minerals,[10, 17-18] layered silicates[11, 19-20] and layered transition metal oxide *via* an ion-exchange mechanism.[12, 21-22]

Four types of surface modifiers, namely alcohols, carboxylic acids, silylation agents and phosphorous coupling agents, have mainly been used for interlayer surface modification involving formation of stable bonds. These four types of surface modifiers form M-O-C bonds through reactions with alcohols and carboxylic acids, M-O-Si bonds through reactions with silylation agents and M-O-P bonds through reactions with phosphorous coupling agents. As concerns stability, M-O-C bonds are known to be easily hydrolyzed, and homocondensation can occur between silylation agents upon hydrolysis. On the other hand, hydrolysis of M-O-P bonds and homocondensation between phosphorous coupling agents seldom occur under mild conditions. Therefore, phosphorous coupling agents form self-assembled monolayers on the surfaces of metal oxides.[23-24] Interlayer surfaces of layered silicates have been modified with alcohols[25] and silylation agents.[26-28] Interlayer surfaces bearing Si-OH group have also been modified with organophosphonic acids, but Si-O-P bonds are easily cleaved by hydrolysis.[23-24] On the other hand, interlayer surfaces of layered transition metal oxides have been modified with alcohols[29] and silylation agents.[30-31] Furthermore, a protonated ion-exchangeable layered perovskite, $HLaNb_2O_7 \cdot xH_2O$, has been modified with organophosphonic acids. In this process, $HLaNb_2O_7 \cdot xH_2O$ was first modified with *n*-propanol, and the resultant

n-propoxy-derivative was then modified with *n*-decanol to expand the interlayer distance through an alcohol-exchange-type reaction. Finally, this *n*-decoxy-derivative was modified with various organophosphonic acids (Figure 1.1).[14]

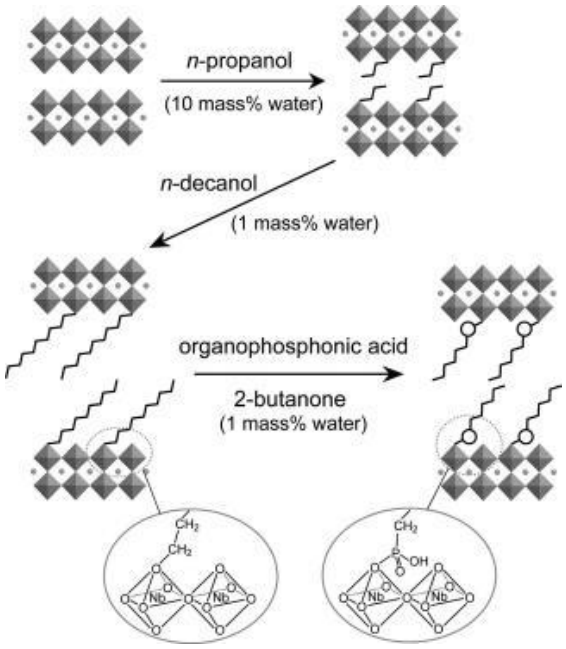

Figure 1.1 Overview of the modification of ion-exchangeable layered perovskite $HLaNb_2O_7 \cdot xH_2O$ with organophosphonic acids.[14]

"Reprinted with permission from A. Shimada, Y. Yoneyama, S. Tahara, P. H. Mutin and Y. Sugahara, Interlayer Surface Modification of the Protonated Ion-exchangeable Layered Perovskite $HLaNb_2O_7 \cdot xH_2O$ with Organophosphonic Acids, *Chem. Mater.*, **21,** 4155-4162 (2009)., Copyright 2009 American Chemical Society."

1.1.2 Exfoliation of layered metal oxides

Nanosheets prepared by exfoliation of layered materials have been applied as

nanofillers for various polymers [32] and for preparation of thin films[33] and nanotubes.[34] Various methods have been reported for exfoliation of layered metal oxides (Figure 1.2). The simplest method of exfoliation is dispersion of layered materials in water. This method is mainly applied to clay minerals, such as montmorillonite contained in bentonite, because of their low layer charge density.[35] These clay minerals swell and exfoliate easily in water, since they accommodate water molecules in their interlayers. Layered materials with high layer charge densities, on the other hand, are exfoliated *via* intercalation of bulky ions, such as tetrabutylammonium ion.[36-38] The distance between the negative layer charge and positive cation charge is increased by intercalation of the bulky ammonium ions, and exfoliation proceeds due to a decreased coulomb interaction between the negative charge and positive charge. These two methods proceed in water. Swelling and exfoliation processes conducted in organic solvents have also been reported using layered materials in which organic moieties with a high affinity to organic solvents were immobilized.[39] Mechanical exfoliation by ultrasonication can be used if spontaneous exfoliation does not proceed.[40] *In-situ* polymerization in interlayers from immobilized initiators, the so-called ”grafting-from” method, is also used for exfoliation since polymer chains can expand the interlayer distance.[41-42] An ion-exchangeable layered perovskite was exfoliated by the “grafting-from” method *via*

polymerization of poly(*N*-isopropylacrylamide) (PNIPAAm) in its interlayer.[43]

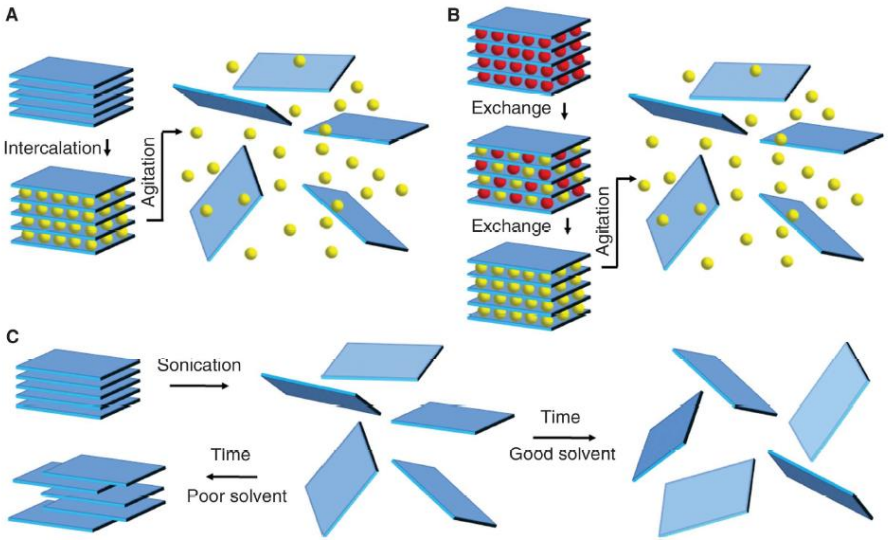

Figure 1.2 Schematic description of the main liquid exfoliation mechanisms. (A) Ion intercalation, (B) Ion exchange and (C) Sonication-assisted exfoliation.[15]

"V. Nicolosi, M. Chhowalla, M. G. Kanatzidis, M. S. Strano, J. N. Coleman, Liquid Exfoliation of Layered Materials, *Science*, 340(6139), 1226419 (2013). Copyright © 2013, American Association for the Advancement of Science"

1.1.3 Layered hexaniobate $K_4Nb_6O_{17}\cdot 3H_2O$

A layered hexaniobate, $K_4Nb_6O_{17}\cdot 3H_2O$, has been used as a host for intercalation of cations and has been modified with a silylation agent and organophosphonic acid. Since highly reactive interlayer I and less reactive interlayer II appear alternately in $K_4Nb_6O_{17}\cdot 3H_2O$ (Figure 1.3),[44] however, different intercalation behaviors are observed for interlayers I and II upon intercalation, interlayer surface modification

and exfoliation. The difference in reactivities between interlayers I and II originates from the hydration state of interlayer K^+ ions; the K^+ ions in interlayer I are hydrated, while the K^+ ions in interlayer II are not hydrated.[8] Therefore, unique intercalation behavior was observed for ion-exchange reactions with metal cations.[45] Monovalent metal cations were intercalated into both interlayers, whereas divalent metal cations were intercalated only into interlayer I.[46] As regards ion exchanges with organic cations *via* intercalation, meanwhile, bulky dioctadecyldimethylammonium ions were intercalated only into interlayer I, while less bulky *n*-dodecylammonium ions were intercalated into both interlayers.[47-48] In addition, interlayer surface modification of $K_4Nb_6O_{17}\cdot 3H_2O$ using a silylating agent was reported.[39] Using its unique intercalation and grafting reaction behavior, surface modification only in interlayer I or in both interlayer I and interlayer II can be achieved using organophosphonic acid.[49] Interlayer I was expanded by intercalation of dioctadecyldimethylammonium ions, and the resulting intercalation compound was reacted with phenylphosphonic acid. In the resulting derivative, designated as A-type, only interlayer I was modified with phenylphosphonic acid. On the other hand, interlayers I and II were expanded by intercalation of dodecylammonium ions, and the resulting intercalation compound was reacted with phenylphosphonic acid. In the resulting derivative, classified as B-type, both interlayers were modified with phenylphosphonic acid. Furthermore, these derivatives were exfoliated in acetonitrile. The A-type derivative was exfoliated only at interlayer I to form a

dispersion containing double-layered nanosheets. On the other hand, the B-type derivative was exfoliated at both interlayer I and interlayer II, resulting in the formation of a dispersion containing single-layered nanosheets.

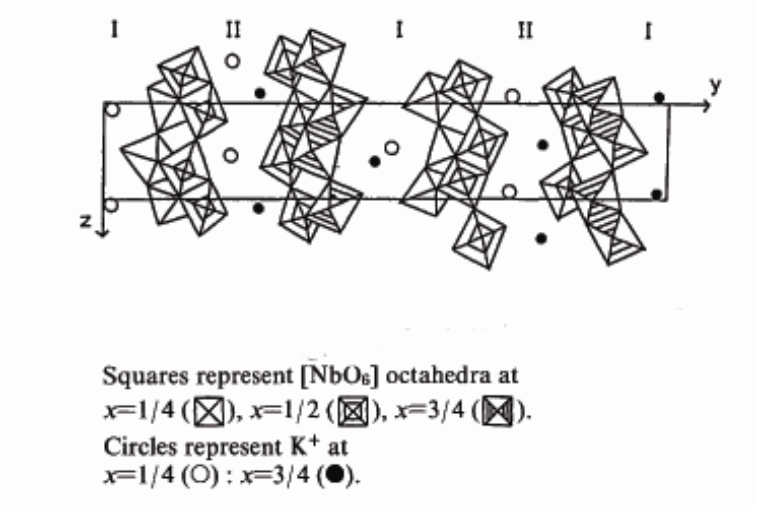

Figure 1.3 Structure of $K_4Nb_6O_{17}\cdot 3H_2O$.[44]

"Reprinted with permission from T. Nakato, K. Kuroda and C. Kato, Syntheses of Intercalation Compounds of Layered Niobates with Methylviologen and their Photochemical Behavior, *Chem. Mater*., **4**, 128-132 (1992)., Copyright 1992 American Chemical Society."

1.2 Janus Materials

1.2.1 Janus Materials and Their Classification

"Janus" is the name of the Roman god who has two faces, one each on the front and back of his head, and Janus materials have two distinct surfaces with different surface chemical properties (Figure 1.4).[50] Janus materials are expected to be applied to various fields, such as electrochemistry,[51] surface chemistry,[52] biochemistry,[53]

optics[54] and catalysts.[55]

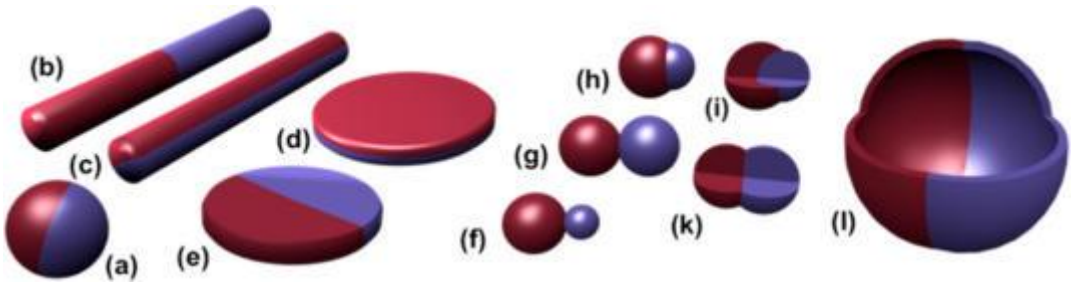

Figure 1.4 (a) Janus particles, (b, c) two types of Janus cylinders, (d, e) Janus discs, (f-k) various kinds of dumbbell-shaped Janus nanoparticles and (l) Janus vesicles or capsules.[50]

"Reprinted with permission from T A. Walther and A. H. E. Müller, Janus Particles: Synthesis, Self-Assembly, Physical Properties, and Applications, *Chem. Rev.*, **113**, 5194-5261 (2013)., Copyright 2020 American Chemical Society."

The concept of a "Janus grain" was introduced by de Denne at his Nobel lecture in 1991.[56] In this lecture, he referred to two Janus materials. One of his two examples was polystyrene nanoparticles, whose hemisphere was modified to produce Janus beads possessing two hemisphere surfaces with different chemical properties.[57] The other example was crushed silica core shell nanoparticles, whose outer shell was modified by lipophilic moieties to produce Janus sheets which had two surfaces with different chemical properties.[58]

To date, Janus materials with various shapes have been prepared. For example, zero-dimensional materials such as particles, one-dimensional materials such as rods and cylinders, and two-dimensional materials such as sheets and discs were

reported.[59] Regardless of the shape, as described above, it is necessary that Janus materials have two distinct surfaces with different chemical properties.[60]

1.2.2 Preparation of Janus Nanomaterials and Their Applications

There are a large number of reports on preparation of Janus nanoparticles and various preparation methods have been developed, including preparation by masking nanoparticle hemispheres and subsequence surface modification of unmasked surfaces and preparation by self-assembly of polymers or oligomers.[61] In a report by Takei *et al*, hemispheres of gold nanoparticles were masked by anchoring them on a polymer substrate and then modifying the unmasked surfaces by sputtering.[62] Polystyrene-based Janus nanoparticles were also prepared by this method.[63] Also, preparing Janus nanoparticles by self-assembly of triblock copolymers was first reported. Polystyrene-*block*-polybutadiene-*block*-poly(methyl methacrylate) was aligned on an air-liquid interface, and the polybutadiene block, its middle block, was crosslinked. The resulting product consisted of nanoparticles bearing two different moieties on two hemispheres.[64] Various Janus nanoparticles have been prepared by this mothed, since it can be applied to various triblock copolymers.[65] Also, Janus nanoparticles with a hydrophilic surface and a lipophilic surface were applied as solid surfactants, and these Janus nanoparticles stabilized emulsions better than nanoparticles with isotropic surfaces.[66] Besides these applications, Janus nanoparticles were also applied as optical materials,[67] biorecognition-signaling

elements[68] and as compatibilizers of polymers for polymer blends.[69] Janus nanoparticles with optical properties were prepared by assembly of Au nanoparticles on hemispheres of SiO_2 nanoparticles and are expected to be applied as sensing materials due to the plasmon resonance of Au nanoparticles.[67] Biorecognition-signaling elements have two functions, biorecognition due to surface modification using streptavidin and electrochemical reactivity due to surface modification using horseradish peroxidase. These Janus nanoparticles could therefore recognize biotin by adsorption of streptavidin surfaces and obtained signals through a reaction of horseradish peroxidase.[68] Janus nanoparticles where individual nanoparticles possessed a poly(2,6-dimethyl-1,4-phenyleneether) (PPE) surface and a poly(styrene-*co*-acrylonitrile) (SAN) surface formed a polymer blend composed of PPE and SAN due to the Pickering effect.[69]

There are few reports on preparation and simulation related to adsorption behavior at the interface[70-71] of Janus nanorods and Janus nanocylinder. Müller *et al.* prepared Janus nanocylinders which had two distinct surfaces parallel to a long axis.[72] Crosslinking of polystyrene-*block*-polybutadiene-*block*-poly(methylmethacrylate) (SBM) triblock copolymers provided Janus nanocylinders whose core was a polybutadiene block. Janus nanocylinders can also be prepared by surface modification of the limited surfaces of nanocylinders anchored on substrates by the same method as that used to prepare Janus nanonanoparticles.[73] Application of Janus nanocylinders based on their shapes were reported.[74] Janus nanocylinders were

adsorbed at the liquid-liquid interface at a fixed angle, and this angle was affected by the balance between the lipophilicity and hydrophilicity of the surfaces and the Janus nanocylinder aspect ratio. Also, Janus nanocylinders whose two surfaces were located perpendicular to the log axis were assembled by gathering the heads of nanocylinders.[75]

Janus nanosheets and Janus nanodiscs exhibit especially high anisotropy among Janus nanomaterials. In particular, Janus nanosheets have been expected to stabilize emulsions due to their high anisotropy and rotation restriction.[76] Most Janus nanosheets have been prepared using polymers. Stupp *et al.*[77] prepared Janus nanosheets by aligning oligomers which had a functional group for polymerization on one terminal and a group for promoting two-dimensional assembly on the other terminal. There was also a chiral center in the middle of these oligomers. Walther *et al.* reported preparing Janus nanosheets using a triblock copolymer.[78] Janus nanosheets can be formed by crystallization of poly(ε-caprolactone) at the interface between water and pentyl acetate.[79] Also, assembly of peptides can form self-supporting Janus nanosheets measuring several nm in thickness.[80] For preparing polymer-based Janus nanosheets, it is important to align functional groups by self-assembly and to immobilize aligned functional groups by crosslinking or crystallization.

The most common application of polymer-based Janus nanosheets is stabilization of emulsions.[81-82] Liu *et al.* prepared an emulsion using Janus nanosheets with

PNIPAAm chains.[83] PNIPAAm chains have a random coil structure that exhibits hydrophilicity at low temperatures, while PNIPAAm exhibits lipophilicity upon formation of a globular structure at high temperatures. This coil-globule transition occurs at a lower critical solution temperature (LCST). Janus nanosheets have lipophilic polystyrene on one side and PNIPAAm chains on the other. When PNIPAAm chains exhibited hydrophilicity at below LCST, the emulsions were stabilized by Janus nanosheets. On the other hand, when PNIPAAm chains exhibited lipophilicity at above LCST, the emulsions were not stabilized by Janus nanosheets. Also, Janus nanosheets bearing poly(maleic acid) chains on one side can stabilize emulsions, but emulsions were destabilized by decreasing the pH.[84] In addition to these application, Janus nanosheets can be applied as biosensing materials[85] and as separators between water and oil for distillation of water.[86]

1.3 Inorganic Janus Nanosheets

The polymer-based Janus nanosheets described in the previous section have certain drawbacks, such as swelling and deformation in organic solvents.[87] On the other hand, inorganic Janus nanosheets are likely stable in organic solvents. Therefore, methods of preparing inorganic Janus nanosheets have been developed. So far, however, there have been many fewer reports on preparing inorganic Janus nanosheets than on preparing polymer-based Janus nanosheets. The inorganic Janus nanosheets prepared have consisted of silica made by the sol-gel method or inorganic

layered materials.

1.3.1 Silica-based Janus Nanosheets prepared by the Sol-gel Method

The key process in preparing sol-gel silica-based Janus nanosheets involves crushing silica core shell nanoparticles to obtain nanosheet structures. As described above, this process was reported by Gruning *et al.* In this report, the outer surfaces of purchased silica core shell particles were modified for purposes of functionalization.[58]

On the other hand, Lian *et al*. also prepared silica-based Janus nanosheets by crushing core shell nanoparticles.[88] Two solvents which can form emulsions, water and paraffin, and two kinds of trialkoxysilanes, one bearing a lipophilic group and the other bearing a hydrophilic group, were used to prepare silica-based Janus nanosheets. Trialkoxysilanes were assembled at the interfaces of paraffin droplets in emulsion. Lipophilic groups or hydrophilic groups of trialkoxysilanes were faced with a solvent with higher affinity. Then, hydrolysis and condensation were carried out to form Si-O-Si bonds. The resultant core shell nanoparticles have different functional groups at the inner and outer surfaces. Sol-gel silica-based Janus nanosheets were then obtained by crushing the core shell nanoparticles using ultrasonication (Figure 1.5). This method was considered as a smart method, since formation of an Si-O-Si network and functionalization of the surfaces were achieved in one step. Also, a polymer composite of silica-based Janus nanosheets was prepared using this method by changing functional group of trialkoxysilanes and

grafting polymers onto the lipophilic side of Janus nanosheets.[89]

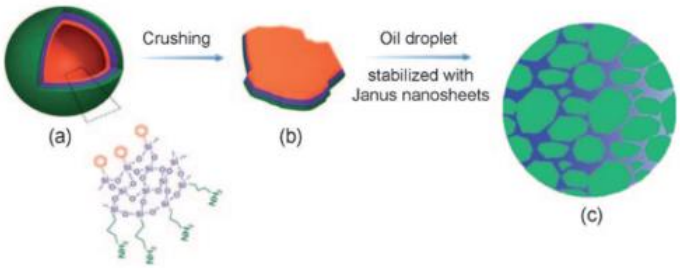

Figure 1.5 Preparation methods of silica-based Janus nanosheets (a) silica Janus hollow spheres formed onto micelle interface using two organosilane, (b) crushing the silica Janus hollow spheres and (c) stabilized emulsion by obtained Janus nanosheets.[88]

"F. Liang, K. Shen, X. Qu, C. Zhang, Q. Wang, J. Li, J. Liu and Z. Yang, Inorganic Janus Nanosheets, Angew. Chem. Int. Ed., 50, 2379 -2382 (2011). Copyright © 2011 WILEY‐VCH Verlag GmbH & Co. KGaA, Weinheim"

The Janus nanosheets prepared using the above-mentioned method had a disadvantage: the relatively large thickness of the obtained Janus nanosheets. Then, in 2015, a decrease in the thickness of silica-based Janus nanosheets was achieved.[90] First, 3-butyldianhydridemercaptopropyltrimethoxysilane (BDMPS) was used to form a self-assembly monolayer on a template comprising $CaCO_3$ nanoparticles. Hydrolysis and condensation of BDMPS were carried out, and an Si-O-Si network was formed. The surfaces of these particles were then modified with octadecyltrichlorosilane. After acid treatment to remove the $CaCO_3$ template and subsequent ultrasonication to crush the silica shells, thin Janus nanosheets measuring

about 3.5 ± 0.2 nm were obtained. Still, there were two issues raised by this method: a limitation of available organosilanes because of the required adsorption of organosilanes onto the template surface and the impossibility of reusing the template nanoparticles. Thus, a method of using acrylamide particles as a template was reported.[91] Acrylamide particles can interact with several trialkoxysilanes, including 3-(2-aminoethylamino)propyltrimethoxysilane, γ-ureidopropyltrimethoxysilane and BDMPS. Previously prepared core shell particles were crushed, and the resulting Janus nanosheets were removed from the template surface by ultrasonication in ethanol. Janus nanosheets and acrylamide particles can be separated easily in ethanol due to a difference in their sedimentation rates.

Furthermore, control of the Janus nanodisc shapes, which were uncontrollable with the methods using silica core shell nanoparticles, was achieved.[92] First, Ag nanoparticles were partially deposited on the surfaces of Fe_3O_4 particles covered with SiO_2. Then, the exposed SiO_2 surfaces were masked by *n*-octyltrimethoxysilane. Next, Ag nanoparticles were dissolved, and the patchy unmasked SiO_2 surface was modified with 4-(chloromethyl)phenyltrimethoxysilane. These particles can adsorb amino groups of 3-aminopropyltrimethoxysilane (APTMS) by forming an imine bond to form a monolayer of APTMS. The APTMS then formed an Si-O-Si network by the sol-gel process to obtain a patchy silica layer. Next, Janus nanodiscs were removed from the core shell surface by breaking the imine bond under acidic conditions. These Janus nanodiscs were also easily corrected, because Fe_3O_4 can be

removed by applying a magnetic field.

It is clear from these reports that the important factors in preparation of silica-based Janus nanosheets are organosilanes, solvents and templates for adsorption of organosilanes onto liquid-liquid interfaces or template surfaces. Most of the inorganic Janus nanosheets were prepared using this type of method and various applications were reported.

Yang *et al.* reported preparation of stimulus-responsive Janus nanosheets with properties as a surfactant.[93] The Janus nanosheets had an octyl group on one side and a poly-2-(dimethylamino)ethyl methacrylate (PDEAEMA) moiety on the other side. When the pH of their aqueous dispersion was lower than 7.2, pK_a of PDEAEMA, the PDEAEMA chains were protonated and became hydrophilic to provide the Janus nanosheets with amphiphilicity. On the other hand, when the pH of dispersion was higher than 7.2, the PDEAEMA chains were aggregated and became lipophilic to provide the Janus nanosheets with lipophilicity on both surfaces. Therefore, the Janus nanosheets worked as surfactants only when the pH of the dispersion was lower than 7.2 (Figure 1.6). In addition, photoresponsive Janus nanosheets were also reported.[94]

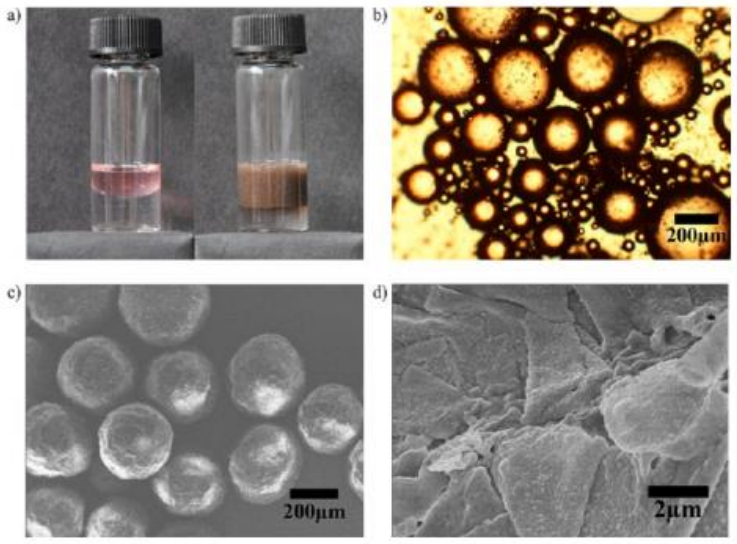

Figure 1.6 (a) left: immiscible mixture of toluene (top) and water (bottom); right: toluene-in-water emulsion stabilized with the Janus composite nanosheet; (b) optical microscopy image of the emulsion droplets; (c) SEM image of the frozen paraffin-in-water emulsion stabilized with the Janus composite nanosheet (d) SEM image of the Janus nanosheet onto the frozen paraffin droplets as shown in (c).[93]

"Reprinted with permission from Z. Zhao, F. Liang, G. Zhang, X. Ji, Q. Wang, X. Qu, X. Song and Z. Yang, Dually Responsive Janus Composite Nanosheets, *Macromolecules*, **48**, 3598-3603 (2015)., Copyright 2015 American Chemical Society."

Janus nanosheets can also be applied as catalysts.[95] Xu *et al.* prepared Janus nanosheets that had amino groups and Au nanoparticles on one side and phenyl groups on the other side. This type of Janus nanosheets can stabilize an emulsion and work as a catalyst for reduction of *p*-nitrophenol at the interface of droplets because

of the effect of the Au nanoparticles. Furthermore, catalytic Janus nanosheets with mesopores were prepared.[96] The mesopores were used as pathways for molecules during catalytic reactions. Mesoporous silica shells were prepared on polystyrene particle surfaces using a surfactant and silica source. Then, the surfaces of the mesoporous silica were modified with *n*-octyltrimethoxysilane. Polystyrene particles and the surfactant were dissolved in ethanol containing HCl and THF. Finally, the hollow mesoporous silica spheres were crushed. The resulting mesoporous silica nanosheets had hydrophilicity on one side and lipophilicity on the other.

In addition, various applications for Janus nanosheets with other types of functionalization were reported. Janus nanosheets functionalized by ionic liquid moieties were reported as stabilizers for emulsions and as a catalyst on an interface.[97-99] Amphiphilic Janus nanosheets can be applied to enhance oil recovery.[100] Janus nanosheets deposited on Fe_3O_4 particles showed magnetic field responsivity for catalytic applications.[101] Janus nanosheets can also be applied to purification of materials for synthesis of medicines by selective capture and fast separation of 2'-deoxyadenosine, which is adsorbed on one side of the Janus nanosheets, and Fe_3O_4 nanoparticles attached to the other side of Janus nanosheets for collection by applying an external magnetic field.[102] Investigations of the dispersion and aggregation behavior of Janus nanosheets were also reported.[103-104]

1.3.2 Layered Materials-based Inorganic Janus Nanosheets

Preparation methods for inorganic Janus nanosheets using layered materials were also reported. Nanosheets derived from layered materials are extremely thin,[105-107] and are considered as stable starting materials for preparing Janus nanosheets with high anisotropy. Preparation methods for obtaining Janus nanosheets from layered materials are classified into two methods. One is the substitution of atoms in nanosheets. This method was applied to transition metal dichalcogenide.[108] The other is selective surface modification of nanosheets. This method was applied to graphene[109] and clay minerals, such as fluorohectorite and laponite.[110-111]

1.3.2.1 Transition Metal Chalcogenide-based Janus Nanosheets

Transition metal dichalcogenides consist of stacked nanosheets whose composition is represented as MX_2 (M = Mo, W and X = S, Se, Te).[105] Janus nanosheets were also prepared from transition metal dichalcogenides, and their compositions were represented as MXY(Y = S, Se, Te).[108] In other words, half of the X atoms in MX_2 were replaced with other atoms. Based on molecular-dynamics calculations, it was reported that MoSSe, WSSe, WSeTe and WSTe can be stable with layered structures.[112] Transition metal dichalcogenide-based Janus nanosheets were prepared using $MoSe_2$ and S by the CVD method.[113] Single-layered $MoSe_2$ was heated at 800°C at the center of a reactor. The heated $MoSe_2$ was then exposed to S vapor (Figure 1.7). There were a few reports of preparing transition metal

dichalcogenide-based Janus nanosheets. And a large number of simulation studies on transition metal dichalcogenide-based Janus nanosheets were reported for their applications in electrochemical[114-115] and catalytic fields.[116-119]

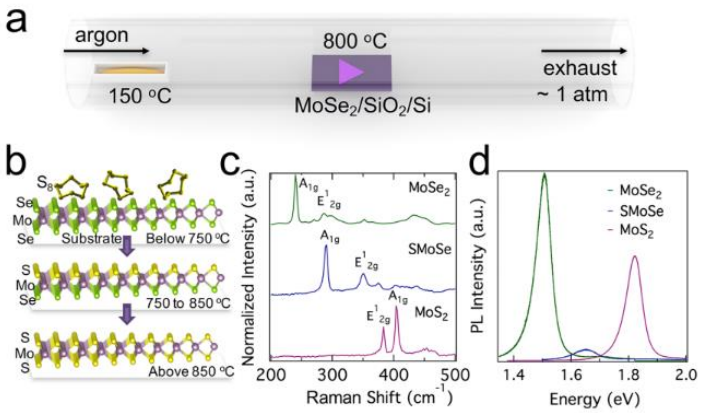

Figure 1.7 (a) Scheme of preparation of Janus nanosheets, MoSSe, the left image with yellow color; S and the center image with purple color; $MoSe_2$ on SiO_2/S substrate, (b) proposed reaction mechanism for the sulfurization of monolayer $MoSe_2$ on substrate at different temperatures, (c, d) Raman and photoluminescence (under 532 nm diode laser excitation) spectra of $MoSe_2$, SMoSe (Janus nanoshessts), and MoS_2 corresponding to the diagram in (b).[113]

1.3.2.2 Graphene-based Janus Nanosheets

Graphene nanosheets consist of C atoms connected with sp^2 bonds.[106] Graphene

oxide (GO), which can be derived from graphene *via* oxidation, has OH groups, carboxylic groups and epoxy groups on its surface and can thus be modified by various modifiers.[120] When the surface of graphene is modified without exfoliation, only the outer surface of the stacked graphene is modified. Exfoliation of graphene is therefore necessary for modification of all the sheets surface. Single-layered graphene nanosheets are obtained by sonication, jet cavitation and high-shear mixing of graphite, and a bottom-up process such as CVD.[121] Both sides of exfoliated individual graphene nanosheets exhibit the same reactivity. Therefore, both sides of these exfoliated graphene nanosheets should be modified. Thus, singe-layered graphene nanosheets with only one side masked are necessary to prepare graphene-based Janus nanosheets.

A single-sided hydrogenated graphene structure, called a graphone, is considered as Janus nanosheets with a very simple structure[122] and is expected to be applied to field effect transistors and ferroelectrics. However, there has been no report on preparation of graphones.[123-124]

Zhang *et al.* prepared graphene-based Janus nanosheets by two-step surface modification.[109] First, one side of graphene nanosheets anchored on Cu film prepared by CVD was modified. Then, the unmodified surface of the graphene nanosheets was exposed by transferring them to a polymethyl methacrylate (PMMA) film. The newly exposed surface of the graphene was then modified. Finally, graphene-based Janus nanosheets were obtained by removing the PMMA (Figure 1.8).

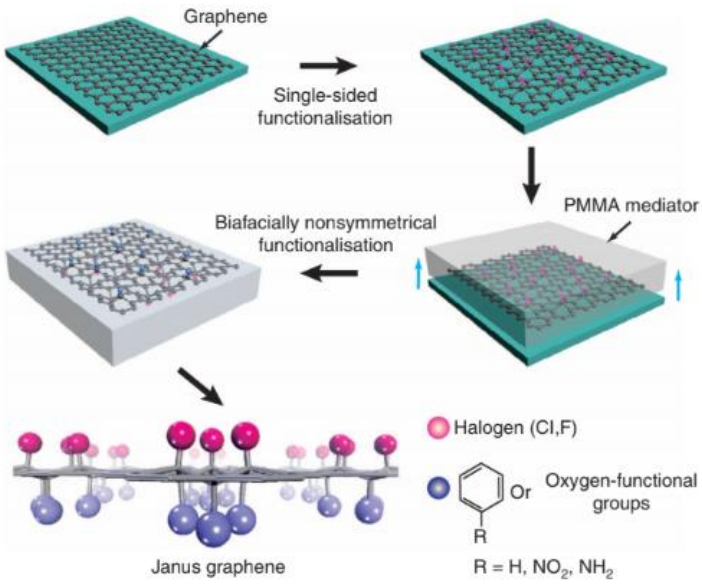

Figure 1.8 Scheme of preparation graphene-based Janus nanosheets. [109]

"L. Zhang, J. Yu, M. Yang, Q. Xie1, H. Peng and Z. Liu, Janus Graphene from Asymmetric Two-dimensional Chemistry, *Nature Commun.*, 2464, (2013). Copyright © 2013, Springer Nature"

There were few reports of preparation of graphene-based Janus nanosheets using a one-pot process.[125-127] A Pickering emulsion was prepared using GO nanosheets with an acryl group on both sides. GO nanosheets bearing acryl groups were modified with thiol-terminated polystyrene dissolved in oil droplet in an o/w emulsion, and surface modification of one side was achieved *via* a thiol-ene reaction.[125] This method was considered easier than the two-step method described above, because the masking and regioselective surface modification were carried out in one process.

Masking of graphene was achieved using not only an emulsion but also positively charged polystyrene particles. Negatively-charged GO nanosheets were assembled on particles of cationic polystyrene and the exposed surface of GO was modified. Simultaneously, the other surface of the graphene nanosheets was modified with cationic polystyrene by forming ionic bonds. Graphene-based Janus nanosheets were obtained by dissolving the polystyrene particles in tetrahydrofuran.[128]

On the other hand, masking can also be achieved by forming hydrogen bonds between GO nanosheets and templates.[129] GO nanosheets were adsorbed on the surfaces of tapioca starch particles by forming hydrogen bonds in water. This method had environmental and economic advantages, such as limited use of an organic solvent and a high yield.

Various applications were reported for graphene-based Janus nanosheets. TiO_2 nanoparticles were deposited on one side and Pt nanoparticles on the other sides of GO nanosheets, and these graphene-based Janus nanosheets exhibited a charge separation ability.[130] Electrons were generated by light irradiation of the deposited TiO_2 nanoparticles, and photogenerated electrons were transferred to the deposited Pt nanoparticles through GO nanosheets. Thus, the holes and electrons were separated to the TiO_2 nanoparticle side and Pt nanoparticle side, respectively.

Dual-functional Janus nanosheets which can adsorb organic and inorganic targets were also reported.[131] Graphene-based Janus nanosheets with an octadecyl group on one side and ethylenediaminetetraacetic acid moiety on the other side were prepared.

These Janus nanosheets can collect pollutants such as perfluorooctanesulfonic acid, Pb(II) ions and Ni(II) ions from aqueous solutions. Graphene-based Janus nanosheets were also expected to be applied in drug delivery,[132] secondary oil recovery,[133-135] surface chemistry [136-137] and electrochemistry.[138]

1.3.2.3 Clay Minerals-based Janus Nanosheets

Fluorohectorite is a clay mineral which consists of negatively charged silicate nanosheets and interlayer cations. These cations can be exchanged with other cations through ion-exchange reactions.[139] Möller *et al.* prepared a product which has two interlayers with two different cation layers appearing alternately by exchanging a part of interlayer Na^+ ions with the other metal cations.[140-141] Therefore, Janus nanosheets could be prepared using the resulting two types of interlayers.[110] First, fluorohectorite with two types of interlayers was prepared by a partial ion-exchange reaction between a part of Na^+ and NH_4^+. Then, the product was dispersed in water, and double-layered nanosheets were obtained by exfoliation at the Na^+-containing interlayer. The exposed surfaces of the double-layered nanosheets were modified using a type of cationic polymer by forming ionic bonds. The product was then dispersed in an LiOH aqueous solution, and single-layered nanosheets were obtained by exfoliation at the NH_4^+-containing interlayer. Finally, the unmodified surface of the nanosheets was modified using another type of cationic polymer, also by forming ionic bonds. The resultant nanosheets have one cationic polymer on one side and the

other polymer on the other side (Figure 1.8). This method produced Janus nanosheets using heterogeneous interlayer reactivities by regioselective ion exchange. Also, Janus nanosheets of this type have ionic bonds between the surface of the nanosheets and the cationic polymers, which limits their applications.

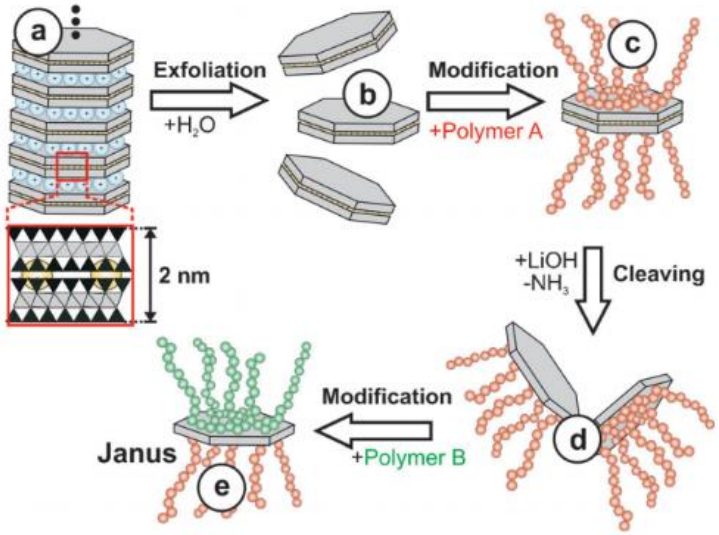

Figure 1.9 Preparation scheme of fluorohectorite-based Janus nanosheets: ⓐ fluorohectorite possessing hydrated Na^+ (blue) and NH_4^+(yellow), alternately, ⓑ highly selective exfoliation at interlayer of Na^+ into bilayers, ⓒ external modification with a polymer A (red),ⓓBilayers was cleaved under LiOH andⓔUn modified surface was further reacted with polymer B (green).[110]

Laponite can also be used for preparing Janus nanosheets. Laponite can be exfoliated by dispersing it in water, and the resultant nanosheets have a negative charge. [142] These exfoliated nanosheets were absorbed on the surface of positively charged polystyrene particles. Laponite-based Janus nanosheets were then obtained by dissolving the positively charged polystyrene nanoparticles, and the resultant Janus nanosheets had a surface bonded with positively charged polystyrene and an unmodified surface. In another method of preparation of laponite-based Janus nanosheets, one surface of laponite nanosheets adsorbed on positively charged polystyrene particles can be modified using cationic polymers, quaternized poly(2-(dimethylamino)ethyl methacrylate) (q-PDMAEMA), or positively charged cross-linked polymeric micelles. The resultant Janus nanosheets had one surface modifier on one side of the individual laponite nanosheets and another modifier on the other side (Figure 1.10).[111] This type of nanosheet also has ionic bonds between the nanosheet surfaces and the surface modifiers.

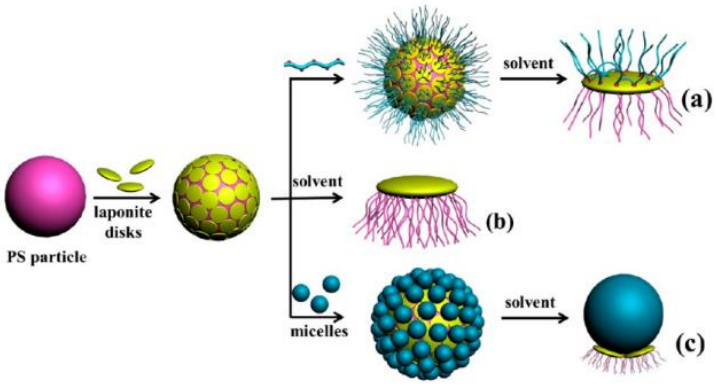

Figure 1.10 Preparation scheme of laponite-based Janus nanosheets (a) Janus

nanosheets modified with two cationic polymers, (b) Janus nanosheets possessing polymer on one surface and unmodified surface and (c) Janus nanosheets possessing polymer on one surface and micelles on the other surface. [111]

1.4 Objectives of This Thesis

Based on the background presented above, it is clear that preparing a lamellar structure and conducting regioselective surface modification by controlling reaction sites are necessary for preparation of Janus nanosheets. In the case of silica-based Janus nanosheets, self-assembly of organosilanes on liquid-liquid interfaces and templates were used for preparation of lamellar structures and functionalization of both the sheet surfaces. When using layered materials originally consisting of stacked nanosheets, on the other hand, precise control of the reaction sites for functionalization was necessary. Masking of single-layered graphene and laponite for precise control of the reaction sites was achieved by adsorption onto substrates or templates. In the case of the fluorohectorite in which heterogeneous interlayers can be achieved by selective ion-exchange, selective exfoliation was the key process for controlling the reacting interlayers for regioselective surface modification.

Therefore, there were several issues concerning the preparation of inorganic Janus nanosheets. For silica-based Janus nanosheets, usable types of organosilanes for preparing the emulsion and adsorbing interface were limited. For clay-based Janus nanosheets, surface modifiers were bonded to the nanosheet surfaces with ionic bonds. In other words, the raw materials available for designing reaction systems were limited. The applications for Janus nanosheets with ionic bonds between the nanosheet surface and modifier could be limited, moreover, because they can be utilized only in specific solvents.

On the other hand, interlayers of $K_4Nb_6O_{17}\cdot 3H_2O$ can be modified regioselectively when nanosheets maintain a stacked structure.[49] It is thus expected that Janus nanosheets can be prepared without using a masking method due to the unique reactivity of $K_4Nb_6O_{17}\cdot 3H_2O$ by applying certain strategies. In the first strategy, interlayer I is modified first using one type of phosphorous coupling agent. Then, interlayer II is modified using the other type of phosphorous coupling agent. Homocondensation of the phosphorous coupling agents and exchange reactions between the phosphorous coupling agents and immobilized organophosphonate moiety should scarcely proceed. Interlayers I and II could therefore be modified ideally by two different types of phosphorous coupling agent. Finally, the product is exfoliated into single-layered Janus nanosheets. In the second strategy, the exfoliation of the A-type organophosphonate derivative of $K_4Nb_6O_{17}\cdot 3H_2O$ could produce Janus nanosheets with an organophosphonate moiety on one side and an

unmodified surface on the other side. It should be noted that no complicated pretreatment, such as masking, is required before surface modification.

The use of phosphorous coupling agents is one characteristic of this study. Since various phosphorous coupling agents, such as hydrophilic phosphoric acid and lipophilic organophosphonic acids including one with a polymerization initiator group,[143] have been reported, desirable coupling agents can be selected for the intended properties. Phosphorous coupling agents have a particularly huge advantage, since they can be synthesized by facile methods such as the Arbuzov reaction.[144] Another advantage to the use of phosphorous coupling agents is avoidance of homocondensation, which is disadvantageous for regioselective surface modification. In addition, the use of phosphorous coupling agents provides stable Nb-O-P bonds between the nanosheet surface and the modifier, and the resulting Janus nanosheets could thus be applied in various solvents.

The contents are described in three chapters, and the conclusions are shown in Chapter 5. Brief introductions to Chapters 2, 3 and 4 are presented below.

In Chapter 2, the preparation method of $K_4Nb_6O_{17}\cdot 3H_2O$-based Janus nanosheets is described. Based on a previous study,[49] an A-type alkylphosphonate derivative of $K_4Nb_6O_{17}\cdot 3H_2O$ was prepared. Interlayer II of the product was expanded by dodecylammonium ions. The expanded interlayer II was then modified with carboxyalkylphosphonic acid. The product was exfoliated in an organic solvent, and a Janus nanosheet dispersion was obtained.

In Chapters 3 and 4, functionalization of $K_4Nb_6O_{17}\cdot 3H_2O$-based Janus nanosheets by changing of the phosphonate coupling agents from those used in Chapter 2 are described. In Chapter 3, Janus nanosheets with surface active performance were prepared and their effects on the liquid-air interface and liquid-liquid interface were investigated. In Chapter 4, dual-functional Janus nanosheets with two independent functions, a cation adsorption ability and thermoresponsivness, were prepared. The combination of these two functions enable these Janus nanosheets to work as cation adsorbents.

References

1 M. Osada and T. Sasaki, Exfoliated Oxide Nanosheets: New Solution to Nanoelectronics. *J. Mater. Chem*., **19**, 2503-2511 (2009).

2 E. Joussein, S. Petit, J. Churchman, B. Theng, D. Righi and B. Delvaux, Halloysite Clay Minerals-a Review, *Clay Miner*., **40(04)** 383-426 (2005).

3 J. Madejova, FTIR Techniques in Clay Mineral Studies, *Vib. Spectrosc*., **31(1)**, 1-10 (2003).

4 K. Kosuge, A. Yamazaki, A. Tsunashima and R. Otsuka, Hydrothermal Synthesis of Magadiite and Kenyaite, *J. Ceram. Soc. Jpn*., **100(3)**, 326-331 (1992).

5 G. W. Brindley, Uunit Cell of Magadiite in Air, in Vacuo, and Under Other Conditions, *Am. Miner.*, **54(11-1)**, 1583-1591 (1969).

6 F. Wolf and W. Schwieger, Ion Exchange of Monovalent Cations in Synthetic

Sodium Polysilicates with Layer Structure, *Anorg. Allg. Chem*., **457(1)**, 224-228 (1979).

7 T. Sasaki and M. Watanabe, Osmotic Swelling to Exfoliation. Exceptionally High Degrees of Hydration of a Layered Titanate, *J. Am. Chem. Soc*., **120(19)**, 4682-4689 (1998).

8 M. A. Bizeto, A. L. Shiguihara and V. R. L. Constantino, Layered Niobate Nanosheets: Building Blocks for Advanced Materials Assembly, *J. Mater. Chem.*, **19**, 2512-2525 (2009).

9 M. Osada and T. Sasaki, Two-Dimensional Dielectric Nanosheets: Novel Nanoelectronics From Nanocrystal Building Blocks, *Adv. Mater*., **24**, 210-228 (2012).

10. G. Lagaly and K. Beneke, Intercalation and Exchange Reactions of Clay Minerals and Non-clay Layer Compounds, *Colloid Polym. Sci.*, **269(12)**, 1198-1211 (1991).

11. G. Lagaly, Interaction of Alkylamines with Different Types of Layered Compounds, *Solid State Ion.*, **22**, 43-51 (1986).

12. M. Ogawa and K. Kuroda, Photofunctions of Intercalation Compounds, *Chem. Rev*., **1995**, 95(2), 399-438.

13 H. He, J. Duchet, J. Galy, and J. F. Gerard, Grafting of Swelling Clay Materials with 3-aminopropyltriethoxysilane, *J. Colloid Interface Sci.*, **288(1)**, 171-176 (2005).

14 A. Shimada, Y. Yoneyama, S. Tahara, P. H. Mutin and Y. Sugahara, Interlayer

Surface Modification of the Protonated Ion-exchangeable Layered Perovskite $HLaNb_2O_7 \cdot xH_2O$ with Organophosphonic Acids, *Chem. Mater.*, **21,** 4155-4162 (2009).

15 V. Nicolosi, M. Chhowalla, M. G. Kanatzidis, M. S. Strano, J. N. Coleman, Liquid Exfoliation of Layered Materials, *Science*, **340(6139)**, 1226419 (2013)

16 P. Podsiadlo, A. K. Kaushik, E. M. Arruda, A. M. Waas, B. S. Shim, J. Xu, H. Nandivada, B. G. Pumplin, J. Lahann, A. Ramamoorthy, N. A. Kotov, Ultrastrong and Stiff Layered Polymer Nanocomposites, *Science,* **318(5847)**, 80-83 (2007).

17 T. Arbeloa and I. L. Arbeloa, Photoresponse and Anisotropy of Rhodamine Dye Intercalated in Ordered Clay Layered Films, *J. Photochem. Photobiol. C*, **8,** 85-108 (2007).

18 W. Matthes, F. W. Madsen and G. Kahr, Sorption of Heavy-Metal Cations by Al and Zr-Hydroxyintercalated and Pillered Bentnite, *Clays Clay Miner.*, **47(5)**, 617-629 (1999).

19 M. Mokhta, Application of Synthetic Layered Sodium Silicate Magadiite Nanosheets for Environmental Remediation of Methylene Blue Dye in Water, *Materials*, **10(7)**, 760 (2017).

20 R. KIler, Ion Exchange Properties of a Crystalline Hydrated Silica, *J. Colloid Sci.*, **19(7)**, 648-657 (1964).

21 R. Shinozaki and T. Nakato, Photochemical Behavior of Rhodamine 6G Dye Intercalated in Photocatalytically Active Layered Hexaniobate, *Microporous*

Mesoporous Mater., **113(1-3)**, 81-89 (2008).

22 D. Yang, Z. Zheng, H. Liu, H. Zhu, X. Ke, Y. Xu, D. Wu and Y. Sun, Layered Titanate Nanofibers as Efficient Adsorbents for Removal of Toxic Radioactive and Heavy Metal Ions from Water, *J. Phys. Chem. C*, **112(42)**,16275-16280 (2008)

23 G. Guerrero, J. G. Alauzun, M. Granier, D. Laurencin and P. H. Mutin, Phosphonate Coupling Molecules for the Control of Surface/interface Properties and the Synthesis of Nanomaterials, *Dalton Trans.*, **42**, 12569-12585 (2013).

24 G. Guerrero, P. H. Mutin and A. Vioux, Anchoring of Phosphonate and Phosphinate Coupling Molecules on Titania Particles, *Chem. Mater*, **13**, 4367-4373 (2001).

25 L. Mercier, Glenn A. Facey and Christian Detellier, Organo-layered Silicates. Interlamellar Intercation and Grafting of Ethylene Glycol in Magadiite, *J. Chem. Soc., Chem. Commun*., 2111-2112 (1994).

26 T. Yanagisawa, K. Kuroda and C. Kato, Organic Derivatives of Layered Polysilicates. II. Reaction of Magadiite and Kenyaite with Diphenylmethylchlorosilane, *Bull. Chem. Soc. Jpn*., **61**, 3743-3745 (1988).

27 I. Fujita, K. Kuroda and M. Ogawa, Synthesis of Interlamellar Silylated Derivatives of Magadiite and the Adsorption Behavior for Aliphatic Alcohols, *Chem. Mater.*, **15**, 3134-3141 (2003).

28 D. Mochizuki, A. Shimojima and K. Kuroda, Formation of a New Crystalline Silicate Structure by Grafting Dialkoxysilyl Groups on Layered Octosilicate, *J. Am.*

Chem. Soc., **124**, 12082-12083 (2002).

29 Y. Asai, Y. Ariake, H. Saito, N. Idota, K. Matsukawa, T. Nishino and Y. Sugahara, Layered Perovskite Nanosheets Bearing Fluoroalkoxy Groups, *RSC Adv*., **4**, 26932-26939 (2014).

30 Y. Ide and M. Ogawa, Surface Modification of a Layered Alkali Titanate with Organosilanes, *Chem. Commun*., 1262-1263 (2003).

31 T. Nakato and S. Hashimoto, Dispersion of Layered Hexaniobate in Organic Solvents through Silylation and Liquid Crystalline Behavior of the Colloidal Suspension, *Chem. Lett*., **36**, 1240-1241 (2007).

32 C. Zilg, F. Dietsche, B. Hoffmann, C. Dietrich, R. Mühlhaupt, Nanofillers Based upon Organophilic Layered Silicates, *Macromol. Symp.*, **169(1)**, 65-77 (2001).

33 T. Sasaki, Fabrication of Nanostructured Functional Materials Using Exfoliated Nanosheets as a Building Block, *J. Ceram. Soc. Jpn.*, **115(1337)**, 9-16 (2007).

34 R. E Schaak, T. E Mallouk, Prying Apart Ruddlesden-Popper Phases: Exfoliation into Sheets and Nanotubes for Assembly of Perovskite Thin Films, *Chem. Mater.*, **12**, 3427-3434 (2000).

35 P. F. Luckham and S. Rossi, The Colloidal and Rheological Properties of Bentonite Suspensions, *Adv. Colloid Interface Sci.,* **82(1-3)**, 43-92 (1999).

36 T. Sasaki, M. Watanabe, H. Hashizume, H. Yamada, H. Nakazawa, Macromolecule-like Aspects for a Colloidal Suspension of an Exfoliated Titanate. Pairwise Association of Nanosheets and Dynamic Reassembling Process Initiated

from It, *J. Am. Chem. Soc.*, **118**, 8329-8335 (1996).

37 Z. Liu, K. Ooi, H. Kanoh, W. Tang and T. Tomida, Swelling and Delamination Behaviors of Birnessite-type Manganese Oxide by Intercalation of Tetraalkylammonium Ions, *Langmuir*, **16**, 4154-4164 (2000).

38 A. Takagaki, D. Lu, J. N. Kondo, M. Hara, S. Hayashi and K. Domen, Exfoliated HNb_3O_8 Nanosheets as a Strong Protonic Solid Acid, *Chem. Mater.*, **17(10)**, 2487-2489 (2005).

39 N. Teruyuki and H. Sachika, Dispersion of Layered Hexaniobate in Organic Solvents through Silylation and Liquid Crystalline Behavior of the Colloidal Suspension, *Chem. Lett*., **36(10)**, 1240-1241 (2007).

40 C. Backes, T. M. Higgins, A. Kelly, C. Boland, A. Harvey, D. Hanlon and J. N. Coleman, Guidelines for Exfoliation, Characterization and Processing of Layered Materials Produced by Liquid Exfoliation, *Chem. Mater.*, **29(1)**, 243-255 (2017).

41 J. S. Bergman, H. Chen, E. P. Giannelis, M. G. Thomasc and G. W. Coates, Synthesis and Characterization of Polyolefin-silicate Nanocomposites: a Catalyst Intercalation and in situ Polymerization Approach, *Chem. Commun*., 2179-2180 (1999).

42 R. K. Layek and A. K. Nandi, A Review on Synthesis and Properties of Polymer Functionalized Graphene. *Polymer*, **54(19)**, 5087-5103 (2013).

43 N. Idota, S. Fukuda, T. Tsukahara, Y. Sugahara, Preparation of Thermoresponsive Nanosheets Exhibiting Phase Transitions in Water *via* Surface

Modification of Layered Perovskite Nanosheets with Poly(*N*-isopropylacrylamide) (PNIPAAm), *Chem. Lett.*, **44(2)**, 203-205 (2015).

44 T. Nakato, K. Kuroda and C. Kato, Syntheses of Intercalation Compounds of Layered Niobates with Methylviologen and their Photochemical Behavior, *Chem. Mater.*, **4**, 128-132 (1992).

45 N. Kinomura, N. Kumada and F. Muto, Ion Exchange of $K_4Nb_6O_{17}\cdot 3H_2O$, *J. Chem. Soc., Dalton Trans.*, 2349-2351 (1985).

46 T. Nakato, D. Sakamoto, K. Kuroda and C. Kato, Synthesis of Two Types of Intercalation Compounds of $K_4Nb_6O_{17}$ with Tris(2,2'-bipyridyl) Metal Complex Ions, *Bull. Chem. Soc. Jpn.*, **65(2)**, 322-328 (1992).

47 T. Nakato, M. Kameyama, Q. Wei and J. Haga, Structural Response of Organically Modified Layered Niobate $K_4Nb_6O_{17}$ to the Adsorption of 2,4-Dichlorophenol, *Microporous Mesoporous Mater.*, **110**, 223-231 (2008).

48 Q. Wei and T. Nakato, Competitive Adsorption of Phenols on Organically Modified Layered Hexaniobate $K_4Nb_6O_{17}$, *Microporous Mesoporous Mater.*, **96**, 84-91 (2006).

49 N. Kimura, Y. Kato, R. Suzuki, A. Shimada, S. Tahara, T. Nakato, K. Matsukawa, P. H. Mutin and Y. Sugahara, Single- and Double-layered Organically Modified Nanosheets by Selective Interlayer Grafting and Exfoliation of Layered Potassium Hexaniobate, *Langmuir*, **30**, 1169-1175 (2014).

50 A. Walther and A. H. E. Müller, Janus Particles: Synthesis, Self-Assembly,

Physical Properties, and Applications, *Chem. Rev.*, **113**, 5194-5261 (2013).

51 T. Nishisako, T. Torii, T. Takahashi, Y. Takizawa. Synthesis of Monodisperse Bicolored Janus Particles with Electrical Anisotropy using a Microfluidic Co-flow system. *Adv. Mater.*, **18**, 1152-1156 (2006).

52 B. P. Binks and P. D. I. Fletcher, Particles Adsorbed at the Oil-water Interface: A Theoretical Comparison between Spheres of Uniform Wettability and "Janus" Particles. *Langmuir*, **17(16)**, 4708-4710 (2001).

53 K. D. Seo, J. Doh, D. S. Kim, Onestep Microfluidic Synthesis of Janus Microhydrogels with Anisotropic Thermo-responsive Behavior and Organophilic/hydrophilic Loading Capability, *Langmuir*, **29**, 15137-15141 (2013).

54 M. Kim, S. A. Anthony and S. Granick, Activated Surface Diffusion in a Simple Colloid System. *Phys. Rev. Lett*., **102**, 178303 (2009).

55 Z. Wua, L. Li, T. Liao, X. Chena, W. Jianga, W. Luoa, J. Yanga, Z. Sunb, Janus Nanoarchitectures: From Structural Design to Catalytic Applications, *Nano Today*, **22** 62-82 (2018).

56 P. G. de Gennes, Soft Matter (Nobel Lecture), *Angew. Chem. Int. Ed. Engl.*, **31**, 842-845 (1992).

57 C. Casagrande, P. Fabre, E. Raphael and M. Veyssie, "Janus Beads": Realization and Behaviour at Water/Oil Interfaces, *Europhys. Lett.*, **9(3)**, 251-255 (1989).

58 B. Gruning, U. Holtschmidt, G. Koerner, G. Rossmy, Particles, Modified at their Surface by Hydrophilic and Hydrophobic Groups, 1987, U. S. Patent 4, 715, 1986.

59 Y. Liang, J. Shi, P. Xiao, J. He, F. Ni, J. Zhang, Y. Huang, C. Huang and T. Chen, A Lotus-inspired Janus Hybrid Film Enabled by Interfacial Self-assembly and in situ Asymmetric Modification, *Chem. Commun.*, **54**, 12804-12807 (2018).

60 S. Jiang, Q. Chen, M. Tripathy, E. Luijten, K. S. Schweizer, and S. Granick, Janus Particle Synthesis and Assembly. *Adv. Mater*., **22**, 1060-1071 (2010).

61 M. Lattuada and T. A. Hatton, Synthesis, Properties and Applications of Janus Nanoparticles, *Nano Today*, **6**, 286-308 (2011).

62 H. Takei and N. Shimizu, Gradient Sensitive Microscopic Probes Prepared by Gold Evaporation and Chemisorption on Latex Spheres, *Langmuir*, **13(7)**, 1865-1868 (1997).

63 L. Y. Wu, B. M. Ross, S. G. Hong and L. P. Lee, Bioinspired Nanocorals with Decoupled Cellular Targeting and Sensing Functionality, *Small*, **6**, 503-507 (2010).

64 H. Xu, R. Erhardt, V. Abetz, A. H. E. Müller and W. A. Goedel, Janus Micelles at the Air/Water Interface, *Langmuir*, **17(22)**, 6787-6793 (2001).

65 V. Sfika, C. Tsitsilianis, A. Kiriy, G. Gorodyska and M. Stamm, pH Responsive Heteroarm Starlike Micelles from Double Hydrophilic ABC Terpolymer with Ampholitic A and C Blocks, *Macromolecules*, **37(25)**, 9551-9560 (2004).

66 B. P. Binks, Particles as Surfactants-similarities and Differences, *Curr. Opin. Colloid Interface Sci.*, **7(1-2)**, 21-41 (2002).

67 M. D. McConnell, M. J. Kraeutler, S. Yang and R. J. Composto, Patchy and Multiregion Janus Particles with Tunable Optical Properties, *Nano Lett.*, **10(2)**, 603-

609 (2010).

68 A. Sánchez, P. Díez, P. Martínez-Ruíz, R. Villalonga and J. M. Pingarrónac, Janus Au-mesoporous Silica Nanoparticles as Electrochemical Biorecognition-signaling System, *Electrochem. Commun.*, **30**, 51-54 (2013).

69 R. Bahrami, T. I. Lobling, A. H. Groschel, H. Schmalz, A. H. E. Muller and V. Altstadtm, The Impact of Janus Nanoparticles on the Compatibilization of Immiscible Polymer Blends under Technologically Relevant Conditions, *ACS Nano*, **8(10)**, 10048-10056, (2014).

70 A. Kharazmi and N. V. Priezjev, Molecular Dynamics Simulations of the Rotational and Translational Diffusion of a Janus Rod-Shaped Nanoparticle, *J. Phys. Chem. B*, **121**, 7133-7139 (2017).

71 B. J. Park, C. H. Choi, S. M. Kang, K. E. Tettey, C. S. Lee and D. Lee, Double Hydrophilic Janus Cylinders at an Air-Water Interface, *Langmuir*, **29**, 1841-1849 (2013).

72 Y. Liu, V. Abetz and A. H. E. Müller, Janus Cylinders, *Macromolecules*, **36(21)**, 7894-7898 (2003).

73 C. J. Murphy, and C. J. Orendorff, Alignment of Gold Nanorods in Polymer Composite and on Polymer Surface, *Adv. Mater.*, **17**, 2173-2177 (2005).

74 T. M. Ruhland, A. H. Grüschel, Andreas Walther and A. H. E. Müller, Janus Cylinders at LiquidLiquid Interfaces, *Langmuir*, **27**, 9807-9814 (2011).

75 K. Chaudhary, Q. Chen, J. J. Juarez, S. Granick and J. A. Lewis, Janus Colloidal

Matchsticks, *J. Am. Chem. Soc*., **134**, 12901-12903 (2012).

76 A. C. de Leon, B. J. Rodier, Q. Luo, C. M. Hemmingsen, P. Wei, K. Abbasi, R. Advincula and E. B. Pentzer, Distinct Chemical and Physical Properties of Janus Nanosheets, *ACS Nano*, **11(7)**, 7485-7493 (2017).

77 S. I. Stupp, S. Son, H. C. Lin and L. S. Li, Synthesis of Two-dimensional Polymers, *Science*, **259**, 59-63 (1993).

78 A. Walther, X. Andre, M. Drechsler, V. Abetz and A. H. E. Muller, Janus Discs, *J. Am. Chem. Soc.*, **129**, 6187-6198 (2007).

79 H. Qi, W. Wang and C. Y. Li, Janus Polymer Single Crystal Nanosheet via Evaporative Crystallization, *ACS Macro Letters*, **3**, 675-678 (2014).

80 Y. Lin, M. R. Thomas, A. Gelmi, V. Leonardo, E. T. Pashuck, S. A. Maynard, Y. Wang and M. M. Stevens, Self-Assembled 2D Free-Standing Janus Nanosheets with Single-Layer Thickness, *J. Am. Chem. Soc*., **139**, 13592-13595 (2017).

81 Q. Wang, Yi. Liu, X. Qu, Q. Wang, F. Liang and Z. Yang, Janus Nanosheets by Emulsion Interfacial Crosslinking of Reactive Surfactants, *Colloid Polym. Sci.*, **293**, 2609-2615 (2015).

82 R. Deng, F. Liang, P. Zhou, C. Zhang, X. Qu, Q. Wang, J. Li, J. Zhu and Z. Yang, Janus Nanodisc of Diblock Copolymers, *Adv. Mater*., **26**, 4469-4472 (2014).

83 Y. Liu, X. Xu, F. Liang and Z. Yang, Polymeric Janus Nanosheets by Template RAFT Polymerization, *Macromolecules*, **50**, 9042-9047 (2017).

84 P. Zhou, Q. Wang, C.-L. Zhang, F.-X. Liang, X.-Z. Qu, J.-L. Li and Z.-Z. Yang,

pH responsive Janus polymeric nanosheets, *Chin. Chem. Lett.*, **26,** 657-661 (2015).

85 N. Nishi, I. Yajima, K. Amano and T. Sakka, Janus-Type Gold/Polythiophene Composites Formed via Redox Reaction at the Ionic Liquid Water Interface, *Langmuir*, **34**, 2441-2447 (2018).

86 T. Li, F. Liu, S. Zhang, H. Lin, J. Wang and C. Y. Tang, Janus Polyvinylidene Fluoride Membrane with Extremely Opposite Wetting Surfaces via One Single-Step Unidirectional Segregation Strategy, *ACS Appl. Mater. Interfaces*, **10**, 24947-24954 (2018).

87 A. Walther, M. Drechsler, A. H. E. Muller, Structures of Amphiphilic Janus Discs in Aqueous Media. *Soft Matter*, **5**, 385-390 (2009).

88 F. Liang, K. Shen, X. Qu, C. Zhang, Q. Wang, J. Li, J. Liu and Z. Yang, Inorganic Janus Nanosheets, *Angew. Chem. Int. Ed.*, **50**, 2379 -2382 (2011).

89 Y. Chen, F. Liang, H. Yang, C. Zhang, Q. Wang, X. Qu, J. Li, Y. Cai, D. Qiu and Z. Yang, Janus Nanosheets of Polymer-Inorganic Layered Composites, *Macromolecules*, **45**, 1460-1467 (2012).

90 Y. Liu, F. Liang, Q. Wang, X. Qu and Z. Yang, Flexible Responsive Janus Nanosheets, *Chem. Commun.*, **51**, 3562-3565, (2015).

91 T. Yin, Z. Yang, M. Lin, J. Zhang and Z. Dong, Preparation of Janus Nanosheets via Reusable Cross-linked Polymer Microspheres Template, *Chem. Eng. J.*, **371**, 507-515 (2019).

92 D. Xue, X. Song and F. Liang, Ultrathin Janus Nanodiscs, *RCS Adv.*, **7**, 25450-

25454 (2017).

93 (a) H. Yang, F. Liang, X. Wang, Y. Chen, C. Zhang, Q. Wang, X. Qu, J. Li, D. Wu and Z. Yang, Responsive Janus Composite Nanosheets, *Macromolecules*, **46**, 2754-2759 (2013). (b) Z. Zhao, F. Liang, G. Zhang, X. Ji, Q. Wang, X. Qu, X. Song and Z. Yang, Dually Responsive Janus Composite Nanosheets, *Macromolecules*, **48**, 3598-3603 (2015).

94 Z. Cao, G. Wang, Y. Chen, F. Liang and Z. Yang, Light-Triggered Responsive Janus Composite Nanosheets, *Macromolecules*, **48**, 7256-7261 (2015).

95 X. Xu, Y. Liu, Y. Gao and H. Li, Preparation of Au@silica Janus Nanosheets and their Catalytic Application, *Colloid Surface A*, **529**, 613-620 (2017).

96 S. Yan, H. Zou, S. Chen, N. Xue and H. Yang, Janus Mesoporous Silica Nanosheets with Perpendicular Mesochannels: Affording Highly Accessible Reaction Interfaces for Enhanced Biphasic Catalysis. *Chem. Commun.*, **54**, 10455-10458 (2018).

97 X. Ji, Q. Zhang, F. Liang, Q. Chen, X. Qu, C. Zhang, Q. Wang, J. Li, X. Song and Z. Yang, Ionic Liquid Functionalized Janus nanosheets, *Chem. Commun*., **50**, 5706-5709, (2014).

98 Q. B. Meng, P. Yang, T. Feng, X. Ji, Q. Zhang, D. Liu, S. Wu, F. Liang, Z. Zheng and X. Song, Phosphomolybdic Acid-responsive Pickering Emulsions Stabilized by Ionic Liquid Functionalized Janus nanosheets, *J. Colloid Interface Sci.*, **507**, 74-82(2017).

99 X. Ji, Q. Zhang, X. Qu, Q. Wang, X. Song, F. Liang and Z. Yang, Poly (ionic liquid) Janus Nanosheets towards Dye Degradation, *RSC Adv*., **5**, 21877-21880 (2015).

100 T. Yin, Z. Yang, Z. Dong, M. Lin and J. Zhang, Physicochemical Properties and Potential Applications of Silica-based Amphiphilic Janus Nanosheets for Enhanced Oil Recovery, *Fuel*, **237**, 344-351 (2019).

101 D. Xue, Q. B. Meng and X. Song, Magnetic-Responsive Janus Nanosheets with Catalytic Properties, *ACS Appl. Mater. Interfaces*, **11**, 10967-10974 (2019).

102 P. Wang, J. Liu, X. Chen, X. Ma, D. Guo, Z. Li and J. Pan, Janus Silica Nanosheets-based MMIPs Platform for Synergetic Selective Capture and Fast Separation of 2'-deoxyadenosine: Two Different Components Segmented on the Surface of One Object, *Chem. Eng. J.*, **369**, 793-802 (2019).

103 Y. Liu, Q. Wang, X. Qu, F. Liang and Z. Yang, Amine/acid Composite Janus Nanosheets, *Sci. China Mater.*, **58**, 126-131 (2015).

104 T. Yin, Z. Yang, M. Lin, J. Zhang and Z. Dong, Aggregation Kinetics and Colloidal Stability of Amphiphilic Janus Nanosheets in Aqueous Solution, *Ind. Eng. Chem. Res.*, **58**, 4479-4486 (2019).

105 M. Pumera, Z. Soferb and A. Ambrosia, Layered Transition Metal Dichalcogenides for Electrochemical Energy Generation and Storage, *J. Mater. Chem. A,* **2**, 8981-8987 (2014).

106 K. S. Novoselov, A. K. Geim, S. V. Morozov, D. Jiang, Y. Zhang, S. V. Dubonos,

I. V. Grigorieva and A. A. Firsov, Electric Field Effect in Atomically Thin Carbon Films, *Science*, **306(5696)**, 666-669 (2004).

107 M. F. Brigatti, E. Galán, and B. K. G. Theng, Chapter 2 - Structure and Mineralogy of Clay Minerals, *Developments in Clay Science*, **5**, 21-81 (2013).

108 R. Li, Y. Cheng and W. Huang, Recent Progress of Janus 2D Transition Metal Chalcogenides: From Theory to Experiments, *Small*, **14**, 1802091 (2018).

109 L. Zhang, J. Yu, M. Yang, Q. Xie1, H. Peng and Z. Liu, Janus Graphene from Asymmetric Two-dimensional Chemistry, *Nature Commun.*, 2464, (2013).

110 M. Stçter, S. Gçdrich, P. Feicht, S. Rosenfeldt, H. Thurn, J. W. Neubauer, M. Seuss, P. Lindner, H. Kalo, M. Mçller, A. Fery, S. Fçrster, G. Papastavrou and J. Breu, Controlled Exfoliation of Layered Silicate Heterostructures into Bilayers and Their Conversion into Giant Janus Platelets, *Angew. Chem. Int. Ed.*, **55**, 7398 -7402 (2016).

111 J. Liu, G. Liu, M. Zhang, P. Sun and H. Zhao, Synthesis and Self-Assembly of Amphiphilic Janus Laponite Disks, *Macromolecules*, **46**, 5974-5984 (2013).

112 Y. C. Cheng, Z. Y. Zhu, M. Tahir and U. Schwingenschlögl, Spin-orbit-induced Spin Splittings in Polar Transition Metal Dichalcogenide Monolayers, *Europhys. Lett.*, **102**, 57001 (2013).

113 J. Zhang, S. Jia, K. Iskandar, L. Dong, D. Er, W. Chen, H. Guo, Z. Jin, V. B. Shenoy, L. Shi and J. Lou, Janus Monolayer Transition-Metal Dichalcogenides, *ACS Nano*, **11(8)**, 8192-8198 (2017).

114 C. Yu, X. Cheng, C. Wang and Z. Wang, Tuning the n-type Contact of Graphene on Janus MoSSe Monolayer by Strain and Electric Field, *Physica E: Low-dimens. Syst. Nanostruct.*, **110**, 148-152 (2019).

115 M. Ren, M. Li, M. Yuan, P. Li and X. Chen, Two-dimensional InSeF Heterostructure: A Tunable Direct/indirect Band Gap, Semiconductor with Nontrivially Topological Properties, *Physica E: Low-dimens. Syst. Nanostruct.*, **106**, 73-77 (2019).

116 W. Shi, K. Fan and Z. Wang, Catalytic Activity for the Hydrogen Evolution Reaction of Edges in Janus Monolayer MoXY (X/Y = S, Se, and Te), *Phys. Chem. Chem. Phys.*, **20**, 29423-29429 (2018).

117 L. Hu and D. Wei, Janus Group-III Chalcogenide Monolayers and Derivative Type-II Heterojunctions as Water-Splitting Photocatalysts with Strong Visible-Light Absorbance, *J. Phys. Chem. C*, **122**, 27795-27802 (2018).

118 A. Huang, W. Shi and Z. Wang, Optical Properties and Photocatalytic Applications of Two-Dimensional Janus Group-III Monochalcogenides, *J. Phys. Chem. C*, **123**, 11388-11396 (2019).

119 W. Shi, G. Li and Z. Wang, Triggering Catalytic Active Sites for Hydrogen Evolution Reaction by Intrinsic Defects in Janus Monolayer MoSSe, *J. Phys. Chem. C*, **123**, 12261-12267 (2019).

120 D. Chen, H. Feng and J. Li, Graphene Oxide: Preparation, Functionalization, and Electrochemical Applications, *Chem. Rev*., **112(11)**, 6027-6053 (2012).

121 Y. Xu, H. Cao, Y. Xue, B. Li and W. Cai, Liquid-Phase Exfoliation of Graphene: An Overview on Exfoliation Media, Techniques, and Challenges, *Nanomaterials*, **8**, 942 (2018).

122 J. Zhou, Q. Wang, Q. Sun, X. S. Chen, Y. Kawazoe and P. Jena, Ferromagnetism in Semihydrogenated Graphene Sheet. *Nano Lett*., **9(11)**, 3867-3870 (2009).

123 Q. Peng, A. K. Dearden, J. Crean, L. Han, S. Liu, X. Wen and S. De, New Materials Graphyne, Graphdiyne, Graphone, and Graphane: Review of Properties, Synthesis, and Application in Nanotechnology, *Nanotechnol. Sci. Appl.*, **7**, 1-29 (2014).

124 J. Zhou and Q. Sun, How to Fabricate a Semihydrogenated Graphene Sheet? A Promising Strategy Explored., *Appl Phys Lett.*, **101**, 073114 (2012).

125 B. T. McGrail, J. D. Mangadlao, B. J. Rodier, J. Swisher, R. Advincula and E. Pentzer, Selective Mono-facial Modification of Graphene Oxide Nanosheets in Suspension, *Chem. Commun.*, **52**, 288-291 (2015).

126 H. Wu, W. Yi, Z. Chen, H. Wang and Q. Du, Janus Graphene Oxide Nanosheets Prepared *via* Pickering Emulsion Template, *Carbon*, **93**, 473-483 (2015).

127 A. C. de Leon, B. J. Rodier, Q. Luo, C. M. Hemmingsen, P. Wei, K. Abbasi, R. Advincula and E. B. Pentzer, Distinct Chemical and Physical Properties of Janus Nanosheets, *ACS Nano*, **11**, 7485-7493 (2017).

128 Y. Yang, L. Zhang, X. Ji, L. Zhang, H. Wang, H. Zhao, Preparation of Janus Graphene Oxide (GO) Nanosheets Based on Electrostatic Assembly of GO

Nanosheets and Polystyrene Microspheres, *Macromol. Rapid Commun*., **37**, 1520-1526 (2016).

129 D. Luo, F. Wang, B. V. Vu, J. Chen, J. Bao, D. Cai, R. C. Willson and Z. Ren, Synthesis of Graphene-based Amphiphilic Janus Nanosheets *via* Manipulation of Hydrogen bonding, *Carbon*, **126**, 105-110 (2018).

130 A. Holm, J. Park, E. D. Goodman, J. Zhang, R. Sinclair, M. Cargnello and C. W. Frank, Synthesis, Characterization, and Light-Induced Spatial Charge Separation in Janus Graphene Oxide, *Chem. Mater*., **30**, 2084-2092 (2018).

131 K. Yuan, Y. Li, X. Huang, Y. Liang, Q. Liu and G. Jiang, Templated Synthesis of a Bifunctional Janus Graphene for Enhanced Enrichment of both Organic and Inorganic Targets, *Chem. Commun*., **55**, 4957-4960 (2019).

132 V. Bekiari, A. Karakassides, S. Georgitsopoulou, A. Kouloumpis, D. Gournis and V. Georgakilas, Self-assembly of One-side-functionalized Graphene Nanosheets in Bilayered Superstructures for Drug Delivery, *J. Mater. Sci.*, **53**, 11167-11175 (2018).

133 D. Luo, F. Wang, J. Zhu, F. Cao, Y. Liu, X. Li, R. C. Willson, Z. Yang, C. Chu and Z. Ren, Nanofluid of Graphene-based Amphiphilic Janus Nanosheets for Tertiary or Enhanced Oil Recovery: High Performance at Low Concentration, *Proc. Natl. Acad. Sci. USA*, **113(28)**, 7711-7716 (2016).

134 D. Luo, F. Wang, J. Zhu, L. Tang, Z. Zhu, J. Bao, R. C. Willson, Z. Yang and Z. Ren, Secondary Oil Recovery Using Graphene-Based Amphiphilic Janus

Nanosheet Fluid at an Ultralow Concentration, *Ind. Eng. Chem. Res.*, **56**, 11125-11132 (2017).

135 D. Luo, F. Wang, J. Chen, F. Zhang, L. Yu, D. Wang, R. C. Willson, Z. Yang and Z. Ren, Poly(sodium 4-styrenesulfonate) Stabilized Janus Nanosheets in Brine with Retained Amphiphilicity, *Langmuir*, **34**, 3694-3700 (2018).

136 D. Luo, F. Wang, M. K. Alam, F. Yu, I. K. Mishra, J. Bao, R. C. Willson and Z. Ren, Colloidal Stability of Graphene-Based Amphiphilic Janus Nanosheet Fluid, *Chem. Mater*., **29**, 3454-3460 (2017).

137 D. Luo, F. Zhang, H. Zheng, Z. Ren, L. Jiang and Z. Ren, Electrostatic-attraction-induced High Internal Phase Emulsion for Large-scale Synthesis of Amphiphilic Janus Nanosheets, *Chem. Commun*., **55**, 1318-1321 (2019).

138 F. Li and Y. Li, Band Gap Modulation of Janus Graphene Nanosheets by Interlayer Hydrogen Bonding and the External Electric Field: a Computational Study, *J. Mater. Chem. C*, **3**, 3416-3421 (2015).

139 W. L. Ijdo and T. J. Pinnavaia, Staging of Organic and Inorganic Gallery Cations in Layered Silicate Heterostructures, *J. Solid State Chem.*, **139(2)**, 281-289 (1998).

140 M. W. Möller, D. Hirsemann, F. Haarmann, J. Senker and J. Breu, Facile Scalable Synthesis of Rectorites, *Chem. Mater.*, **22(1)**, 186-196 (2010).

141 M. Stöter, B. Biersack, N. Reimer, M. Herling, N. Stock, R. Schobert and J. Breu, Ordered Heterostructures of Two Strictly Alternating Types of Nanoreactors, *Chem. Mater*., **26(18)**, 5412-5419, (2014)

142 T. Nicolai and S. Cocard, Light Scattering Study of the Dispersion of Laponite, *Langmuir*, **16**, 8189-8193 (2000).

143 R. Boissezon, J. Muller, V. Beaugeard, S. Monge and J. J. Robin, Organophosphonates as Anchoring Agents onto Metal Oxide-based Materials: Synthesis and Applications, *RSC Adv.*, **4**, 35690-35707 (2014).

144 C. M. Sevrain, M. Berchel, H. Couthon and P. A. Jaffrès, Phosphonic Acid: Preparation and Applications, *Beilstein J. Org. Chem*., **13**, 2186-2213 (2017).

Chapter 2

Preparation of $K_4Nb_6O_{17}\cdot 3H_2O$-based Janus Nanosheets bearing Stable Bonds with Two Organophosphonic Acids by Regioselective Interlayer Surface Modification

Ryoko Suzuki, Mitsuhito Sudo, Megumi Hirano, Naokazu Idota, Masashi Kunitake, Taisei Nishimi and Yoshiyuki Sugahara, Inorganic Janus nanosheets bearing two types of covalently bound organophosphonate groups *via* regioselective surface modification of $K_4Nb_6O_{17}\cdot 3H_2O$, *Chem. Commun.*, 2018, **54**, 5756-5759 - Reproduced by permission of The Royal Society of Chemistry

Available from: DOI : 10.5772/intechopen.84228

2.1 Introduction

Janus nanosheets exhibit the highest anisotropy among Janus compounds with various shapes[1-9] and have been expected to be applied as emulsifiers.[10] Inorganic Janus nanosheets are attracting particular attention because the swelling and deformation observed in inorganic Janus nanosheets in organic solvents seldom occur.[11-18] Earlier reports raised issues concerning the preparation of inorganic Janus nanosheets, as described in Chapter 1.[12-18] Inorganic Janus nanosheets, which have no limitation on the choice of functional groups and have stable bonds between the nanosheets surface and surface modifier, are desirable for their possible uses in various solvents, including water.

Layered hexaniobate ($K_4Nb_6O_{17}\cdot 3H_2O$) has two types of interlayers, denoted interlayer I and interlayer II, that are stacked alternately and exhibit different reactivities.[19-20] Compounds in which only interlayer I is modified are called A-type, and compounds in which both interlayers I and II are modified are called B-type. Kimura *et al*. achieved selective interlayer surface modification of $K_4Nb_6O_{17}\cdot 3H_2O$, and obtained A-type and B-type phenylphosphonic acid derivatives of $K_4Nb_6O_{17}\cdot 3H_2O$.[21]

In this chapter, the preparation of Janus nanosheets is achieved by taking advantage of the presence of two types of interlayers with different reactivities in $K_4Nb_6O_{17}\cdot 3H_2O$. Interlayer II of an A-type organophosphonic acid derivative of $K_4Nb_6O_{17}\cdot 3H_2O$ was reacted with another type of organophosphonic acid. Both

sides of niobate nanosheets were modified by two organophosphonic acids regioselectively, because organophosphonic acid could not undergo an exchange reaction with immobilized organophosphonate moieties and homocondensation.[22] Janus nanosheets could be obtained by exfoliation of the product into single-layered nanosheets in an appropriate solvent, THF. Lipophilic octadecylphosphonic acid (ODPA) and hydrophilic carboxypropylphosphonic acid (CPPA) were chosen as the organophosphonic acid modifiers (Scheme 2.1). The properties of both sides of Janus nanosheets were explored by the AFM phase imaging technique.

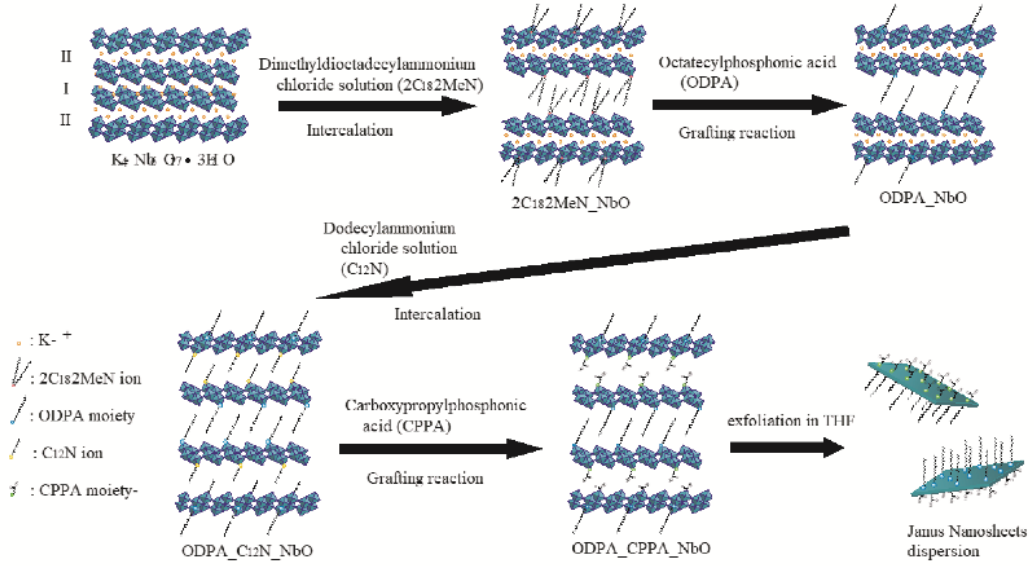

Scheme 2.1 Scheme 1 Preparation of Janus nanosheet.

2.2 Experimental Section

2.2.1Materials.

K_2CO_3 (Tokyo Kasei Co.) and Nb_2O_5 (Wako Pure Chemical Ind. Co.) were used

for preparation of $K_4Nb_6O_{17}\cdot 3H_2O$. Dimethyldioctadecylammonium chloride (Tokyo Kasei Ind.) and dodecylammonium chloride (Tokyo Kasei Ind.) were used as guest species for preparation of intermediates for surface modification. Octadecylphosphonic acid (ODPA) synthesized according to the method in the literature,[23-24] and (3-carboxypropyl)phosphonic acid (CPPA, Wako Pure Chemical Ind.) were used for surface modification. Tetrahydrofuran (THF, Wako Pure Chemical Ind.), 2-butanone, (Kanto Chemical) and hydrochloric acid (Kanto Chemical) were used for surface modification. Only 2-butanone was dehydrated using a molecular sieve 4A before use. All other reagents were used as received without further purification.

2.2.2 Experimental Procedures

2.2.2.1. Preparation of $K_4Nb_6O_{17}\cdot 3H_2O$

$K_4Nb_6O_{17}\cdot 3H_2O$ was prepared by calcination of a mixture of K_2CO_3 (2.83 g, 2.05 $\times 10^{-2}$ mol) and Nb_2O_5 (7.43 g, 2.80 $\times 10^{-2}$ mol) at 1100°C for 10 hours without intermittent grinding. The product was washed with water and dried in air.

2.2.2.2 Preparation of ODPA_NbO

$K_4Nb_6O_{17}\cdot 3H_2O$ (2.60 g, 2.50 $\times 10^{-3}$ mol) and dimethyldioctadecylammonium chloride (5.87g, 1.00 $\times 10^{-2}$ mol) ($K_4Nb_6O_{17}\cdot 3H_2O$ to dimethyldioctadecylammonium chloride molar ratio of 1 : 4) were reacted in water (200 mL) at 50°C for 7 days to expand interlayer I. Fifty mg of the product (3.60 ×

10^{-5} mol) was reacted with ODPA (0.048 g, 1.44×10^{-4} mol) (Nb_6O_{17} to ODPA molar ratio of 1 : 4) in 2-butanone (20 mL) at 150°C for 7 days. The crude product, ODPA_NbO, was washed with THF and hydrochloric acid (pH = 3) and dried in air.

2.2.2.3 Preparation of ODPA_CPPA_NbO

ODPA_NbO (0.10 g, 8.57×10^{-5} mol) and dodecylammonium chloride (0.19 g, 8.57×10^{-4} mol) (Nb_6O_{17} to dodecylamine hydrochloride molar ratio of 1 : 10) were reacted in water (10 mL) at 80°C for 3 days to expand interlayer II(ODPA_C_{12}N_NbO). Subsequently, ODPA_C_{12}N_NbO (50 mg, 2.97×10^{-5} mol) was reacted with CPPA (50 mg, 2.97×10^{-4} mol) (Nb_6O_{17} to dodecylammonium chloride molar ratio of 1 : 10) in 2-butanone (10 mL) at 80ºC for 3 days. The crude product was centrifuged and washed with THF twice, hydrochloric acid (pH = 3) twice and THF sequentially. The precipitate remaining after the last washing with THF was identified as ODPA_CPPA_NbO. The supernatant obtained during washing with THF was collected and dried on a glass substrate and called ODPA_CPPA_NbO_evaporation.

2.2.3 Analyses

Solid-state ^{31}P magic angle spinning (MAS) NMR spectra were recorded on a JEOL JNM-ECX400 spectrometer. The measurement conditions were as follows: resonance frequency: 160.26 MHz; pulse angle: 90º; pulse delay: 30 seconds; and MAS frequency: 12 kHz. Triphenylphosphine (-8.4 ppm) was used as a reference.

Solid-state ^{13}C cross polarization (CP)/MAS NMR spectra were recorded on a JEOL JNM-ECX-400 spectrometer. The measurement conditions were as follows: resonance frequency: 99.55 MHz; pulse delay: 5 seconds; contact time: 1.5 m seconds; and MAS frequency: 12 kHz. Hexamethylbenzene (17.4 ppm) was used as a reference. Infrared (IR) adsorption spectra were recorded on a JASCO FT/IR-460 Plus spectrometer by the KBr disk method. Inductively coupled plasma emission spectrometry was performed with a Thermo Jarrell Ash ICAP-574 II instrument by the internal standard method after dissolution of the sample in a mixture of 4 mL of HNO_3, 3 mL of HCl, and 1 mL of HF at 150ºC overnight. The carbon, hydrogen, and nitrogen contents were determined by elemental analysis using a Perkin Elmer PE2400 II instrument. X-ray diffraction (XRD) patterns were recorded on a Rigaku RINT-1000 diffractometer (Mn-filtered FeKα radiation). and a Rigaku SmartLab diffractmeter with Mn-filtered FeKα radiation by the parallel-beam method. Transmission electron microscope (TEM) images were obtained using a JEM-1011 microscope operating at 100 kV. For the electron diffraction (ED) analysis, the incident electron beam was perpendicular to the lateral plane of the nanosheets. A TEM sample was prepared by dropping drops of a dispersion on a Cu 150P grid and drying under reduced pressure. Atomic force microscope (AFM) images were observed with an Agilent 5500 AFM/SPM microscope in the acoustic AC mode under ambient conditions. An ordinary commercial silicon cantilever was used as an AFM tip (e.g., a RTESP-300 from Bruker: resonance frequency ≈ 300 kHz, and

spring constant ≈ 40 N/m). Samples for AFM were prepared by spin-coating of the dispersion on a Si wafer.

2.3 Results and discussion

Figure 2.1 shows ^{13}C CP/MAS NMR spectra of the products. In the spectrum of ODPA_NbO (Figure 2.1a), signals assignable to the octadecyl group were observed. It is likely that the ODPA moiety was introduced into interlayer I, since dioctadecyldimethylammonium ions, whose presence was required for interlayer modification with organophosphonic acids,[21] were present only in interlayer I. In the spectrum of ODPA_C_{12}N_NbO (Figure 2.1b), signals assignable to alkyl chains (octadecyl and dodecyl) were observed at 15-43 ppm.[21] In addition, a signal assignable to a carbon atom adjacent to a nitrogen atom was observed at 43 ppm,[25] indicating the presence of $C_{12}N^+$. Since $C_{12}N^+$ is known to be intercalated into both interlayer I and interlayer II,[19] the intercalation of $C_{12}N^+$ into interlayer II was likely to occur. In the spectrum of ODPA_CPPA_NbO (Figure 2.1c), signals due to alkyl chains were observed at 15-36 ppm. On the other hand, a signal originating from $C_{12}N^+$ at 43 ppm disappeared and a signal due to C=O groups of CPPA was observed at 178 ppm.[26] These results suggest the removal of $C_{12}N^+$ and introduction of the CPPA moiety to ODPA_CPPA_NbO.

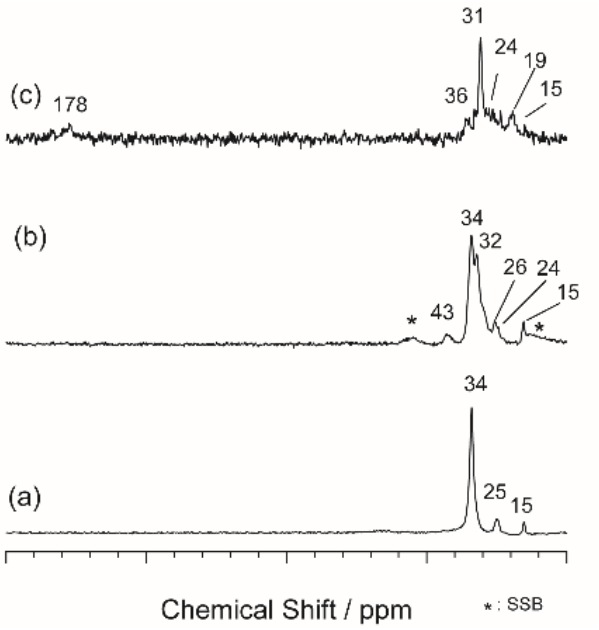

Figure 2.1 ^{13}C CP/MAS NMR spectra of (a) ODPA_NbO, (b) ODPA_C_{12}N_NbO and (c) ODPA_CPPA_NbO.

Figure 2.2 shows IR spectra of the products. In the spectrum of ODPA_NbO (Figure 2.2a), absorption bands due to ν (C-H), δ_s (CH_2) and ν (P-O) modes were observed at 2956 - 2849 cm^{-1}, 1468 cm^{-1} and 1011 cm^{-1}, respectively,[27] the indicating that ODPA moiety was present in ODPA_NbO. In the spectrum of ODPA_C_{12}N_NbO (Figure 2.2b), an adsorption band at 1540 cm^{-1} assignable to the δ (N-H) mode was observed in addition to the aforementioned adsorption band, indicating that octadecylammonium ions were present in ODPA_C_{12}N_NbO. In the spectrum of ODPA_CPPA_NbO (Figure 2.2c), a new adsorption band which was assignable to the δ (C=O) mode of the CPPA moiety was observed at 1700 cm^{-1},[28]

indicating the presence of the CPPA moiety in ODPA_CPPA_NbO. It was reported that an adsorption band due to the ν_{as} (CH_2) of alkyl chain was shifted from 2924.7 cm^{-1} to a lower wavenumber by increasing the packing density of the alkyl chain.[29] In the case of the *all-trans* octadecyl alkyl chain, ν_{as} (CH_2) was observed at 2917.8 cm^{-1}, [29-30] and a δ_s (CH_2) band was observed at 1468 cm^{-1}.[30] In the spectrum of ODPA_NbO, adsorption bands assignable to ν_{as} (CH_2) and ν_s (CH_2) modes were observed at 2918 cm^{-1} and 2848 cm^{-1}, respectively, and a δ_s (CH_2) adsorption band was observed at 1468 cm^{-1}. Thus, the alkyl chain in ODPA_NbO was likely to be in an *all-trans* conformation. On the other hand, ν_{as} (CH_2), ν_s (CH_2) and δ_s (CH_2) adsorption bands were observed at 2923 cm^{-1}, 2852 cm^{-1} and 1456 cm^{-1} in the spectrum of ODPA_CPPA_NbO, respectively, indicating that the alkyl chain in ODPA_CPPA_NbO was likely to contain *gauche-blocks*.

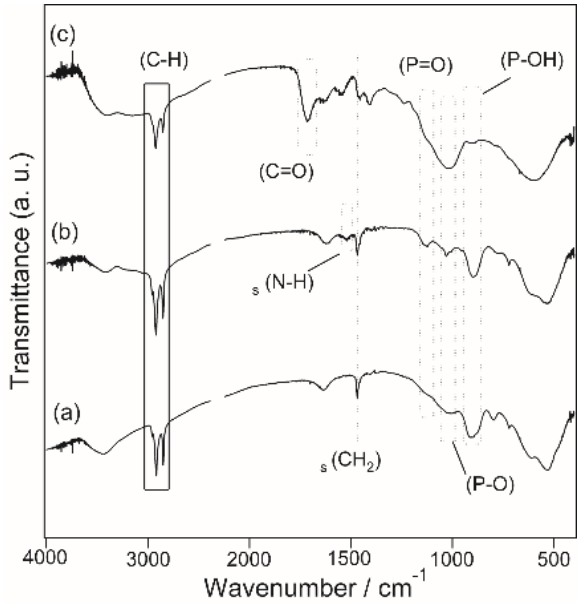

Figure 2.2 IR spectra of (a) ODPA_NbO, (b) ODPA_C12N_NbO and (c) ODPA_CPPA_NbO.

Phosphorous-31 MAS NMR measurements could provide important information on the environments of phosphonate groups immobilized on metal oxide surfaces, because the ^{31}P chemical shifts are affected by the electronegativity values of the second neighbor atoms of ^{31}P atoms and the O-P-O bond angles.[31-32] It was possible to discuss the ^{31}P chemical shift of phosphate species on metal oxides using density functional theory calculations,[33] but only shifts of ^{31}P atoms (normally upfield) upon immobilization on metal oxides such as TiO_2 powders[34-35] and ZrO_2 nanoparticles[36] were reported for organophosphonic acids. Figure 2.3 shows ^{31}P MAS NMR spectra of the products. A signal was observed at 28 ppm in the spectrum of ODPA_NbO (Figure 2.3a). This signal shifted upfield from the chemical shift of the ODPA molecule (33 ppm at ^{31}P MAS NMR) by 5 ppm,

indicating that interlayer surface modification by ODPA had proceeded and an Nb-O-P bond had been formed.[37] In the spectrum of ODPA_C_{12}N_NbO (Figure 2.3b), a signal was observed at 25 ppm. This signal was shifted upfield from 28 ppm, the chemical shift of ODPA_NbO, by 3 ppm. This shift suggests that $C_{12}N^+$ would change the electronic environment around the P atom by an ion exchange reaction with H^+ of the P-OH group,[37] although the details were not yet clarified. Thus, it is likely that $C_{12}N^+$ was intercalated not only in interlayer II, but probably also in interlayer I upon the reaction with ODPA_NbO. In the spectrum of ODPA_CPPA_NbO (Figure 2.3c), a new signal was observed at 31 ppm in addition to the signal at 28 ppm. The signal at 28 ppm was observed in the same position as that of the ODPA moiety of ODPA_NbO, confirming maintenance of the ODPA moiety at interlayer I. Because a signal of a CPPA molecule was observed at 34 ppm,

a signal at 31 ppm was assignable to the CPPA moiety. This signal shifted upfield by 3 ppm, indicating that the CPPA moiety was grafted onto the interlayer surface and a Nb-O-P bond was formed. The above results suggested that both ODPA and CPPA formed Nb-O-P bonds with the $[Nb_6O_{17}]^{4-}$ sheet surface. Since bands assignable to P-OH groups and P=O groups were observed in the IR spectrum of ODPA_CPPA_NbO, ODPA and CPPA were likely to be in a monodentate

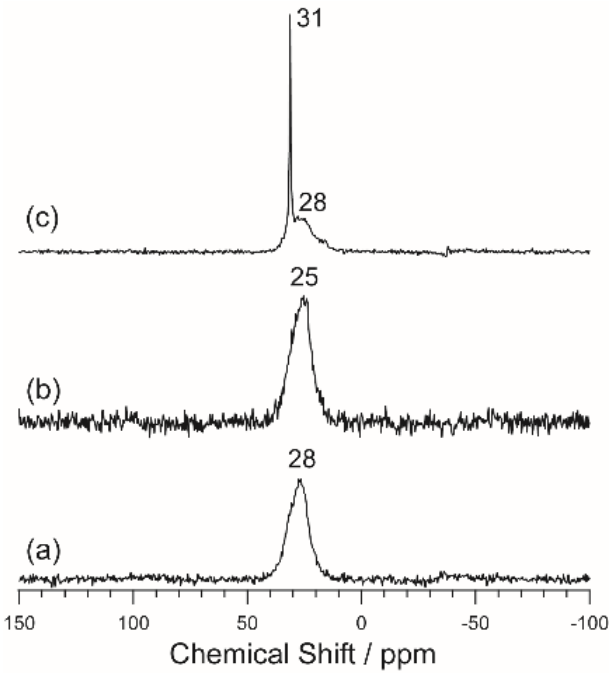

environment on the surface of $[Nb_6O_{17}]^{4-}$.

Figure 2.3 31P MAS NMR spectra of (a) OPDA_NbO, (b) ODPA_C12N_NbO and (c) ODPA_CPPA_NbO.

Table 2.1 shows the molar ratio calculated from the ICP measurement and elemental analysis. The molar ratio of ODPA_NbO was P : Nb = 1.3 : 6.0. On the

other hand, the molar ratios of ODPA_C_{12}N_NbO and ODPA_CPPA_NbO were P : Nb = 1.3 : 6.0 and P : Nb = 3.5 : 6.0, respectively. Intercalation of $C_{12}N^+$ proceeded without release of the ODPA moiety in ODPA_NbO, because the molar ratio of P and Nb of ODPA_NbO did not change after reaction with a dodecylammonium chloride solution. Also, the molar ratio of P to 6 Nb in ODPA_CPPA_NbO increased by 2.2 (3.5 - 1.3), confirming grafting of the CPPA moiety. Assuming Nb = 6.0, the maximum modification amounts for interlayer I and II are 2.0.[21] Since the Nb-O-P bond was stable with respect to hydrolysis and no homocondensation between two P-OH groups of phosphonic acid occurred under mild conditions,[38] the amount of the ODPA moiety in interlayer I was estimated to be 1.3 (65% of the maximum modification amount), that of the CPPA moiety at interlayer I was in the range of 0.2-0.7 (10-35% of maximum modification amount) and that of the CPPA moiety in interlayer II was in the range of 1.5-2.0 (75-100% of the maximum modification amount). Thus, an organic derivative with interlayer I and interlayer II dominantly modified with lipophilic ODPA and hydrophilic CPPA, respectively, were successfully prepared. (Scheme 2.2)

Table 2.1 Molar ratios of Nb, K, P and N in ODPA_NbO, ODPA_C_{12}N_NbO and ODPA_CPPA_NbO

	Nb / -	K / -	P / -	N / -
ODPA_NbO	6.0	2.6	1.3	0.082
ODPA_C_{12}N_NbO	6.0	0.58	1.3	1.8

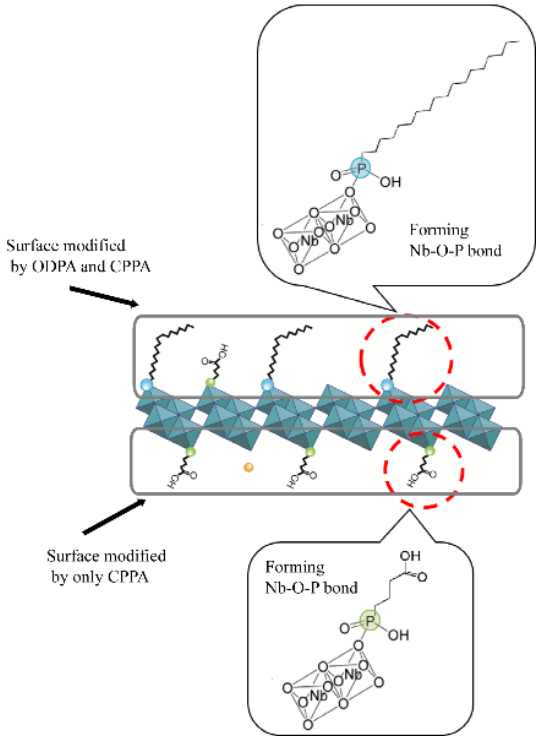

ODPA_CPPA_NbO	6.0	0.49	3.5	-

Scheme 2.2 Proposed structure of ODPA_CPPA_NbO.

Based on the nitrogen ratio of ODPA_NbO, it seems that a small amount of unreacted A-type alkylammonium intercalation compound was present in ODPA_NbO or a small number of released $2C_{18}2MeN$ ions were present in interlayer I *via* ion exchange. Since the amount of K^+ in interlayer II in ODPA_C_{12}N_NbO decreased, an ion exchange reaction between K^+ and H^+ ions proceeded at interlayer II and $C_{12}N^+$. Because no nitrogen was detected in ODPA_CPPA_NbO, $C_{12}N^+$ was completely removed from interlayer I and II after the reaction with CPPA.

A THF dispersion of nanosheets was easily attained by dispersing ODPA_CPPA_NbO in THF. The resulting dispersion was cast on a TEM grid and TEM observation was carried out (Figure 2.4). A sheet-like morphology with low contrast was observed. Spots observed in the electron diffraction (ED) pattern can be assigned to 200, 202 and 002 of the orthorhombic cells and the lattice parameters were calculated to be a = 0.80 nm and c = 0.64 nm. This ED pattern was thus a b-axis incidence pattern of $K_4Nb_6O_{17}\cdot 3H_2O$.[39] Based on these results, ODPA_CPPA_NbO was synthesized while maintaining the crystal structure of the $[Nb_6O_{17}]^{4-}$ nanosheets.

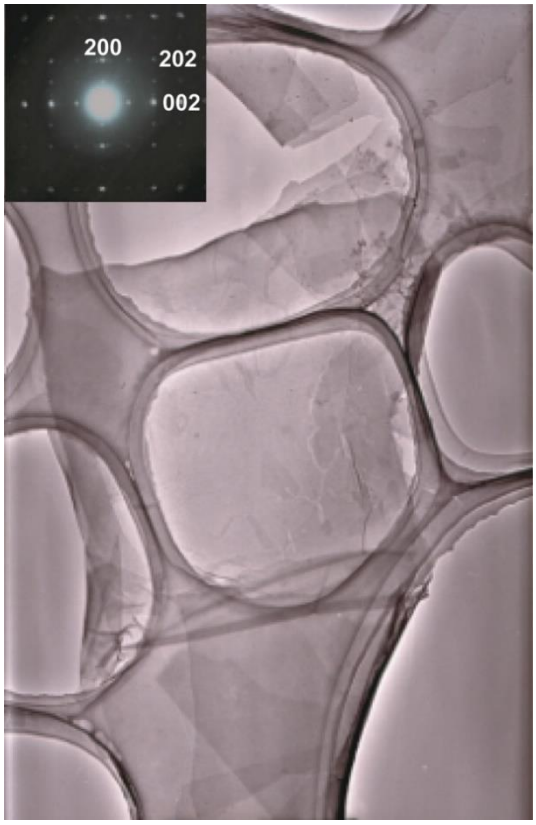

Figure 2.4 TEM image of exfoliated ODPA_CPPA_NbO. The inset shows the corresponding ED pattern.

Figure 2.5 shows XRD patterns of the products. The *d* values of low-angle diffractions due to repeating distances were as follows; the *d* value of ODPA_NbO, A-type derivative (Figure 2.5a), was 5.67 nm and the *d* value of ODPA_C_{12}N_NbO (Figure 2.5b) was 4.03 nm. If intercalation of $C_{12}N^+$ into interlayer II proceeded while maintaining an A-type stacking sequence, the *d* value of ODPA_C_{12}N_NbO is likely to have increased from that of ODPA_NbO. It is possible that a B-type stacking sequence was generated due to exfoliation and restacking during the reaction, resulting in a smaller repeating distance. Also, the *d* values of ODPA_CPPA_NbO (Figure 2.5c) and

ODPA_CPPA_NbO_evaporation (Figure 2.5d) were 2.41 nm and 4.74 nm, respectively. The stacking sequence would therefore be changed by reaction between ODPA_C_{12}N_NbO and CPPA.

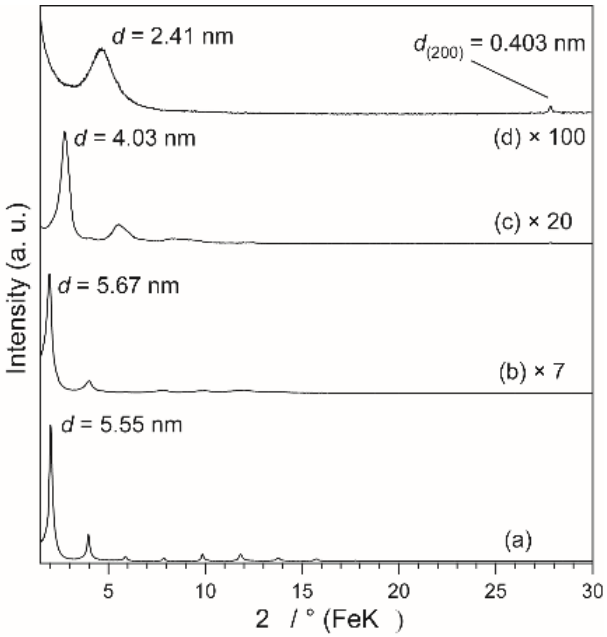

Figure 2.5 XRD patterns of (a) ODPA_NbO, (b) ODPA_C12N_NbO, (c) ODPA_CPPA_NbO and (d) ODPA_CPPA_NbO_evaporation.

Here, the difference between these two *d* values is discussed. If ODPA_CPPA_NbO is a B-type derivative, the thickness of an organic moiety layer (sum of an ODPA monolayer and a CPPA monolayer) can be calculated by subtracting 0.82 nm, the niobate layer thickness, from 2.41 nm to make 1.59 nm.[21] The repeating distance of an A-type derivative could thus be estimated as the sum of a double niobate layer thickness and a double organic layer thickness. The repeating distance of an A-type derivative can

therefore be estimated as follows: (1.59 nm × 2) + (0.82 nm × 2) = 4.82 nm. This value is approximately equal to d = 4.74 nm of ODPA_CPPA_NbO_evaporation. From these estimations, it is proposed that ODPA_CPPA_NbO is a B-type derivative and ODPA_CPPA_NbO_evaporation is an A-type derivative. As shown in Scheme 2.3, a B-type derivative could be generated by forced restacking *via* centrifugation of exfoliated nanosheets (Scheme 2.3 a, b). On the other hand, an A-type derivative, in which hydrophilic groups faced each other and lipophilic groups faced each other, was obtained by slow evaporation under mild conditions (Scheme 2.3 c).

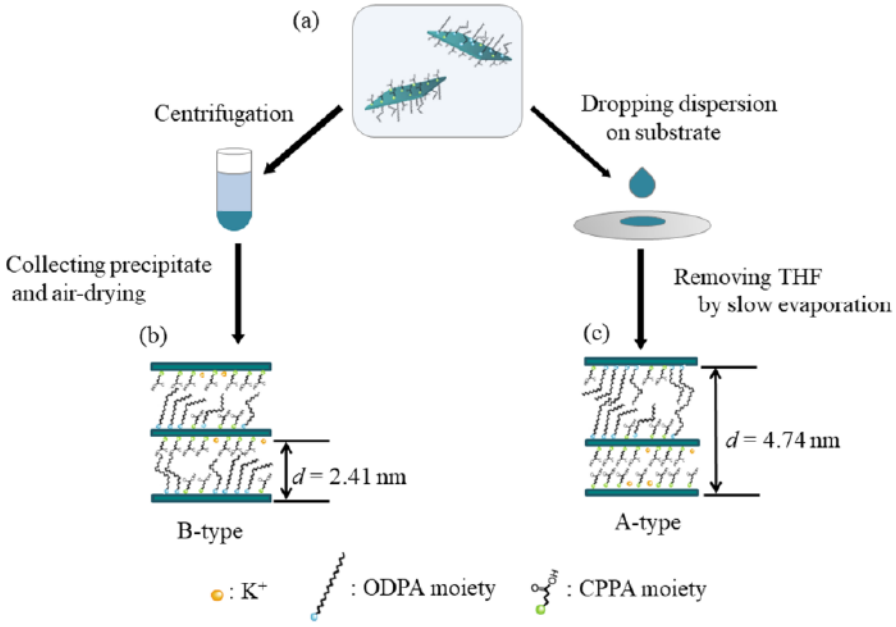

Scheme 3 The estimated structures of ODPA_CPPA_NbO : possible routes from (a) ODPA_C_{12}N_NbO to (b) ODPA_CPPA_NbO and (c) ODPA_CPPA_NbO_evaporation.

The crystallite sizes calculated from diffraction of the repeating distances using Scherrer's formula were 3.67 nm and 7.71 nm for ODPA_CPPA_NbO and

ODPA_CPPA_NbO_evaporation, respectively. The crystallite size of ODPA_CPPA_NbO_evaporation was larger than that of ODPA_CPPA_NbO. It should be noted that underestimation could occur with use of lowest-angle diffractions due to the presence of strain.[40] The crystallite sizes could therefore reflect the average thickness of the particles in the stacking direction, making the number of stacked ODPA_CPPA_NbO nanosheets lower than that of stacked ODPA_CPPA_NbO_evaporation nanosheets. On the other hand, the estimated crystallite size could be interpreted as average thickness of a portion of the stacked sheets with an A-type or B-type stacking sequence. Based on this interpretation, ODPA_CPPA_NbO formed via forced restacking by centrifugation has lower stacking regularity or more random stacking than ODPA_CPPA_NbO_evaporation nanosheets restacked under mild conditions.

Figure 2.6 shows an AFM images of a sample prepared by spin-coating of a THF dispersion of ODPA_CPPA_NbO on a Si wafer. In a topo image (Figure 2.6A), many sheet-like shapes were observed and the height profile from The topo image indicates that the sheet thicknesses were mostly in the range of 2.5-3.0 nm (Figure 2.6A'), which is consistent with the *d* value of ODPA_CPPA_NbO with the B-type stacking sequence (2.41 nm), indicating that nanosheets exfoliated to single layers were successfully cast on the Si substrate. In a previous report, A Janus structure with two chemically different surfaces was confirmed visually using phase AFM imaging, which is frequently used for local mapping of chemical properties.[41] Although there was no distinction between the surfaces of the sheets in the topographic images, the simultaneously recorded phase

images (Figure 2.6B) clearly visualized the existence of two different surfaces of Janus nanosheets as “yellow-green” (16-19 degrees) and “yellow-red” (19-21 degrees) colored terraces in contrast to “purple” color (22-23 degrees) of the substrate. Considered based on the color with the highest degree of surface hydrophilic silicone oxide, the “yellow-red” and “yellow-green” coloring sides might be attributed to hydrophilic surfaces bearing carboxylic groups and lipophilic surfaces bearing alkyl chain groups, respectively. This phase difference in the AFM phase image corresponds to the tapping phase gap in the vibration amplitude, and it was reported that the phase difference could occur with a difference in the crystallinity, viscosity and adhesion of the sample surface.[42-43]

The Janus nanosheets consisted of a lipophilic surface which was dominantly covered with the ODPA moiety and a hydrophilic surface which was modified with the CPPA moiety. As a result, two chemically different surfaces gave different phases due to differences in the interactions between the apex of the AFM probe and the surfaces of the nanosheets and distinguished visually in the phase image. The origin of the phase contrast would be due to differences in viscosity and hydrophilicity / lipophilicity. Since the apex of the AFM probe used in this measurement was hydrophilic, it is likely that the high-phase surface and a low-phase surface were assignable to the hydrophilic CPPA moiety and lipophilic ODPA moiety, respectively.

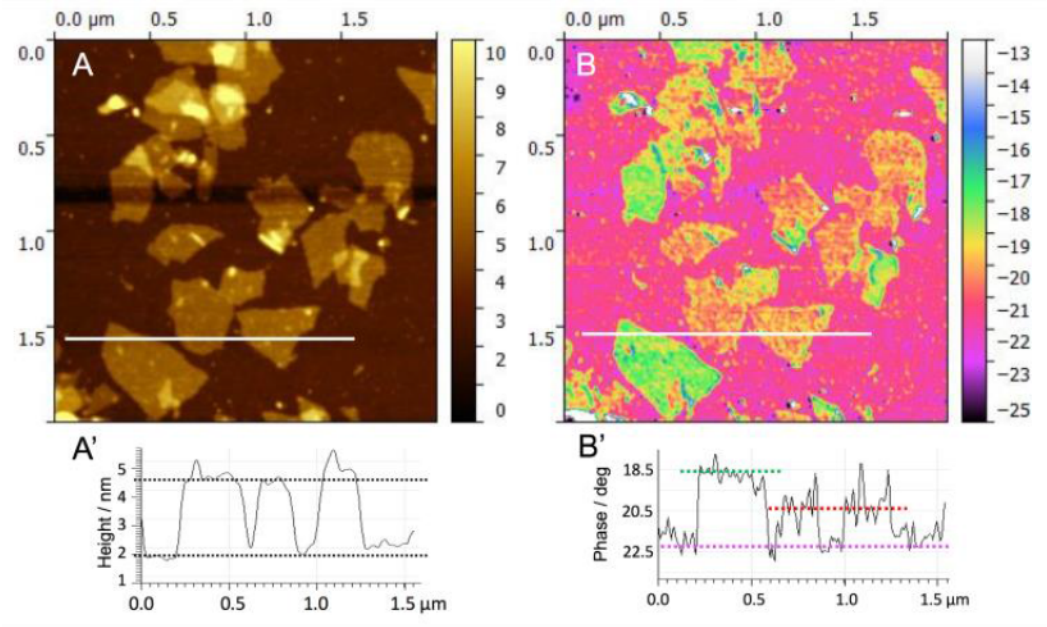

Figure 2.6 Simultaneously recorded topographic (A) and phase (B) atomic force microscopy (AFM) images of the Janus nanosheets on a silicon wafer, and the corresponding cross sections (A' and B') at the line marked by the white lines in the images.

Partially overlapping moieties of the nanosheets formed during the drying process in the sample preparation were frequently observed, as shown in Figure 2.7. From the difference in the height of the terrace of the sheets (Figure 2.7A) and the difference in the color of the phase image (Figure 2.7B), it is possible to determine the overlapping state consisting of three nanosheets, as shown in Figure 2.7C. The differences in the colors (phases) of the top surfaces clearly indicate that the same surfaces of the sheets were facing each other in the stack. Although it could be possible to interpret as showing the topographic image (Figure 2.7A), two small sheets were placed on a single large sheet, an interpretation based on a comparison between the topographic and phase images

elucidates that two nanosheets (a and c) are partially overlapping on the nanosheet (b). The solid and dotted closed lines in Figure 2.7B indicate the boundaries of the upper nanosheets (a and c) and the lower nanosheet (b), respectively. This hydrophilic "face to face" arrangement was generally observed as an overlapping arrangement, probably due to an attractive interaction.

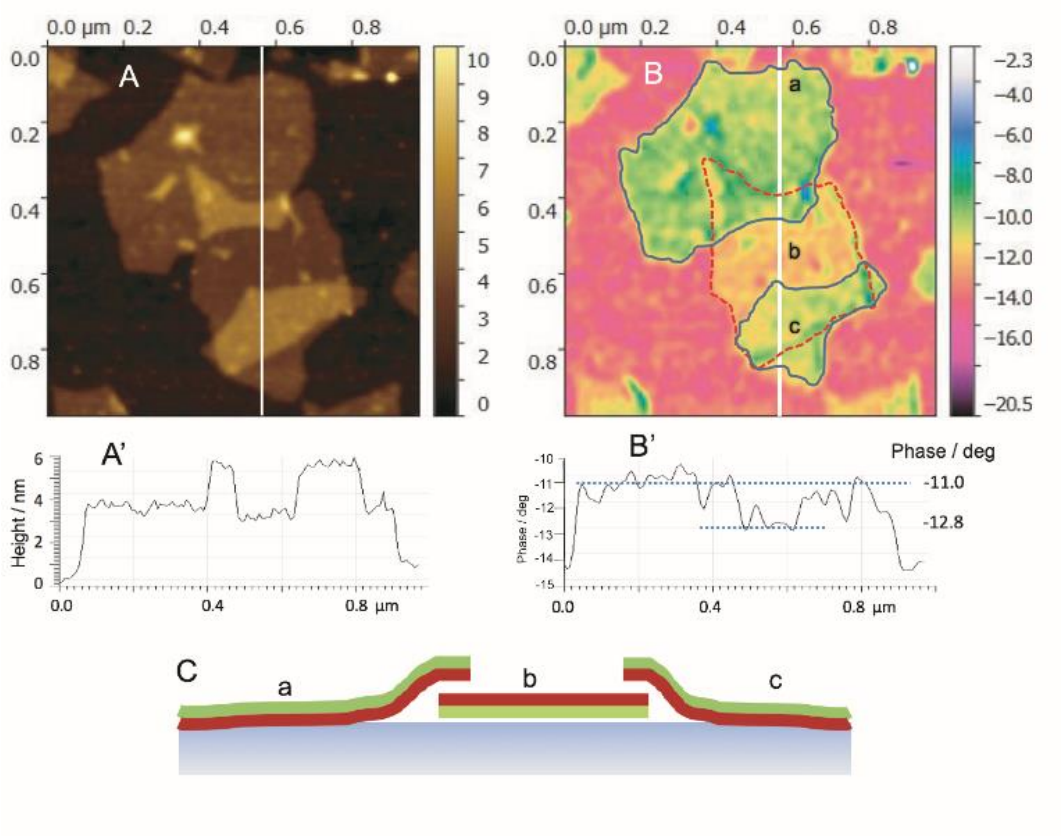

Figure 2.7 Simultaneously recorded topographic (A) and phase (B) atomic force microscopy (AFM) images of the Janus nanosheets on a silicon wafer, and the corresponding cross sections (A' and B') at the line marked by the white lines in the images and the schematic representation of partially overlapped Janus nanosheets (C). The solid and dotted closed lines in b indicate the boundaries of upper nanosheets (a and b) and a lower nanosheet, respectively.

2.4 Conclusions

Janus nanosheets were successfully prepared by regioselective and sequential surface modification and exfoliation of $K_4Nb_6O_{17}\cdot 3H_2O$, whose interlayer I and interlayer II were dominantly modified by ODPA and CPPA, respectively. Since organophosphonic acids bearing various functional groups can be easily synthesized, Janus nanosheet surfaces can exhibit various properties in addition to lipophilicity and hydrophilicity. The Janus nanosheets prepared by the present method can be dispersed in many solvents, moreover, because organophosphonic moieties are bound to niobate nanosheets by stable Nb-O-P bonds. The Janus nanosheets prepared in this chapter can be expected to be applied in surface chemistry research because of the lipophilicity and hydrophilicity on opposing sides of the nanosheets. Also, by changing the functional groups of organophosphonic acids, novel two-dimensional materials with various functions with potential applications in various fields can be realized.

References

1 P. G. de Gennes, Soft Matter (Nobel Lecture), *Angew. Chem. Int. Ed*., **31(7)**, 842-845 (1992).

2 T. Nishisako, T. Torii, T. Takahashi and Y. Takizawa, Synthesis of Monodisperse Bicolored Janus Particles with Electrical Anisotropy Using a Microfluidic Co-Flow System, *Adv. Mater*., **18**, 1152-1156 (2006).

3 B. P. Binks and P. D. I. Fletcher, Particles Adsorbed at the Oil-Water Interface: A

Theoretical Comparison between Spheres of Uniform Wettability and “Janus” Particles, *Langmuir*,**17**, 4708-4710 (2001).

4 M. Kim, S. A. Anthony and S. Granick, Activated Surface Diffusion in a Simple Colloid System, *Phys. Rev. Lett*., **102**, 178303 (2009).

5 A. Walther and A. H. E. Muller, Janus Particles: Synthesis, Self-Assembly, Physical Properties, and Applications, *Chem. Rev*., **113**, 5194-5261 (2013).

6 M. Lattuada and T. A. Hatton, Synthesis, Properties and Applications of Janus Nanoparticles, *Nano Today*, **6**, 286-308 (2011).

7 S. Jiang, Q. Chen, M. Tripathy, E. Luijten, K. S. Schweizer and S. Granick, Janus Particle Synthesis and Assembly, *Adv. Mater*., **22**, 1060-1071 (2010).

8 R. Erhardt, M. Zhang, A. Boker, H. Zettl, C. Abetz, P. Frederik, G. Krausch, V. Abetz and A. H. E. Muller, Amphiphilic Janus Micelles with Polystyrene and Poly(methacrylic acid) Hemispheres, *J. Am. Chem. Soc*., **125**, 3260-3267 (2003).

9 H. Qi, W. Wang and C. Y. Li, Janus Polymer Single Crystal Nanosheet via Evaporative Crystallization, *ACS Macro Lett*., **3**, 675-678 (2014).

10 A. C. de Leon, B. J. Rodier, Q. Luo, C. M. Hemmingsen, P. Wei, K. Abbasi, R. Advincula and E. B. Pentzer, Distinct Chemical and Physical Properties of Janus Nanosheets, *ACS Nano.*, **11**, 7485-7493 (2017).

11 A. Walther, M. Drechsler and A. H. E. Muller, Structures of Amphiphilic Janus Discs in Aqueous Media, *Soft Matter*., **5**, 385-390 (2009).

12 F. Liang, K. Shen, X. Qu, C. Zhang, Q. Wang, J. Li, J. Liu and Z. Yang, Inorganic

Janus Nanosheets, *Angew. Chem. Int. Ed*., **50**, 2379-2382 (2011).

13 H. Yang, F. Liang, X. Wang, Y. Chen, C. Zhang, Q. Wang, X. Qu, J. Li, D. Wu and Z. Yang, Responsive Janus Composite Nanosheets, *Macromolecules*, **46**, 2754-2759 (2013).

14 Y. Liu, F. Liang, Q. Wang, X. Qu and Z. Yang, Flexible Responsive Janus Nanosheets, *Chem. Commun.*, **51**, 3562-3565 (2015).

15 L. Zhang, J. Yu, M. Yang, Q. Xie, H. Peng and Z. Liu, Janus Graphene from Asymmetric Two-Dimensional Chemistry, *Nature Commun*., **4**, 1443 (2013).

16 H. Wu, W. Yi, Z. Chen, H. Wang and Q. Du, Janus Graphene Oxide Nanosheets Prepared via Pickering Emulsion Template, *Carbon*, **93**, 473-483 (2015).

17 M. Stçter, S. Gçdrich, P. Feicht, S. Rosenfeldt, H. Thurn, J. W. Neubauer, M. Seuss, P. Lindner, H. Kalo, M. Mçller, A. Fery, S. Fçrster, G. Papastavrou and J. Breu, Controlled Exfoliation of Layered Silicate Heterostructures into Bilayers and Their Conversion into Giant Janus Platelets, *Angew. Chem. Int. Ed*., **55**, 7398-7402 (2016).

18 J. Liu, G. Liu, M. Zhang, P. Sun and H. Zhao, Synthesis and Self-Assembly of Amphiphilic Janus Laponite Disks, *Macromolecules*, **46(15)**, 5974-5984 (2013).

19 T. Nakato, K. Kuroda and C. Kato, Syntheses of Intercalation Compounds of Layered Niobates with Methylviologen and Their Photochemical Behavior, *Chem. Mater*., **4**, 128-132 (1992).

20 Q. Wei and T. Nakato, Competitive Adsorption of Phenols on Organically Modified Layered Hexaniobate $K_4Nb_6O_{17}$, *Microporous Mesoporous Mater*., **96**, 84-91 (2006).

21 N. Kimura, Y. Kato, R. Suzuki, A. Shimada, S. Tahara, T. Nakato, K. Matsukawa, P. H. Mutin and Y. Sugahara, Single- and Double-Layered Organically Modified Nanosheets by Selective Interlayer Grafting and Exfoliation of Layered Potassium Hexaniobate, *Langmuir*, **30**, 1169-1175 (2014).

22 G. Guerrero, J. G. Alauzun, M. Granier, D. Laurencin and P. H. Mutin, Phosphonate Coupling Molecules for the Control of Surface / Interface Properties and the Synthesis of Nanomaterials, *Dalton Trans.*, **42**, 12569-12585 (2013).

23 J. T. Woodward, A. Ulman and D. K. Schwartz, Self-Assembled Monolayer Growth of Octadecylphosphonic Acid on Mica, *Langmuir*, **12**, 3626-3629 (1996).

24 B. Y. Kim, E. L. Ratcliff, N. R. Armstrong, T. Kowalewski and J. Pyun, Ferrocene Functional Polymer Brushes on Indium Tin Oxide via Surface-Initiated Atom Transfer Radical Polymerization, *Langmuir*, **26**, 2083-2092 (2010).

25 M. R. Mello, D. Phanon, G. Q. Silveira, P. L. Llewellyn and C. M. Ronconi, Amine-modified MCM-41 Mesoporous Silica for Carbon Dioxide Capture, *Microporous Mesoporous Mater.*, **143**, 174-179 (2011).

26 S. Ghosh, W. Z. Yu, S. Kang, P. C. Bhowmik and B. S. Xing, Sorption and Fractionation of a Peat Derived Humic Acid by Kaolinite, Montmorillonite, and Goethite, *Pedosphere*, **19(1)**, 21-30 (2009).

27 H. F. Shurvell, Spectra-Structure Correlations in the Mid- and Far-Infrared, in *Handbook of Vibrational Spectroscopy. Vol. 3 Sample Characterization and Spectral Data Processing*, ed. J. M. Chalmers and P. R. Griffiths, John Wiley & Sons, Chichester,

1783-1816 (2002).

28 Y. Katsumoto, T. Tanaka, H. Sato and Y. Ozaki, Conformational Change of Poly(*N*-isopropylacrylamide) during the Coil-Globule Transition Investigated by Attenuated Total Reflection/Infrared Spectroscopy and Density Functional Theory Calculation, *J. Phys. Chem. A*, **106**, 3429-3435 (2002).

29 R. Quinones, K. Rodriguez and R. J. Iuliucci, Investigation of Phosphonic Acid Surface Modifications on Zinc Oxide Nanoparticles under Ambient Conditions, *Thin Solid Films*, **565**, 155-164 (2014).

30 R. A. Vaia, R. K. Teukolsky, E. P. Giannelis, Interlayer Structure and Molecular Environment of Alkylammonium Layered Silicates, *Chem. Mater*., **6**, 1017-1022 (1994).

31 W. Gao, L. Dickinson, C. Grozinger, F. G. Morin and L. Reven, Self-Assembled Monolayers of Alkylphosphonic Acids on Metal Oxides, *Langmuir*, **12**, 6429-6435 (1996).

32 F. B. Severac, G. Guerrero, J. Maquet, P. Florian, C. Gervais and P. H. Mutin, High-Field ^{17}O MAS NMR Investigation of Phosphonic Acid Monolayers on Titania, *Chem. Mater.*, **20**, 5191-5196 (2008).

33 F. Tielens, C. Gervais, G. Deroy, M. Jaber, L. Stievano, C. C. Diogo and J. F. Lambert, Characterization of Phosphate Species on Hydrated Anatase TiO_2 Surfaces, *Langmuir*, **32**, 997-1008 (2016).

34 P.Falaras, I. M. Arabatzis, T. Stergiopoulos, G. Papavassiliou and M. Karagianni, Modification of TiO_2 Semiconductor with Molecules bearing Functional Phosphonic

Groups: a ^{31}P Solid State NMR Study, *J. Mater. Process. Technol*., **161(1-2)**, 276-281 (2005).

35 P. H. Mutin, V. Lafond, A. F. Popa, M. Granier, L. Markey and A. Dereux, Selective Surface Modification of SiO_2-TiO_2 Supports with Phosphonic Acids, *Chem. Mater.*, **16**, 5670-5675 (2004).

36 S. Pawsey, K. Yach and L. Reven, Self-Assembly of Carboxyalkylphosphonic Acids on Metal Oxide Powders, *Langmuir*, 18, 5205-5212 (2002).

37 A. Shimada, Y. Yoneyama, S. Tahara, P. H. Mutin and Y. Sugahara, Interlayer Surface Modification of the Protonated Ion-Exchangeable Layered Perovskite $HLaNb_2O_7 \cdot xH_2O$ with Organophosphonic Acids, *Chem. Mater*., **21**, 4155-4162 (2009).

38 G. Guerrero, P. H. Mutin and A. Vioux, Anchoring of Phosphonate and Phosphinate Coupling Molecules on Titania Particles, *Chem. Mater*., **13**, 4367-4373 (2001).

39 K. Nassau, W. Shiever, J. L. Bernstein, Crystal Growth and Properties of Mica-Like Potassium Niobates, *J. Electrochem. Soc*., **116**, 348-353 (1969).

40 T. Sasaki and M. Watanabe, Osmotic Swelling to Exfoliation. Exceptionally High Degrees of Hydration of a Layered Titanate, *J. Am. Chem. Soc*., **120(19)**, 4682-4689 (1998).

41 K. Sakata, S. Kashiyama, G. Matsuo, S. Uemura, N. Kimizuka and M. Kunitake, Growth of Two‐Dimensional Metal-Organic Framework Nanosheet Crystals on Graphite Substrates by Thermal Equilibrium Treatment in Acetic Acid Vapor, *ChemNanoMat*, **1(4)**, 259-263 (2015).

42 D. Ricci and P. C. Braga, Imaging Methods in Atomic Force Microscopy, In *Atomic Force Microscopy Biomedical Methods and Applications*, ed. D. Ricci and P. C. Braga, Humana Press, New York City, 13-23 (2014).

43 S. N. Magonov and M. H. Whangbo, Phase Imaging and Stiffness in Tapping-Mode Atomic Force Microscopy, *Surface Sci*., **375**, L385-L391 (1997).

Chapter 3

Effect of Water-dispersible Janus Nanosheets Derived from $K_4Nb_6O_{17}\cdot 3H_2O$ on Air-Liquid and Liquid-Liquid interfaces

3.1 Introduction

Surfactants have hydrophilic (polar) and lipophilic (nonpolar) groups in the same molecule or molecular ion and perform various functions such as stabilizing emulsions and foams due to decreasing surface energy at the interface. [1-3] Surfactants are not limited to molecules and molecular ions. Polymers with specific structures can also act as surfactants. In particular, various polymeric surfactants, including block copolymers and grafted copolymers, were reported.[4] These polymeric surfactants have higher adsorption energy than those of molecular surfactants and were reported to stabilize emulsions.

Also, Janus particles bearing a hydrophilic surface on one side and a lipophilic surface on the other side can work as solid surfactants.[5] They are adsorbed at liquid-liquid interfaces more strongly than particles which have chemically isotropic surfaces and can stabilize emulsions.[6-8] When Janus nanoparticles are adsorbed at the water-oil interface, water and oil face directly at the interface where no particles are present, leading to facile mass transfer at the water-oil interface, a phenomenon which differs from that observed in the biphasic systems with surfactant molecules and ions which align minutely at the interface.[9]

Janus nanosheets, which exhibit the highest anisotropy among Janus materials, have high adsorption energies. Furthermore, their rotation at the liquid-liquid interface is generally restricted, while Janus nanoparticles rotate easily at the interface.[10] Inorganic Janus nanosheets have an advantage over polymer-based Janus

nanosheets, since organic Janus nanosheets can become swollen and deformed in organic solvents.[11] Actually, silica-based Janus nanosheets and graphene-based Janus nanosheets stabilize emulsions.[12-13] On the other hand, clay-based Janus nanosheets have limitations as dispersants due to their ionic bonds between the nanosheet surface and the midofiyer polymers.[14-15] The $K_4Nb_6O_{17}\cdot 3H_2O$-based Janus nanosheets described in Chapter 2 have stable bonds between the niobite nanosheet surface and surface modifiers. Therefore, $K_4Nb_6O_{17}\cdot 3H_2O$-based Janus nanosheets can be dispersed in water and can be applied as surfactants by adjusting the hydrophilicity and lipophilicity on both side of the nanosheets.

In this chapter, the preparation of $K_4Nb_6O_{17}\cdot 3H_2O$-based single-layered Janus nanosheets, which can be dispersed in water, is achieved using phenylphosphonic acid and phosphoric acid as surface modifiers for increasing their hydrophilicity compared to the nanosheets in Chapter 2. Their behavior at an air-water interface was investigated by dynamic surface tension measurement. Furthermore, an emulsion was prepared using an aqueous dispersion of the obtained Janus nanosheets and toluene, and their behavior at the liquid-liquid interface was investigated by continuous optical microscopic observation.

3.2 Experimental Section

3.2.1 Materials

K_2CO_3 (Tokyo Kasei Co.) and Nb_2O_5 (Wako Pure Chemical Ind. Co.) were used

for preparation of $K_4Nb_6O_{17}\cdot 3H_2O$. Dimethyldioctadecylammonium chloride (FUJIFILM Wako Pure Chemical Co.) and dodecylammonium chloride (Tokyo Kasei Ind.) were used for preparation of intermediates for surface modification. Phenylphosphononic acid (PPA) and phosphoric acid (PA) were used as surface modifiers for interlayer I and interlayer II, respectively. For surface modification, 2-butanone was used as a solvent for surface modification. Toluene and oil orange(Tokyo Kasei Ind.) was used for preparing the emulsion.

3.2.2 Experimental Procedures

3.2.2.1. Preparation of $K_4Nb_6O_{17}\cdot 3H_2O$

$K_4Nb_6O_{17}\cdot 3H_2O$ was prepared by calcination of a mixture of K_2CO_3 (2.83 g, 2.05 × 10^{-2} mol) and Nb_2O_5 (7.43 g, 2.80 × 10^{-2} mol) at 1100°C for 10 hours without intermittent grinding. The product was washed with water and dried in air.

3.2.2.2 Preparation of PPA_ NbO[16]

$K_4Nb_6O_{17}\cdot 3H_2O$ (2.60 g, 2.50 × 10^{-3} mol) and dimethyldioctadecylammonium chloride (5.87 g, 1.00 × 10^{-2} mol) ($K_4Nb_6O_{17}\cdot 3H_2O$ to dimethyldioctadecylammonium chloride molar ratio 1 : 4) were reacted in water (200 mL) at 50°C for 7 days to expand interlayer I. The intermediate was centrifuged, washed with water and dried in air. Next, the product (1.0 g, 1.4× 10^{-3} mol) and PPA (0.90 g, 5.7 × 10^{-3} mol) (Nb_6O_{17} to PPA molar ratio 1 : 4) were added

to 2-butanone (40 mL) and reacted at 80°C for 1 day to modify the surface of interlayer I. This reaction was repeated four times. The product was washed twice with hydrochloric acid (pH = 3) and three times with acetone. Then the product was air-dried (PPA_NbO).

3.2.2.3 Preparation of PPA_PA_NbO

PPA_NbO (0.1 g, 1.0×10^{-4} mol) and dodecylammonium chloride (0.23 g, 1.0×10^{-3} mol) (Nb_6O_{17} to dodecylammonium chloride molar ratio 1 : 10) were reacted in water (20 mL) at 80°C for 3 days to expand of interlayer II as described in Chapter 2. The intermediate was centrifuged and washed with water three times and dried in air. The intermediate (0.2 g, 1.4×10^{-4} mol) and PA (0.056 g, 5.7×10^{-4} mol) (Nb_6O_{17} to PA molar ratio 1 : 4) were reacted in 2-butanone (40 mL) at 50°C for 1 day under an N_2 atmosphere. This reaction was repeated four times. Finally, the product was washed with acetone three times and dried in air (PPA_PA_NbO).

3.2.2.4 Preparation of PPA_PA_NbO dispersion

PPA_PA_NbO (100 mg) was dispersed in water (100 mL), stirred overnight and ultrasonicated for exfoliation. Ultrasonication was carried out for 2 hours (with a 2-s interval for every 2-s irradiation) in an ice bath using a BRANSON Advanced Digital Sonifier. The obtained dispersion was then centrifuged at 4500 rpm for 15 minutes and the supernatant was collected (PPA_PA_NS dispersion).

4.2.3 Analyses

X-ray diffraction (XRD) patterns were recorded on a Rigaku RINT-1000 diffractometer (Mn-filtered Fe Kα radiation). Solid-state ^{31}P NMR spectra were obtained with a magic angle spinning (MAS) technique only (pulse delay, 30 s; spinning rate, 12 kHz) using a JEOL JNM-ECX 400 spectrometer at 160.26 MHz. Triphenylphosphine (-8.4 ppm) was used as an external standard for ^{31}P NMR. Inductively coupled plasma emission spectrometry was performed with a Thermo Jarrell Ash ICAP-574 II instrument by the internal standard method after dissolution of the sample in a mixture of 4 mL of HNO_3, 3 mL of HCl, and 1 mL of HF at 150ºC overnight. Atomic force microscope (AFM) images were obtained with a Digital Instruments Nanoscope III using the tapping mode. The surface tension was measured by the Wilhelmy plate method using a Kyowa DY-300 instrument. Image analysis of the emulsions was carried out using Image J (Wayne Rasband (NIH)) and the sphericity was calculated as $4\pi \times$ (area of sphere) / (square of circumference).

3. 3 Results and discussions

Figure 3.1 shows an AFM image of PPA_PA_NS cast on an Si wafer. A sheet-like shape with a lateral dimension of about 1 μm was observed and the thickness of the sheet was 1.9 nm. From its XRD measurement (Figure 3.2), the *d* value

corresponding to the repeating distance was determined to be 3.62 nm. In Chapter 2, Janus nanosheets collected by centrifugation possessed an A-type stacking sequence, where two different interlayers appeared alternately in the stacking direction. Assuming that PPA_PA_NS collected by centrifugation was also an A-type derivative, the thickness of a single-layer nanosheet was estimated by halving the repeating distance: 3.62 nm ÷ 2 =1.81 nm, which is very similar to the thickness of a nanosheet observed from AFM, 1.9 nm. Based on these results, regioselective surface modification and exfoliation into single-layered nanosheets proceeded.

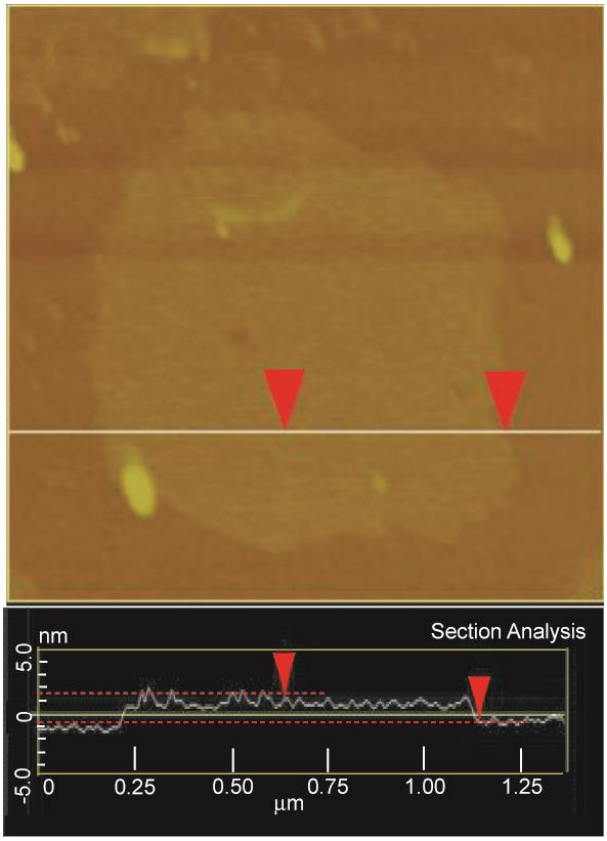

Figure 3.1 AFM image of PPA_PA_NS.

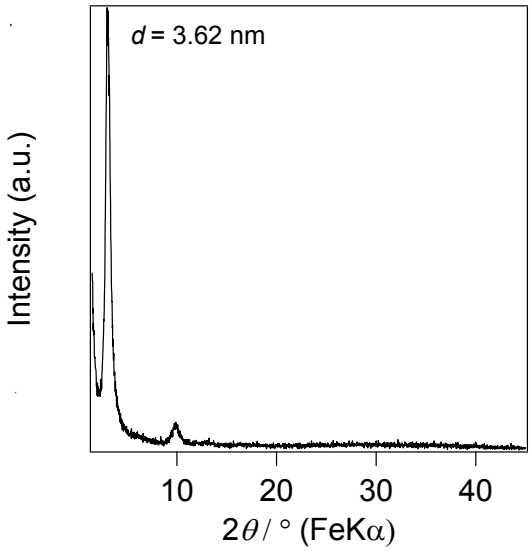

Figure 3.2 XRD pattern of PPA_PA_NbO.

Figure 3.3 shows ^{31}P MAS NMR spectra of the products. In the spectrum of PPA_NbO (Figure 3.3a), a signal assignable to a PPA−related species was observed. The signal was shifted upfield from that of the PPA molecule, 22 ppm, to 16 ppm, indicating formation of Nb-O-P bonds between the niobate nanosheet surface and PPA moiety.[16] In the spectrum of PPA_PA_NbO (Figure 3.3b), two signals were observed at 16 ppm and -4 ppm. The presence of the 16-ppm signal confirms that Nb-O-P bonds between the niobate nanosheets and PPA moiety were maintained. Also, the other signal was shifted upfield from that of the PA molecule, whose chemical shift was 0 ppm, to -4 ppm, indicating formation of Nb-O-P bonds between the niobate nanosheet surface and PA moiety.[16]

The amounts of the PPA moiety and PA moiety on both sides of the nanosheets

were calculated based on the ICP results. In PPA_C_{12}N_NbO, which was estimated to be an A-type derivative, the Nb : P molar ratio was calculated to be 6.0 : 1.9. Since the molar ratio for the maximum modification amount of interlayer I was Nb : P = 6.0 : 2.0,[16] 95% of interlayer I of PPA_C_{12}N_NbO was modified by PPA. Also, the molar ratio of Nb : P was calculated as 6.0 : 3.4 in PPA_PA_NbO, indicating that the relative molar ratio of P increased from PPA_C_{12}N_NbO by 1.5 (per 6 Nb). Since the maximum modification amounts of interlayer I and II were both Nb : P =6.0 : 2.0,[16] it is considered that the possible molar amounts of the modified PA moieties relative to 6 Nb were in the ranges of 0-0.1 (0 %-5 %) at interlayer I and 1.4-1.5 (70 %-75 %) at interlayer II. From these results, it is concluded that interlayer I was modified mainly with the PPA moiety while interlayer II was modified only with the PA moiety. It is therefore concluded that single-layered water-dispersible Janus nanosheets modified with PA moiety on one side and PA moiety on the other side of individual nanosheets were successfully prepared.

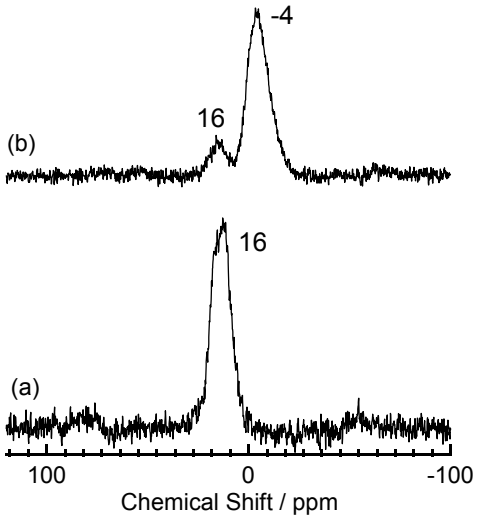

Figure 3.3 ^{31}P MAS NMR spectra of (a) PPA_NbO and (b) PPA_PA_NbO.

Figure 3.4 shows the results of dynamic surface tension measurements of water, a PPA aqueous solution (1 mg / L) and a PPA_PA_NS dispersion (1 mg / L). PPA (Figure 3.4b) did not decrease the surface tension effectively, and the surface tension curve was very similar to that of water (Figure 3.4a). It was considered that PPA was stably dissolved in water and the PPA molecules were not present at the air-liquid interface. On the other hand, the PPA_PA_NS dispersion (Figure 3.4c) affected the surface tension, which gradually decreased with time and became 59.5 mN/m after 20,000 s. Since PPA_PA_NS decreased the surface tension, it is concluded that PPA_PA_NS behaved as a solid surfactant. It is likely that PPA_PA_NS can be considered to be a two-dimensional assembly of PPA molecules, which does not show surface activity by itself, and that assembly of PPA and PA moieties on the nanosheet surfaces provided sufficient liphophilicity on one

side and lipophilicity on the other side of the individual nanosheet, leading to the fact that the obtained nanosheets exhibited surface activity. Furthermore, PPA_PA_NS required a far longer period of time to decrease surface tension than a low molecular surfactant, which normally needs several seconds to decrease surface tension.[17] β-Casein, a protein with a much larger molecular weight of about 24,000 as compared to those of standard surfactants, also required a long period time to decrease surface tension, probably because the proteins moved slowly to the air-liquid interface due to their large molecular weights.[18] Assuming that PPA_PA_NS was a square plate with a 1.0-μm lateral size based on its AFM image (Figure 3.1), the weight of PPA_PA_NS was calculated to be 7.0×10^{-15} g, which was heavier than those of one of typical molecular surfactants, hexaethylene glycol mono hexadecyl ether, and protein, whose weights were calculated at 8.4×10^{-22} g and 4.0×10^{-20} g, respectively,[17-18] and PPA_PA_NS should move more slowly than low molecular weight surfactants. Therefore, a longer period of time was required to decrease surface tension in the PPA_PA_NS dispersion.

On the other hand, the surface tension at 60 s after of the start of measurement was 64.6 mN/m, which was lower than that of water, as shown in Figure 3.4a; the PPA_PA_NS dispersion had already decreased surface tension at the start of measurement. It was considered that wide nanosheet size distribution of PPA_PA_NS, which was not controllable, could affect this decrease in surface tension; very small PPA_PA_NS could be rapidly adsorbed at the air-liquid

interface, and the surface tension could thus be decreased at the start of measurement.

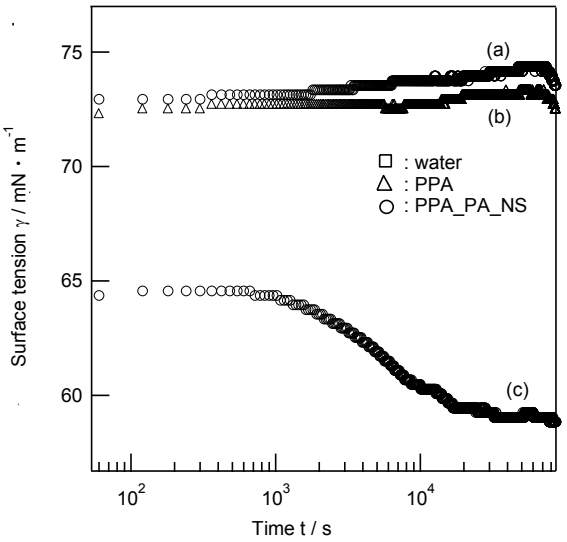

Figure 3.4 Dynamic surface tension of (a) water, (b) PPA and (c) PPA_PA_NS water dispersion.

Figure 3.5 shows optical microscopic images of the PPA_PA_NS dispersion/toluene emulsion at the time of the start of measurement, after 44 min and after 60 min. Toluene droplets colored by oil orange were observed, and the formation of an o/w emulsion was clearly demonstrated. The total number of oil droplets in Figure 3a, the image of the emulsion as prepared, was 114. On the other hand, after 60 min, the total number of oil droplets in the same frame (Figure 3c) decreased to 78. A closer look at the images suggests that coalescence and Ostwald ripening occurred. Oil droplets (i) and (ii) in Figure 3a coalesced and formed oil droplet (iii) with a non-spherical shape in Figure 3b. Furthermore, oil droplet (iii) in

Figure 3.5c maintained an ellipsoidal shape. The sphericity of the oil droplet in Figure 3b upon coalescence was 0.88 and that of the droplet in Figure 3.5c, 16 min after coalescence, was 0.91. Oil droplet (iii) maintained a non-spherical shape for 16 min and the shape changed from a non-spherical shape toward a true spherical shape over time. The non-spherical oil droplet was transitional during coalescence, and the oil droplet stabilized by the low molecular surfactant transformed immediately to a true spherical shape after coalescence.[19] It is likely that the slow movement of PPA_PA_NS, the assumed phenomenon observed in dynamic surface tension measurement, also affected the shape changing rate of coalesced oil droplets (Scheme 3.1a). Therefore, the transitional shapes of coalesced oil droplets could be observed in the emulsion for over 10 min.

On the other hand, the sizes of oil droplets (iv), (v) and (vi) were changed in Figure 3.5c from those in Figure 3.5a. In Figure 3.5a, the diameters of oil droplets (iv) and (v) were 4.7 and 3.1 μm, respectively. In Figure 3.5c, the diameters of oil droplets (iv) and (v) decreased to 2.8 and 2.3 μm, respectively. On the other hand, the diameter of large oil droplet (vi) near oil droplets (iv) and (v) increased slightly from 14.2 μm in Figure 3.5a to 14.3 μm in Figure 3.5c. This phenomena, a reduction in the diameters of the small droplets and an increase in the diameter of the large droplet, are likely due to Ostwald ripening. It is generally accepted that Ostwald ripening of emulsions stabilized with standard molecular and ionic surfactants proceeds slowly, with the theoretical ripening rate of emulsions calculated as

9.2×10^{-22} $m^3\cdot s^{-1}$.[20] The size change of the oil droplets in the present PPA_PA_NS dispersion/toluene emulsion, on the contrary, proceeded within 60 min based on optical microscopic observation, indicating that Ostwald ripening in the present system proceeded significantly faster than usual. It was reported that Ostwald repining of a Pickering emulsion stabilized by silica nanoparticles was faster than that stabilized by a low molecular-weight surfactant and that the ripening rate was about 10^{-18} $m^3\cdot s^{-1}$.[20] It was proposed that Ostwald ripening proceeded rapidly when oil molecules were dissolved from gaps between silica nanoparticles on small oil droplets to the aqueous phase, with subsequent molecular diffusion into larger oil droplets. In the emulsion stabilized by PPA_PA_NS, nanosheets cannot cover the oil droplet surface completely, and toluene molecules could be dissolved gaps between nanosheets with the ripening rate calculated at about 1.2×10^{-20} $m^3\cdot s^{-1}$, which is faster than that of molecular surfactants (Scheme 3.1b). Therefore, the Ostwald ripening process of oil droplets can be observed in a short period of time. The dynamic behavior and adsorption states of Janus nanosheets at the air-liquid interface and liquid-liquid interface were not estimated precisely, however, because the adsorption state has not been investigated.

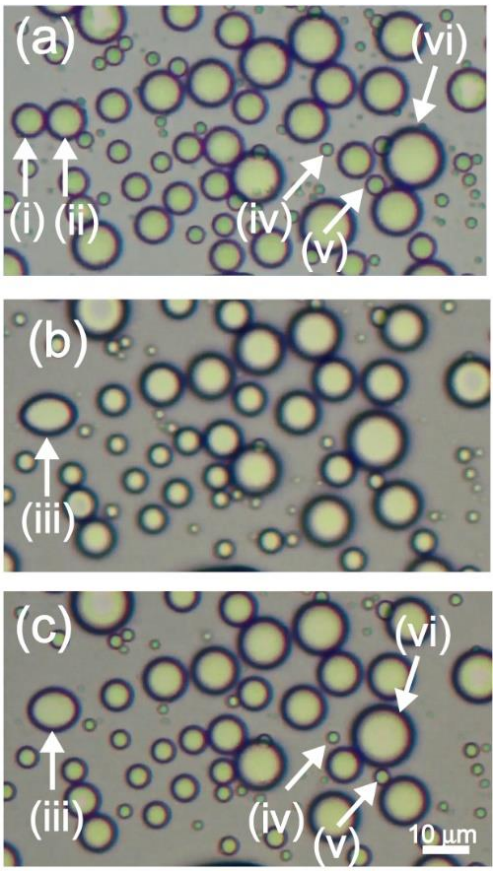

Figure 3.5 Optical microscope images of micelles of PPA_PA_NS water dispersion and toluene (a) at time of starting measurement (0 minute), after (b) 44 minutes and (c) 60 minutes.

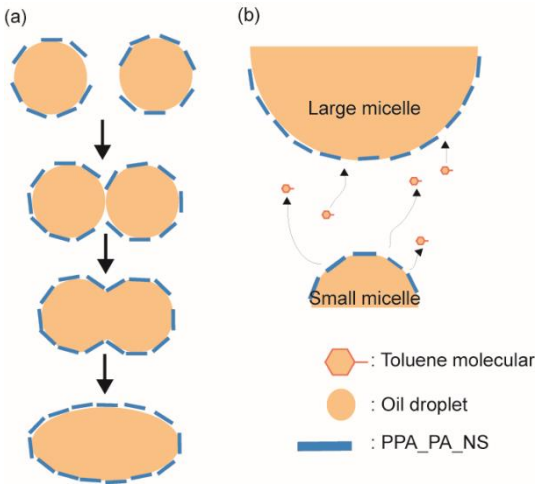

Scheme 3.1 (a) coalescence process and (b) Ostwald ripening images of micelles covered by PPA_PA_NS

3.4 Conclusions

Single-layered Janus nanosheets dispersible in water were successfully prepared by changing the surface modifiers from the ODPA and CPPA used in Chapter 2 to PPA and PA, since the hydrophilicities of PPA and PA are higher than those of the corresponding modifiers, ODPA and CPPA, respectively. Janus nanosheets decreased surface tension over a very long period of time, probably because of their extremely heavy weight in comparison with those of standard surfactants. In the emulsion prepared using a Janus nanosheets dispersion and toluene, dynamic changes in the oil droplets, an oil droplet with a transitional non-spherical shape upon coalescence and rapid Ostwald ripening were observed. The non-spherical shape was likely due to slow movement of the nanosheets, and the rapid Ostwald ripening was probably due to rapid dissolution of toluene from gaps between Janus nanosheets. These results clearly demonstrate that single-layered water-dispersible Janus nanosheets acted as two-dimensional surfactants. Further investigation of the behavior of Janus nanosheets on air-liquid surfaces and liquid-liquid surfaces will be required to improve their performances. This type of two-dimensional surfactant has the potential to form emulsions with various combinations by changing functional groups, moreover, and to adjusting dynamic surface tension

by changing the nanosheets size.

Reference

1 N. Kumar and A. Mandal, Surfactant Stabilized Oil-in-Water Nanoemulsion: Stability, Interfacial Tension, and Rheology Study for Enhanced Oil Recovery Application, *Energy Fuels*, **32(6)**, 6452-6466 (2018).

2 I. Kralova and J. Sjöblom, Surfactants Used in Food Industry: A Review, *J. Disper. Sci. Technol.*, **30**, 1363-1383 (2009).

3 R. J. Pugh, Foaming, Foam Films, Antifoaming and Defoaming, *Adv. Colloid Interface Sci.*, **64**, 67-142 (1996).

4 V. P. Torchilin, Structure and Design of Polymeric Surfactant-based Drug Delivery Systems, *J. Control. Release*, **73**, 137-172 (2001).

5 N. Glaser, D. J. Adams, A. Böker and G. Krausch, Janus Particles at Liquid-Liquid Interfaces, *Langmuir*, **22**(12), 5227-5229 (2006).

6 B. P. Binks, Colloidal Particles at Liquid Interfaces, *Phys. Chem. Chem. Phys*., **9**, 6298-6299 (2007).

7 B. P. Binks and P. D. I. Fletcher, Particles Adsorbed at the Oil-Water Interface: A Theoretical Comparison between Spheres of Uniform Wettability and "Janus" Particles, *Langmuir*, **17**, 4708-4710 (2001).

8 R. Aveyard, Can Janus Particles Give Thermodynamically Stable Pickering Emulsions? *Soft Matter*, **8**, 5233-5240 (2012).

9 J. Faria, M. P. Ruiz, and D. E. Resasco, Phase-Selective Catalysis in Emulsions Stabilized by Janus Silica Nanoparticles, *Adv. Synth. Catal*., **352**, 2359-2364 (2010).

10 (a)Y. Nonomura, S. Komura and K. Tsujii, Adsorption of Disk-shaped Janus Beads at Liquid-Liquid Interfaces, *Langmuir,* **20**, 11821-11823 (2004); (b) Y. Nonomura, S. Komura and K. Tsujii, *J. Phys. Chem. B*, **2006**, 110, 13124-13131.

11 A. Walther, X. Andr, M. Drechsler, V. Abetz and A. H. E. Müller, Janus Discs. *J. Am. Chem. Soc*., **129**, 6187-6198 (2007).

12 D. Xue, X. Song and F. Liang, Ultrathin Janus Nanodiscs, *RSC Adv.*, **7**, 25450-25454 (2017).

13 D. Luo, F. Zhang, H. Zheng, Z. Ren, L. Jiang and Z. Ren, Electrostatic-attraction-induced High Internal Phase Emulsion for Large-scale Synthesis of Amphiphilic Janus Nanosheets, *Chem. Commun.*, **55**, 1318-1321 (2019).

14 M. Stçter, S. Gçdrich, P. Feicht, S. Rosenfeldt, H. Thurn, J. W. Neubauer, M. Seuss, P. Lindner, H. Kalo, M. Mçller, A. Fery, S. Fçrster, G. Papastavrou and J. Breu, Controlled Exfoliation of Layered Silicate Heterostructures into Bilayers and Their Conversion into Giant Janus Platelets, *Angew. Chem. Int. Ed*., **55**, 7398 -7402 (2016).

15 J. Liu, G. Liu, M. Zhang, P. Sun and H. Zhao, Synthesis and Self-Assembly of Amphiphilic Janus Laponite Disks, *Macromolecules*, **46**(15), 5974-5984 (2013).

16 N. Kimura, Y. Kato, R. Suzuki, A. Shimada, S. Tahara, T. Nakato, K. Matsukawa, P. H. Mutin, Y. Sugahara, Single- and Double-Layered Organically Modified Nanosheets by Selective Interlayer Grafting and Exfoliation of Layered Potassium Hexaniobate, *Langmuir*, **30**(4),1169-1175 (2014).

17 B. V. Zhmud, F. Tiberg and J. Kizling, Dynamic Surface Tension in Concentrated Solutions of C_nE_m Surfactants : A Comparison between the Theory and Experiment, *Langmuir*, **16**, 2557-2565 (2000).

18 R. Miller, V. B. Fainerman, E. V. Aksenenko, M. E. Leser and M. Michel, Dynamic Surface Tension and Adsorption Kinetics of *β*-Casein at the Solution/Air Interface, *Langmuir*, **20**(3), 771-777 (2004).

19 I. B. Ivanov and P. A. Kralchevsky, Stability of Emulsions under Equilibrium and Dynamic Conditions, *Colloids Surf. A,* **128**(1-3), 155-175 (1997).

20 J. A. Juárez and C. P. Whitby, Oil-in-water Pickering Emulsion Destabilisation at Low Particle Concentrations, *J. Colloid Interface Sci.*, **368**(1), 319-325 (2012).

Chapter 4

Preparation of $K_4Nb_6O_{17}\cdot 3H_2O$-based Dual-functional Janus Nanosheets with Thermo-responsiveness and a Cation Adsorption Capability

Ryoko Suzuki, Naokazu Idota, Taisei Nishimi and Yoshiyuki Sugahara,

Dual-functional Janus nanosheets with cation exchangeability and thermo-responsiveness prepared via regioselective modification of $K_4Nb_6O_{17}\cdot 3H_2O$, *Chem. Lett.*, Accepted.

4.1 Introduction

Adsorption of target ions and compounds from water plays an important role in many technologies, including water purification[1] and drug delivery systems[2]. There are many reports on adsorption of cations such as heavy metal ions[3], surfactants[4] and dyes[5], and various inorganic solids including clay minerals[6] and zeolites[7] have been applied as adsorbents to take advantages of their negative charges and large surface areas.

Layered potassium hexaniobate, $K_4Nb_6O_{17}\cdot 3H_2O$, consisting of negatively charged hexaniobate layers[8] and interlayer K^+ ions, can also adsorb cations[9-11] *via* ion-exchange with other cations, such as heavy metal ions,[9] alkylammonium ions[10] and cationic dyes.[11]. $K_4Nb_6O_{17}\cdot 3H_2O$ has two interlayers, interlayers I and II, that appear alternately, and exhibit high and low reactivities for intercalation, respectively.[8]

On the other hand, poly(*N*-isopropylacrylamide) (PNIPAAm) exhibits a thermo-responsiveness ascribable to a swollen random coil structure below the lower critical solution temperature (LCST) and the deswollen globule state at above LCST in water.[12-13] By immobilizing PNIPAAm chains on inorganic materials, therefore, control of dispersion and aggregation states of resultant hybrid materials has been achieved. For example, inorganic nanostructures such as SiO_2 nanoparticles[14] and nanosheets derived from the protonated layered perovskite $HLaNb_2O_7\cdot xH_2O$[15] with grafted PNIPAAm chains exhibited dispersion-aggregation

phase transition behavior at the LCST of PNIPAAm chains. Thus, combining the ion-exchange capabilities of negatively-charged surfaces and thermoresponsive PNIAAm chains enables preparation of adsorbents with facile recovery capability. The use of Janus nanomaterials is an ideal option for realization of such dual-functional materials.

As described in Chapter 2, Janus nanosheets possessing two different properties on two faces of each nanosheet were successfully prepared *via* regioselective modification of $K_4Nb_6O_{17}\cdot 3H_2O$ using two organophosphonic acids.

In this chapter, the preparation of dual-functional Janus nanosheets *via* regioselective modification of $K_4Nb_6O_{17}\cdot 3H_2O$ is described. One of their functions is cation adsorption capability originating from the negative charge of the niobate layer. Their other function is thermo-responsiveness of polymer chains prepared by copolymerization of *N*-(hydroxymethyl)acrylamide (HMAAm) bearing OH groups and NIPAAm and bound to one face of each nanosheet. Use of PNIPAAM-based polymer chains increases the dispersibility of Janus nanosheets in water.[16] The adsorption behavior of cationic methylene blue by the Janus nanosheets and the aggregation behavior of the Janus nanosheets in a wide temperature range were studied. Advantages of this design include excellent stability of Nb-O-P bonds with respect to hydrolysis, as described in Chapter 2, and no interference of these two functions because of their presence on two physically-separated surfaces in one nanosheet; cations in aqueous systems could be adsorbed on one of two nanosheet

surfaces without steric hindrance of polymer chains. This is a huge advantage over Janus nanoparticles; if the same two functions are located on a dual-functional Janus nanoparticle, steric hindrance of polymer chains for adsorption of cations could occur near boundaries.

First, potassium ions at interlayer I of $K_4Nb_6O_{17}\cdot 3H_2O$ were exchanged with dioctadecyldimethylammonium ions ($2C_{18}2MeN\_NbO$). Next, interlayer I was modified with *m*-(chloromethyl)phenylmethanoyloxymethylphosphonic acid bearing an initiator group for atom transfer radical polymerization (ATRP), which was synthesized based on the previous report (CPMP_NbO).[17] NIPAAm and HMAAm were then copolymerized at interlayer I with a molar ratio of the CPMP moiety : NIPAAm : HMAAm = 1 : 45 : 5 (P(NH)_NbO). Interlayer II was then exfoliated by intercalation of tetrabutylammonium ions (TBA^+) in water. Interlayer I was simultaneously exfoliated because of the high hydrophilicity of copolymer chains. Finally, the resulting dispersion was centrifuged, and a supernatant was obtained as a nanosheet dispersion (P(NH)_TBA_NS dispersion)(Scheme 4.1). An aqueous dispersion of $K_4Nb_6O_{17}\cdot 3H_2O$ nanosheets *via* intercalation of TBA^+ at both interlayers I and II and subsequent exfoliation (TBA_TBA_NS dispersion), and an aqueous dispersion of nanosheets in which P(NIPAAm-*co*-HMAAm) chains were bonded to interlayer surfaces at both interlayers (P(NH)_P(NH)_NS dispersion) were also prepared.

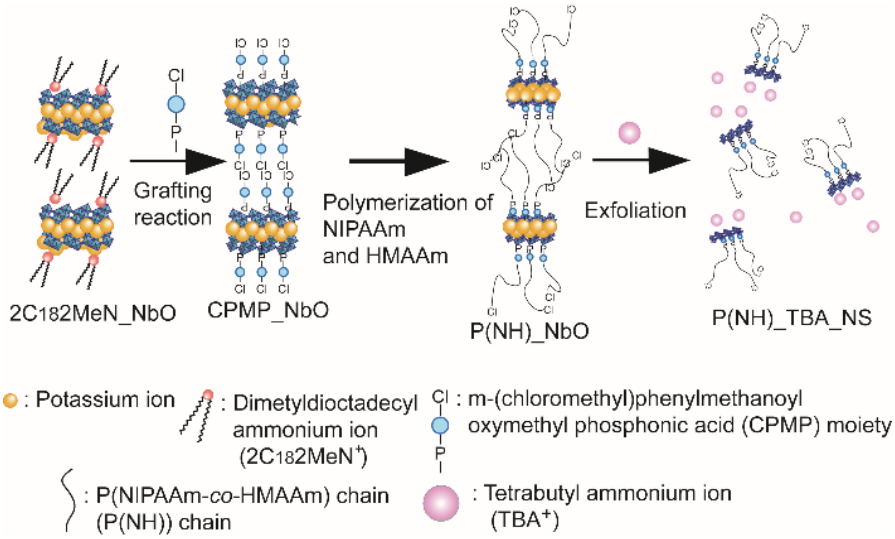

Scheme 4.1 Preparation of dual-functional Janus nanosheets.

4.2 Experimental Section

4.2.1Materials

K_2CO_3 (Tokyo Chemical Industry Co., Ltd.) and Nb_2O_5 (FUJIFILM Wako Pure Chemical Co., Ltd) were used for preparation of $K_4Nb_6O_{17}\cdot 3H_2O$. Trimethylsilyl bromide (TMSBr) (Tokyo Chemical Industry Co., Ltd.), 4-dimethylaminopyridine (Tokyo Chemical Industry Co., Ltd.), diethyl(hydroxymethyl)phosphonate (Tokyo Chemical Industry Co., Ltd.), trimethylamine (FUJIFILM Wako Pure Chemical Co., Ltd) and 3-(chloromethyl)benzoyl chloride (Tokyo Chemical Industry Co., Ltd.) were used to synthesize *m*-(chloromethyl)phenylmethanoylphosphonic acid (CPMP). Dimethyldioctadecylammonium chloride (Tokyo Chemical Industry Co., Ltd.) and dodecylammonium chloride (Tokyo Chemical Industry Co., Ltd.) were used as guest species for preparation of intermediates for surface modification. *N*-isopropylacrylamide (NIPAAm) (FUJIFILM Wako Pure Chemical Co., Ltd),

N-hydroxymethylacrylamide (HMAAm) (Tokyo Chemical Industry Co., Ltd.), CuCl (FUJIFILM Wako Pure Chemical Co., Ltd), $CuCl_2$ (FUJIFILM Wako Pure Chemical Co., Ltd), tris[2-(dimethylamino)ethyl]amine (Me_6TREN) (FUJIFILM Wako Pure Chemical Co., Ltd) were used for preparation of poly(*N*-isopropylacrylamide-*co*-*N*-hydroxymethylacrylamide). Tetrbutylammonium bromide (TBABr) (FUJIFILM Wako Pure Chemical Co., Ltd) was used for exfoliation. Methylene blue (FUJIFILM Wako Pure Chemical Co., Ltd) and methyl orange (FUJIFILM Wako Pure Chemical Co., Ltd) were used for adsorption onto layer surfaces. All materials were used as received without further purification.

4.2.2 Experimental Procedures

4.2.2.1. Preparation of $K_4Nb_6O_{17}\cdot 3H_2O$

$K_4Nb_6O_{17}\cdot 3H_2O$ was prepared by calcination of a mixture of K_2CO_3 (2.83 g, 2.05×10^{-2} mol) and Nb_2O_5 (7.43 g, 2.80×10^{-2} mol) at 1100°C for 10 hours without intermittent grinding. The product was washed with water and dried in air.

4.2.2.2 Synthesis of *m*-(chloromethyl)phenylmethanoyl phosphonic acid (CPMP)

First, 4-dimethylaminopyridine (0.32 g, 2.6×10^{-3} mol), CH_2Cl_2 (30 mL), diethyl(hydroxymethyl)phosphonate (2.0 g, 1.2×10^{-2} mol) and trimethylamine (1.2

g, 2.0×10^{-2} mol) were mixed at 0 °C. Next, 3-(chloromethyl)benzoyl chloride (2.3 g, 1.2×10^{-2} mol) was added and the resulting solution was stirred at room temperature for 1 day. The intermediate compound was collected after extraction with H_2O and washed with a saturated NH_4Cl aqueous solution. The crude product was then purified using a silica gel column with hexane : ethyl acetate = 1 : 5 containing 2% triethylamine. The intermediate compound (1.7 g), CH_2Cl_2 (11 mL) and TMSBr (2.5 g, 1.6×10^{-2} mol) were stirred at room temperature overnight and the volatiles were removed. The crude product was added to methanol and stirred at room temperature for 60 minutes and the volatiles were removed. The product was collected by filtering. The ^{1}H NMR and ^{31}P NMR of the product are shown in Figure 4.1 and Figure 4.2, respectively. The assignments of ^{1}H NMR signals are listed in Table 4.1. In the ^{31}P NMR spectrum, one signal was observed, indicating that the product contained no by-products. The yield of CPMP was 25.1 %.

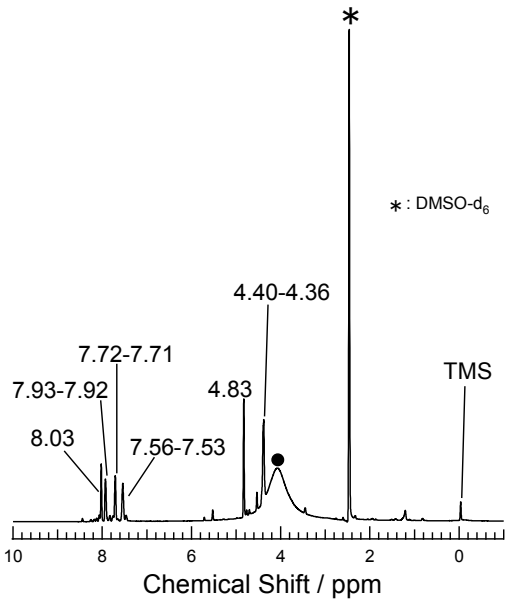

Figure 4.1 ^{1}H NMR spectrum of CPMP.

Signal presented ● could be assigned to impurities, such as H_2O.

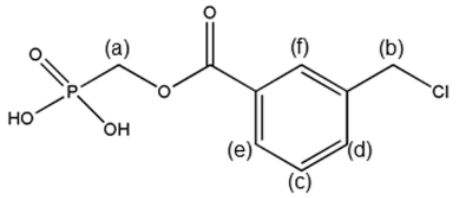

Table 4.1 The assignments of ^{1}H NMR signals of CPMP

	Chemical shift / ppm		integral value
a	4.40-4.36	d	2
b	4.83	s	2
c	7.56-7.53	t	1
d	7.72-7.71	d	1
e	7.92-7.94	d	1
f	8.03	s	1

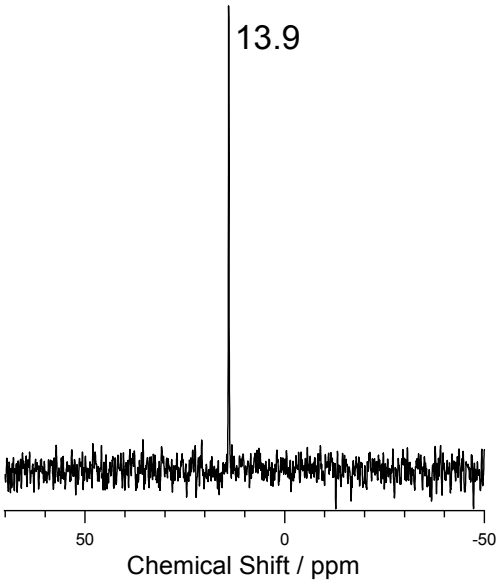

Figure 4.2 ^{31}P NMR spectrum of CPMP.

4.2.2.3 Preparation of $2C_{18}2MeN\_NbO$

$K_4Nb_6O_{17}\cdot 3H_2O$ (2.60 g, 2.50×10^{-3} mol) and dimethyldioctadecylammonium chloride (5.87g, 1.00×10^{-2} mol) ($K_4Nb_6O_{17}\cdot 3H_2O$ to dimethyldioctadecylammonium chloride molar ratio 1 : 4) were reacted in water (200 mL) at 50°C for 7 days to expand interlayer I. The product was centrifuged, washed with water and dried in air.

4.2.2.4 Preparation of CPMP_NbO

$2C_{18}2MeN\_NbO$ (0.35 g, 2.50×10^{-4} mol) and CPMP (0.53 g, 2.00×10^{-3} mol) (Nb_6O_{17} to CPMP molar ratio 1 : 8) were reacted in 2-butanone (14 mL) at 80°C for 2 days for surface modification of interlayer I. The product was centrifuged, washed with acetone three times and dried in air.

4.2.2.5 Preparation of P(NH)_NbO

CPMP_NbO (0.2 g) was placed into a flask connected with other two flasks. NIPAAm (1.2 g, 1.1× 10^{-2} mol), HMAAm (0.12 g, 1.2× 10^{-2} mol), Me_6TREN (61 μL, 2.3× 10^{-4} mol) and 2-propanol (5.6 mL) were entered into another flask. CuCl (21 mg, 2.1× 10^{-4} mol) and $CuCl_2$ (3.3 mg, 2.5× 10^{-5} mol) were then entered into a third flask. The three flasks were then connected and freeze-pump-thaw cycled three times. CuCl and $CuCl_2$ were then added to a 2-propanol solution and dissolved completely. CPMP_NbO was dispersed in this 2-propanol solution and stirred for 1 day at 40ºC for polymerization. The molar ratio was adjusted based on the CPMP moiety as follows: NIPAAm : HMAA : CuCl : $CuCl_2$ = 1 : 45 : 5 : 0.9 : 0.1, and the concentration of the monomer was 2 mol/L. After the reaction, the product was centrifuged, washed twice with 2-propanol and MeOH and dried in air.

4.2.2.6 Preparation of P(NH)_P(NH)_NbO

$K_4Nb_6O_{17}\cdot 3H_2O$ (2.5 g, 2.4 × 10^{-3} mol) and dodecylammonium chloride (4.3g, 1.9 × 10^{-2} mol) ($K_4Nb_6O_{17}\cdot 3H_2O$ to dodecylammonium chloride molar ratio 1 : 8) were reacted in water (33 mL) at 50°C for 5 days to expand interlayers I and II. The product was centrifuged, washed with water and dried in air. The product (0.3 g, 0.21 × 10^{-4} mol) and CPMP (0.87 g, 3.3 × 10^{-3} mol) (Nb_6O_{17} to CPMP molar ratio 1 : 16) were reacted in 2-butanone (14 mL) at 80°C for 2 days for surface

modification of interlayers I and II. The resulting derivative was centrifuged, washed with acetone three times and dried in air. The intermediate derivative (0.2 g) was entered into a flask. NIPAAm (2.2 g, 1.9×10^{-2} mol), HMAAm (0.22 g, 2.2×10^{-3} mol), Me_6TREN (118.46 μL, 4.4×10^{-4} mol) and 2-PrOH (5.6 mL) were entered into another flask. CuCl (39 mg, 3.9×10^{-4} mol) and $CuCl_2$ (5.9 mg, 4.4×10^{-5} mol) were then entered into a third flask. These three flasks were then connected and freeze-pump-thaw cycled three times. CuCl and $CuCl_2$ were added to a 2-propanol solution and completely dissolved. The 2-propanol solution was added to the product and stirred for 1 day at 40ºC for polymerization. The molar ratio was adjusted based on the CPMP moiety as follows: NIPAAm : HMAAm : CuCl : $CuCl_2$ = 1 : 45 : 5 : 0.9 : 0.1, and the monomer concentration was 4 mol/L. After the reaction, the product was centrifuged, washed twice with 2-propanol and MeOH and dried in air.

4.2.2.7 Preparation of nanosheet dispersions

P(NH)_NbO (20 mg), P(NH)_P(NH)_NbO (20 mg) and $K_4Nb_6O_{17}{\cdot}3H_2O$ (20 mg) was added separately to a 36.4 g/L TBABr aqueous solution (22 mL), and the resulting solution was stirred at room temperature for 7 days. The dispersion was centrifuged at 4000 rpm for 15 minutes and the supernatant was collected. The resulting products were called as a P(NH)_TBA_NS dispersion, a P(NH)_P(NH)_NS dispersion and a TBA_TBA_NS dispersion.

4.2.2.8 Reaction between the nanosheet dispersion and dye, methylene blue or methyl orange

First, 0.010 wt% methylene blue or methyl orange (0.1 mL) was added to P(NH)_TBA_NS dispersion, P(NH)_P(NH)_NS dispersion, TBA_TBA_NS dispersion or water (9.9 mL) and heated at 60ºC for 7 days. The supernatant was collected by filtration. The absorbance of each supernatant was measured. The absorption spectrum of mixture of the nanosheet dispersion (2.97 mL) and 1 g/L dye (MB or methyl orange) aqueous solution (30 μL) were recorded with a Shimadzu UV-3100PC UV-vis spectrophotometer.

4.2.3 Analyses

Liquid-state ^{1}H NMR and ^{31}P NMR spectra were recorded with a JEOL JNM-ECZ500R instrument at 500.16 MHz. DMSO-d^6 was used as a deuterated solvent. X-ray diffraction (XRD) patterns were recorded on a Rigaku RINT-1000 diffractometer (Mn-filtered FeKα radiation) and a Rigaku SmartLab diffractometer with Mn-filtered FeKα radiation by the parallel-beam method. Infrared (IR) adsorption spectra were recorded on a JASCO FT/IR-460 Plus spectrometer by the KBr disk method. Inductively coupled plasma emission spectrometry was performed with a Thermo Jarrell Ash ICAP-574 II instrument using the internal standard method after dissolution of each sample in a mixture of 4 mL of HNO_3

(60%), 3 mL of HCl (36 %), and 1 mL of HF(47 %) at 150ºC overnight. Atomic force microscope (AFM) images of P(NH)_TBA_NS, TBA_TBA_NS and P(NH)_P(NH)_NS were obtained with a Shimadzu SPM-9700 HT microscope, Digital Instruments Nanoscope III microscope and Shimadzu SPM-9500J3 microscope, respectively, using the tapping mode. The absorbance of the nanosheet dispersions with changes in temperature was measured using a JASCO V-630 spectrophotometer at a wavelength of 400 nm and a JASCO ETCR-726 temperature control unit. Absorbance was monitored at every one degree from 35 °C to 65 °C under heating conditions of 5-s holding time at target temperature and a heating rate of 1 °C/min (The dispersion was stirred at 800 rpm). The absorbance of the supernatants after reaction with a dye solution was measured using a Shimadzu UV-3100PC UV-vis spectrophotometer.

4. 3 Results and discussions

Figure 4.3 shows XRD patterns of $2C_{18}2MeN\_NbO$, CPMP_NbO and P(NH)_NbO. The *d* value corresponding to repeating distance decreased from 5.39 to 3.58 nm upon reaction between $2C_{18}2MeN\_NbO$ and CPMP. After copolymerization of NIPAAm and HMAAm in CPMP_NbO, no diffraction corresponding to the repeating distance was observed in the XRD pattern of P(NH)_NbO.

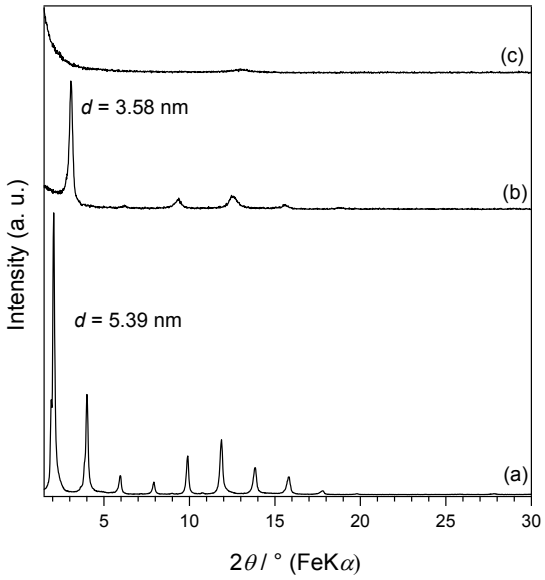

Figure 4.3 XRD patterns of (a) $2C_{18}2MeN\_NbO$, (b) CPMP_NbO and (C) P(NH)_NbO.

Figure 4.4 shows IR spectra of $2C_{18}2MeN\_NbO$, CPMP, CPMP_NbO and P(NH)_NbO. An $\delta(N^+\text{-}CH_3)$ adsorption band[18] assignable to $2C_{18}2MeN^+$ was observed at 1486 cm^{-1} in the spectrum of $2C_{18}2MeN\_NbO$ but was not observed in the spectrum of CPMP_NbO, indicating removal of $2C_{18}2MeN^+$ from interlayer I upon the reaction of $2C_{18}2MeN\_NbO$ with CPMP. This result is consistent with the XRD results showing a decrease in the repeating distance. In the spectrum of CPMP_NbO, adsorption bands due to the ν_{ar}(C-H), ν(P=O), ν(P-O) and ν(P-OH) modes[19] were observed at 3067 cm^{-1}, 1198 cm^{-1}, 1084 cm^{-1} and 925 cm^{-1}, respectively. In addition, the ν(P=O) adsorption band of CPMP_NbO was shifted to a lower wavenumber from the ν(P=O) band position of bulk CPMP (at 1208 cm^{-1}) and broadened, indicating that a grafting reaction of CPMP onto the interlayer

surfaces of hexaniobate layers had proceeded.[20] Also, a ν(NHC=O) band assignable to the PNIPAAm and PHMAAm moieties[21] was observed at 1653 cm^{-1} in the spectrum of P(NH)_NbO. Adsorption bands assignable only to the PHMAAm moiety could not be identified, because they were overlapping with the adsorption bands of other moieties on the nanosheets.[22] By taking the XRD results demonstrating the stacking disorder into account, copolymerization in the interlayer space is confirmed.

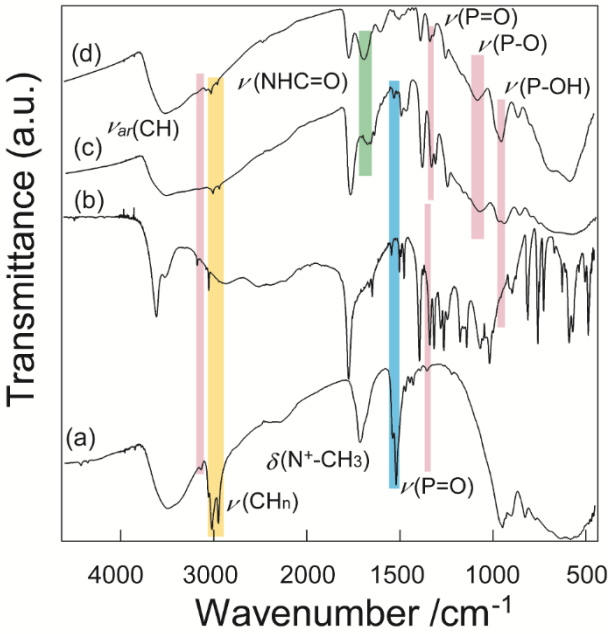

Figure 4.4 IR spectra of (a) $2C_{18}2MeN$_NbO, (b) CPMP, (c) CPMP_NbO and (d) P(NH)_NbO. Adsorption bands in a pink colored area, green colored area and blue colored area are assignable to vibrations of a CPMP molecule, thermos-responsive polymer chains and $2C_{18}2MeN^+$, respectively. Adsorption band in a yellow colored area are assignable to ν(CHn) in $2C_{18}2MeN^+$, CPMP moiety and thermos-responsive polymer chains.

Table 4.2 shows the molar ratios of Nb and P in CPMP_NbO and P(NH)_NbO based on the ICP results. The molar ratio in CPMP_NbO was P : Nb = 1.7 : 6. Since the amount of P per $[Nb_6O_{17}]$ was smaller than 2, a compound in which only interlayer I was modified was obtained.[23] The molar ratio in P(NH)_NbO was also P : Nb = 1.7 : 6, equal to that of CPMP_NbO, indicating that polymerization proceeded with maintenance of the CPMP moiety on the interlayer surface of the hexaniobate layer.

Table 4.2 Molar ratio if Nb and P of CPMP_NbO and P(NH)_NbO

	Nb*	P
CPMP_NbO	6	1.7
P(NH)_NbO	6	1.7

* The amounts of niobium were set to 6.

Based on these results, it is concluded that only interlayer I was regioselectively modified with CPMP. Since copolymerization proceeded only from the initiator groups, it is reasonable to conclude that a P(NH)_NbO nanosheet had polymer chains onto one face of an individual hexaniobate nanosheets *via* the CPMP moiety.

Figure 4.5 shows an AFM image of samples prepared by dropping and drying (a) TBA_TBA_NS dispersion, (b) P(NH)_TBA_NS dispersion and (c)P(NH)_P(NH)_NS dispersion onto an Si wafer. The thickness of a TBA_TBA_NS estimated by AFM was 0.99 nm (Figure 4.5(a)). The reported thickness of double-layered niobate nanosheets exfoliated by TBA^+ was in the range

of 1.5 nm to 2.1 nm.[24] Since 0.99 nm is thinner than double-layered exfoliated nanosheets and thicker than $[Nb_6O_{17}]^{4-}$ nanosheets measuring 0.82 nm,[23] the TBA_TBA_NS dispersion apparently consisted of single-layered nanosheets. In previous reports on single-layered nanosheets exfoliated using TBA^+, the thickness observed by AFM was the same as or slightly greater than the corresponding crystallographic thickness.[25-27] Thus, it is likely that an unreacted interlayer II could be exfoliated by treatment with a TBA^+ solution. In figure 4.5(b), a sheet-like morphology with a thickness of 6.4 nm was observed. On the other hand, the thickness of a nanosheet from the P(NH)_P(NH)_NS dispersion was estimated to be 12 nm by AFM (Figure 4.5(c)). A nanosheet from the P(NH)_TBA_NS dispersion had a P(NH)-chain layer and TBA^+ layer on its individual hexaniobate nanosheets. If the P(NH)_P(NH)_NS dispersion consists of single-layered nanosheets, the thickness of P(NH)_TBA_NS could be calculated as half of sum of the thicknesses of TBA_TBA_NS and P(NH)_P(NH)_NS: (0.99 nm + 12 nm) ÷ 2 = 6.5 nm, which bears a close similarity to the observed value, 6.4 nm. From this relationship, it is

reasonable to conclude that these three types of nanosheets were single-layered in dispersions. The estimated structures and thicknesses of these three nanosheets are shown in scheme 4.2.

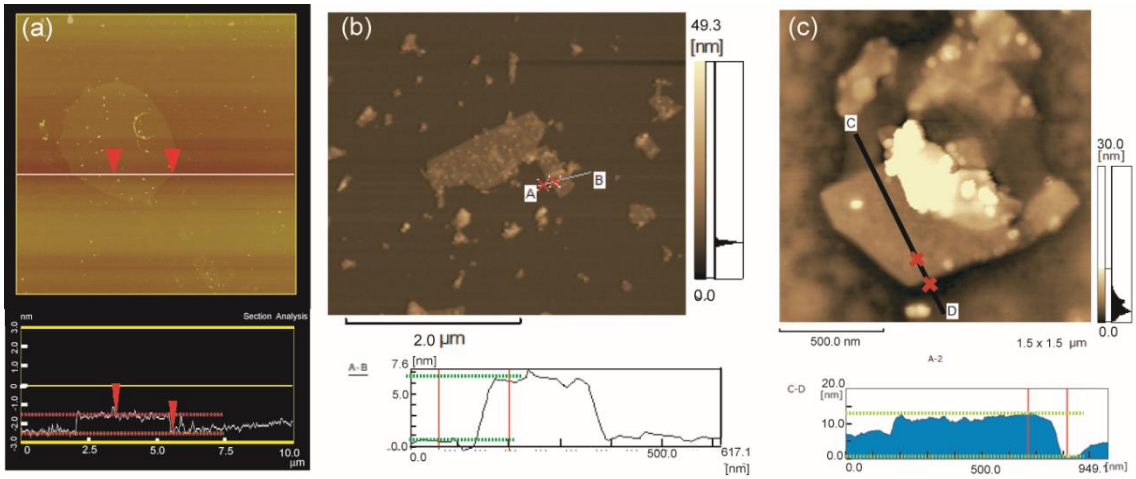

Figure 4.5 AFM images of (a) TBA_TBA_NS, (b)P(NH)_TBA_NS and (c)P(NH)_P(NH)_NS. Particles on nanosheets were likely to be impurities such as precipitated TBABr.

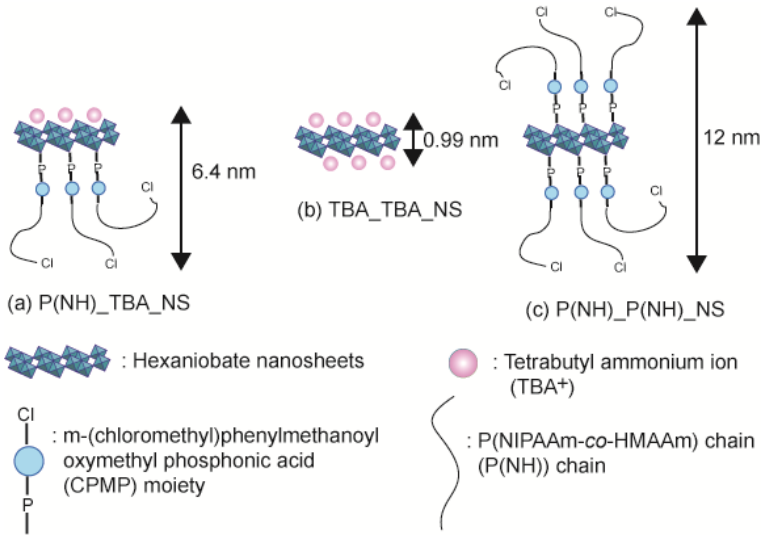

Scheme 4.2 Estimated structures of (a) TBA_TBA_NS, (b)P(NH)_TBA_NS and (c)P(NH)_P(NH)_NS

The temperature-depending absorbance of P(NH)_TBA_NS dispersion is shown in Figures 4.6 A (i) and (ii). The absorbance of the dispersion increased and decreased with heating and cooling, respectively, and sedimentation was observed at high temperatures. This behavior can be interpreted based on conformational changes in PNIPAAm-based polymer chains. Thus, it is likely that the P(NH)_TBA_NS dispersion exhibited a reversible dispersion-aggregation transition due to thermo-responsiveness. Absorption of P(NH)_TBA_NS was changed gradually by changing temperature. Similar behavior was observed in the previous reports due to low mobility of PNIPAAm chains whose one end of was immobilized on substrate and closeness of distance between polymer chains.[15,28] While the LCST of PNIPAAm is 32°C,[12,13] the starting point of turbidity changes for the P(NH)_TBA_NS dispersion was about 45°C. This is probably due to increasing hydrophilicity caused by copolymerization with hydrophilic HMAAm.[16] The absorbance of the TBA_TBA_NS dispersion was then measured with respect to increases in temperature and compared with that of the P(NH)_TBA_NS dispersion (Figures 4.6 A (i) and (iii)). The absorbance of the TBA_TBA_NS dispersion increased gradually from 50°C, while that of the P(NH)_TAB_NS dispersion increased significantly from 45°C, indicating that P(NH)_TBA_NS dispersion started to aggregate at lower temperature than TBA_TBA_NS dispersion because of conformational changes in the thermoresponsive P(NIPAAm-*co*-HMAAm) chains. The P(NH)_TBA_NS dispersion and TBA_TBA_NS dispersion were heated at

60°C for 7 days to monitor their aggregation behavior (Figure 4.6 B and C). Tyndall scattering was observed for both dispersions before heating, indicating the colloidal states of nanosheets. After heating, no Tyndall scattering was observed for the P(NH)_TBA_NS dispersion because of sediment formation. On the other hand, Tyndall scattering was still observed for the TAB_TBA_NS dispersion without sediments. This difference clearly suggests that the nanosheets in the P(NH)_TBA_NS dispersion were aggregated and sedimented at above the LCST. Similar behavior was reported for SiO_2 nanoparticles modified with a

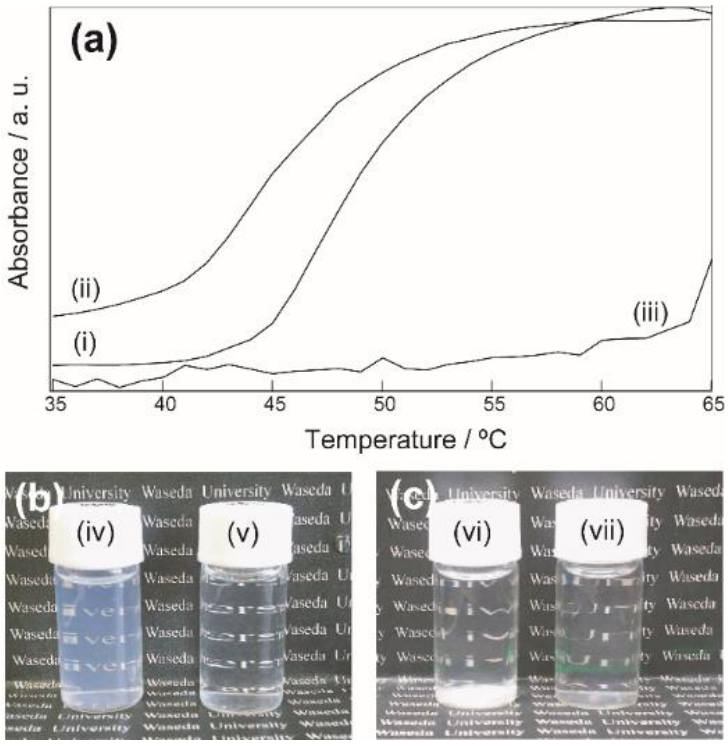

thermoresponsive polymer.[15] These results show that P(NH)_TBA_NS could be collected from water more easily than TBA_TBA_NS from water upon heating.

Figure 4.6 (a) Variation in absorbance at 400 nm for P(NH)_TBA_NS dispersion with (i) increasing, (ii) decreasing temperature and (iii) TBA_TBA_NS dispersion

with increasing temperature, (b) appearances of (iv) P(NH)_TBA_NS dispersion and (v) TBA_TBA_NS dispersion before heating and (c) appearance of (vi) P(NH)_TBA_NS dispersion and (vii) TBA_TBA_NS dispersion after heating at 60°C for 7 days.

Figure 4.7a shows the visible absorption spectra of the P(NH)_TBA_NS dispersion containing MB. Since the spectrum of P(NH)_TBA_NS dispersion containing scattering, this spectrum was obtained via the following modification. The presene of scattering (Figure 4.7b) whose absorbance increases linearly with the decreasing in the wavenumber was assumed. The modified spectrum of the P(NH)_TBA_NS dispersion containing MB (Figure 4.7c) was obtained by subtraction of the absorbance value of Figure 4.7b from that of figure 4.7a.

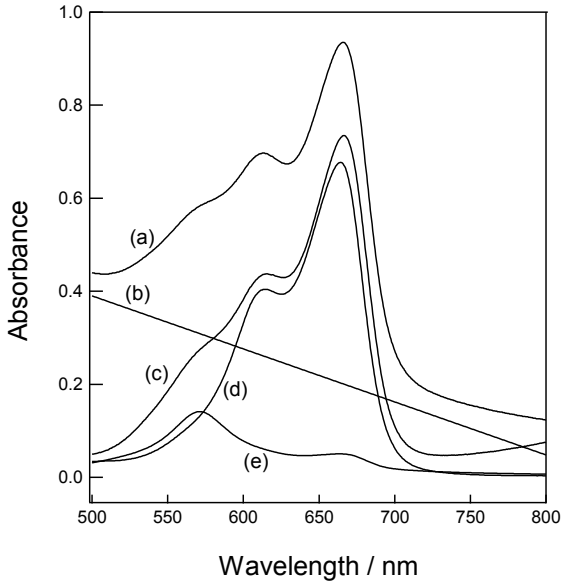

Figure 4.7 (a) original spectrum of P(NH)_TBA_NS dispersion containing MB, (b) a scattering profile and (c) subtract spectrum using (a) and (b). Spectrum (a) could be simulated as sum of (d) 39% of MB aqueous solution (Figure 4.8a), (e) 21% of TBA_TBA_NS dispersion (Figure 4.8b) and estimated scattering (b).

The visible absorption spectrum of the P(NH)_TBA_NS dispersion containing MB was measured to evaluate its ion exchange capability (Figure 4.8). The same measurements were carried out using TBA_TBA_NS and P(NH)_P(NH)_NS dispersions. No notable difference was observed between the spectra of the P(NH)_P(NH)_NS dispersion containing MB (Figure 4.8d) and the MB aqueous solution (Figure 4.8a), whose absorbance peaks were observed at 666 nm with a shoulder at 608 nm, indicating that the organophosphonate moiety and P(NIPAAm-*co*-HMAAm) chains grafted onto nanosheets did not adsorb MB. A new absorption peak was observed, on the other hand, at 572 nm in the spectrum of

the TBA_TBA_NS dispersion containing MB. It was reported that the absorption peak of MB forming H-aggregates on montmorillonite was shifted to a shorter wavelength from those of MB monomers at 665 nm and H-dimers at 605 nm.[29] A similar absorption peak shift was reported when MB was adsorbed onto the $K_4Nb_6O_{17}\cdot H_2O$ interlayer surface.[30] It is thus concluded that MB formed H-aggregates upon adsorption on TBA_TBA_NS *via* ion exchange with TBA^+. When the P(NH)_TBA_NS dispersion containing MB was heated at 60°C, a pink-colored powder was sedimented. This product was filtered and a supernatant was obtained. From 666-nm absorbance values of this supernatant and the original MB solution (Figure 4.8a), the amount of adsorbed MB was calculated to be 29.2% of the total MB, an MB amount equivalent to 3.2% of the cation exchange capacity of an unmodified face of P(NH)_TBA_NS.

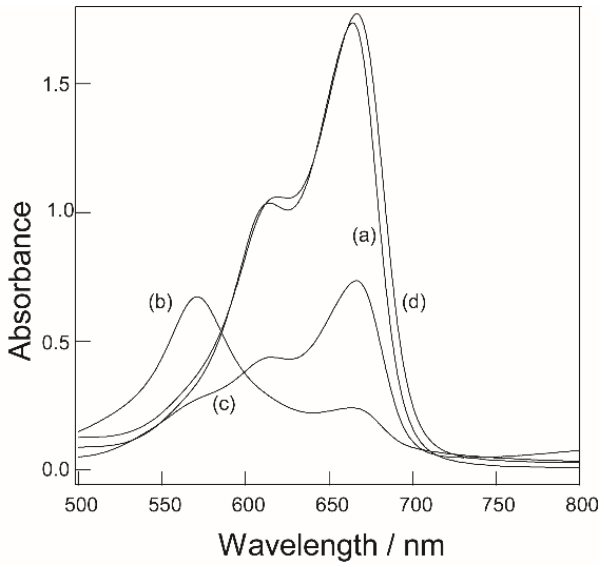

Figure 4.8 Visible adsorption spectra of (a) 0.01 g/L MB aqueous solution, (b)

TBA_TBA_NS dispersion, (c) P(NH)_TBA_NS dispersion and (d) P(NH)_P(NH)_NS dispersion containing MB. The spectrum (c) was modified to reduce the effect of scattering.

The same experiment was carried out using methyl orange, which is an anionic dye, moreover, and no adsorption on P(NH)_TBA_NS was observed (Figure 4.9). Based on these results, it was concluded that unmodified faces of P(NH)_TBA_NS adsorbed cationic MB through an electrostatic interaction.

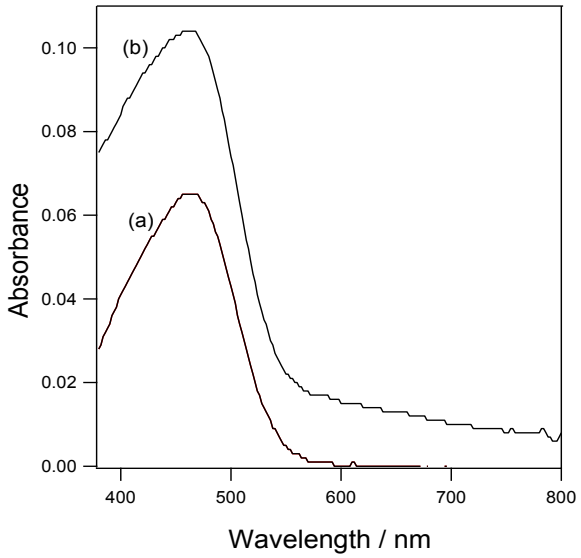

Figure 4.9 Visible absorption spectra of (a) methyl orange aqueous solution and (b) P(NH)_TBA_NS dispersion mixed with methyl orange.

4.4 Conclusions

Interlayer I of $K_4Nb_6O_{17}\cdot 3H_2O$ was regioselectively modified with an organophosphonate moiety bearing an ATRP initiator group, CPMP moiety, the

resultant product was dispersed in the TBA^+ aqueous solution to exfoliate into single-layered nanosheets, leading to the dispersion of Janus nanosheets grafted with P(NIPAAm-*co*-HMAAm) chains onto one of the two faces of the individual nanosheets. It was demonstrated that these Janus nanosheets have two functions: adsorption of cations *via* an ion-exchange mechanism and thermo-responsive aggregation behavior, and that two reactions proceeded independently on two faces of individual nanosheets. The present study reveals that Janus materials bearing two functions which do not interfere each other can be prepared with this strategy. It is therefore expected that dual-functional Janus nanosheets exhibiting various functions and usable in water can be prepared by extending the present approach using $K_4Nb_6O_{17}\cdot 3H_2O$.

References

1 Q. U. Jiuhui, Research Progress of Novel Adsorption Processes in Water Purification: A Review, *J. Environ. Sci*., **20**, 1-13 (2008).

2 A. Kumari, S. K. Yadav and S. C. Yadav, Biodegradable Polymeric Nanoparticles based Drug Delivery Systems, *Colloids Surf. B*, **75**, 1-18 (2010).

3 F. Fu and Q. Wang, Removal of Heavy Metal Ions from Wastewaters: A Review, *J. Environ. Manage.,* **92**(3), 407-418 (2011).

4 M. A. Aboulhassan, S. Souabi, A. Yaacoubi and M. Baudu, Removal of Surfactant from Industrial Wastewaters by Coagulation Flocculation Process, *Int. J. Environ.*

Sci. Technol., **3**(4), 327-332 (2006).

5 P. Sharma and M. R. Das, Removal of a Cationic Dye from Aqueous Solution Using Graphene Oxide Nanosheets: Investigation of Adsorption Parameters, *J. Chem. Eng.*, **58**(1), 151-158 (2013).

6 M. R. M. P. Aguiar, A. C. Novaes and A. W. S. Guariono, Removal of Heavy Metals from Wastewaters by Alminosilicate, *Quimica Nova.*, **25**, 1145-1154 (2002).

7 S. Babel and T. A. Kurniawan, Low-Cost Adsorbents for Heavy Metals Uptake from Contaminated Water: A Review, *J. Hazard. Mater.*, **97**, 219-243 (2003).

8 R. Uppuluri, A. S. Gupta, A. S. Rosasa and T. E. Mallouk, Soft Chemistry of Ion-Exchangeable Layered Metal Oxides, *Chem. Soc. Rev.*, **47**, 2401-2430 (2018).

9 K. Sayama, A. Tanaka, K. Domen, K. Maruya and T. Onishi, Photo-Catalytic Decomposition of Water over Platinum-Intercalated Potassium Niobate ($K_4Nb_6O_{17}$), *J. Phys. Chem.*, **95**(3), 1345-1348 (1991).

10 T. Nakato, D. Sakamoto, K. Kuroda and C. Kato, Synthesis of Two Types of Intercalation Compounds of $K_4Nb_6O_{17}$ with Tris(2,2'-bipyridyl) Metal Complex Ions, *Bull. Chem. Soc. Jpn.*, **65**, 322-328 (1992).

11 R. Shinozaki and T. Nakato, Humidity-Dependent Reversible Aggregation of Rhodamine 6G Dye Immobilized within Layered Niobate $K_4Nb_6O_{17}$, *Langmuir*, **20**(18), 7583-7588 (2004).

12 G. Masci, L. Giacomelli and V. Crescenzi, Atom Transfer Radical Polymerization of *N*-Isopropylacrylamide, *Macromol. Rapid Commun.*, **25**,

559-564 (2004).

13 E. S. Gil and S. M. Hudson, Stimuli-Reponsive Polymers and their Bioconjugates, *Plog. Polym. Sci.*, **29**, 1173-1222 (2004).

14 J. Wang, X. Lu, N. Huang, H. Zhang, R. Li and W. Li, Temperature-Responsive Multifunctional Switchable Nanoreactors of Poly (*N*-Isopropylacrylamide)/SiO_2/Lanthanide-Polyoxometalates/Au: Controlled on/off Catalytic and Luminescent System, *Mater. Sci. Eng. B*, **224**, 1-8 (2017).

15 N. Idota, S. Fukuda, T. Tsukahara and Y. Sugahara, Preparation of Thermoresponsive Nanosheets Exhibiting Phase Transitions in Water *via* Surface Modification of Layered Perovskite Nanosheets with Poly(*N*-Isopropylacrylamide) (PNIPAAm), *Chem. Lett.*, **44**, 203-205 (2015).

16 A. Saeed, D. M. R. Georget and A. G. Mayes, Synthesis, Characterisation and Solution Thermal Behaviour of a Family of Poly (*N*-Isopropyl Acrylamide-*co*-*N*-Hydroxymethyl Acrylamide) Copolymers, *React. Funct. Polym.*, **70**, 230-237 (2010).

17 H. Ma, M. Wells, T. P. Beebe Jr and A. Chilkoti, Surface-Initiated Atom Transfer Radical Polymerization of Oligo (Ethylene Glycol) Methyl Methacrylate from a Mixed Self-Assembled Monolayer on Gold, *Adv. Funct. Mater.*, **16**, 640-648 (2006).

18 N. V. Venkataraman and S. Vasudevan, Conformation of an Alkane Chain in Confined Geometry: Cetyl Trimethyl Ammonium Ion Intercalated in Layered

$CdPS_3$, *J. Phys. Chem. B*, **104**, 11179-11185 (2000).

19 A. Shimada, Y. Yoneyama, S. Tahara, P. H. Mutin and Y. Sugahra, Interlayer Surface Modification of the Protonated Ion-Exchangeable Layered Perovskite $HLaNb_2O_7 \cdot xH_2O$ with Organophosphonic Acids, *Chem. Mater.*, **21**, 4155-4162 (2009).

20 R. Quiñones, K. Rodriguez and R. J. Iuliucci, Investigation of Phosphonic Acid Surface Modifications on Zinc Oxide Nanoparticles under Ambient Conditions, *Thin Solid Films*, **565**, 155-164 (2014).

21 C. M. Schilli, M. Zhang, E. Rizzardo, S. H. Thang, B. Y. K. Chong, K. Edwards, G. Karlsson and A. H. E. Mu1ller, A New Double-Responsive Block Copolymer Synthesized *via* RAFT Polymerization: Poly(*N*-isopropylacrylamide)-block-poly(acrylic acid), *Macromolecules*, **37**, 7861-7866 (2004).

22 H. Wei, W. Chen, C. Chang, C. Cheng, S. Cheng, X. Zhang and R. Zhuo, Synthesis of Star Block, Thermosensitive Poly(*l*-lactide)-star block-poly(*N*-isopropylacrylamide-*co*-*N*-hydroxymethylacrylamide) Copolymers and Their Self-Assembled Micelles for Controlled Release, *J. Phys. Chem. C*, **112**, 2888-2894 (2008).

23 N. Kimura, Y. Kato, R. Suzuki, A. Shimada, S. Tahara, T. Nakato, K. Matsukawa, P. H. Mutin and Y. Sugahara, Single- and Double-Layered Organically Modified Nanosheets by Selective Interlayer Grafting and Exfoliation

of Layered Potassium Hexaniobate, *Langmuir*, **30**, 4, 1169-1175 (2014).

24 G. B. Saupe, C. C. Waraksa, H. N. Kim, Y. J. Han, D. M. Kaschak, D. M. Skinner and T. E. Mallouk, Nanoscale Tubules Formed by Exfoliation of Potassium Hexaniobate, *Chem. Mater*., **12**, 1556-15627 (2000).

25 T. Tanaka, K. Fukuda, Y. Ebina, K. Takada and T. Sasaki, Highly Organized Self-Assembled Monolayer and Multilayer Films of Titania Nanosheets, *Adv. Mater.*, **16**(11), 872-875 (2004).

26 K. Fukuda, K. Akatsuka, Y. Ebina, M. Osada, W. Sugimoto, M. Kimura and T. Sasaki, Photochromogenic Nanosheet Crystallites of Tungstate with a 2D Bronze Structure, *Inorg. Chem*., **51**, 1540-1543 (2012).

27 Y. Song, N. Iyi, T. Hoshide, T. C. Ozawa, Y. Ebina, R. Ma, N. Miyamoto and T. Sasaki, Accordion-like Swelling of Layered Perovskite Crystals *via* Massive Permeation of Aqueous Solutions into 2D Oxide Galleries, *Chem. Commun*., **51**, 17068-17071 (2015).

28 M. Annaka, C. Yahiro, K. Nagase, A. Kikuchi and T. Okano, Real-time observation of coil-to-globule transition in thermosensitive poly(*N*-isopropylacrylamide) brushes by quartz crystal microbalance, *Polymer*, **48**, 5713-5720 (2007).

29 J. Bujdak, N. Iyi and T. Fujita, The Aggregation of Methylene Blue in Montmorillonite Dispersions, *Clay Miner.*, **37**, 121-133 (2002).

30 W. Qu, F. Chen, B. Zhao and J. Zhang, Preparation and Visible Light

Photocatalytic Performance of Methylene Blue Intercalaed $K_4Nb_6O_{17}$, *J. Phys. Chem. Solids*, **71**, 35-41 (2010).

Chapter 5

Conclusions

This thesis describes novel preparation methods for Janus nanosheests using $K_4Nb_6O_{17}\cdot 3H_2O$ and phosphorus coupling agents. In this strategy, the unique reactivity of two kinds of interlayers in $K_4Nb_6O_{17}\cdot 3H_2O$ and the characteristics of phosphorus coupling agents, their freedom from homocondensation under mild conditions and from exchange reactions between phosphorus coupling agents and grafted organophosphonate moieties, play important roles. The resultant Janus nanosheets have stable M-O-P bonds between the niobate nanosheet surface and phosphorus coupling agent moiety, and various functional groups can be immobilized on the surface by changing the type of organophosphonic acid. Due to these advantages, the Janus nanosheets described in this thesis exhibit the potential to be employed as functional materials in various solvents, including water. In order to demonstrate their potential, two types of functional Janus nanosheets which work as a two-dimensional surfactant and a cation adsorbent are presented.

In Chapter 1, previous studies on the reactivity and surface modification of $K_4Nb_6O_{17}\cdot 3H_2O$ and preparation methods and applications for Janus nanosheets are summarized. Based on these previous studies, it is demonstrated that the preparation methods previously used for inorganic Janus nanosheets have drawbacks, including low versatility concerning functional groups for sol-gel-derived Janus nanosheets and difficulty in the use of clay-derived Janus nanosheets in water. To overcome these drawbacks, a new strategy for preparation

of Janus nanosheets using $K_4Nb_6O_{17}\cdot 3H_2O$ and phosphorus coupling agents is introduced.

In Chapter 2, preparation of inorganic Janus nanosheets from $K_4Nb_6O_{17}\cdot 3H_2O$ according to a strategy using regioselective surface modification and an evaluation of the resulting Janus nanosheets are described. First, interlayer I of $K_4Nb_6O_{17}\cdot 3H_2O$ was modified using lipophilic octadecylphosphonic acid. Next, interlayer II was modified using hydrophilic carboxypropylphosphonic acid. Finally, the product was exfoliated into single-layered nanosheets. Phase images obtained by AFM visibly revealed differences in the surface properties of the two types of the surfaces of the resultant nanosheets, which could be assigned to lipophilicity and hydrophilicity of the surfaces. These results demonstrate that inorganic Janus nanosheets can be prepared using $K_4Nb_6O_{17}\cdot 3H_2O$ and organophosphonic acids.

In Chapter 3, preparation from $K_4Nb_6O_{17}\cdot 3H_2O$ of functional Janus nanosheets that acted as two-dimensional surfactants is described. The surface modifiers for preparation of Janus nanosheets in Chapter 2 were changed to phenylphosphonic acid and phosphoric acid to increase hydrophilicity of Janus nanosheets, and the resultant nanosheets could be exfoliated into single-layered nanosheets in water. These Janus nanosheets exhibited surface activity demonstrated by the reduction of air-liquid surface tension, probably over a long period of time due to their heavy weight. In an emulsion prepared from the Janus nanosheet aqueous

dispersion and toluene, coalescence proceeded slowly and Ostwald ripening proceeded rapidly. These results are very different from the behavior of conventional molecular or ionic surfactants, demonstrating the unique characteristics of this type of Janus nanosheets.

In Chapter 4, preparation of dual-functional Janus nanosheets that acted as cation adsorbents from $K_4Nb_6O_{17}\cdot 3H_2O$ is described. Cation adsorption onto Janus nanosheets was achieved by ion exchangeability originating from the intrinsic negative charge of niobite nanosheets. On the other hand, recovery of nanosheets from water was achieved by their aggregation due to the thermoresponsiveness of poly(*N*-isopropylamide)-based polymer chains. These Janus nanosheets exhibited two different functions, an ion exchange capability and thermo-responsive aggregation on each side of individual nanosheets. This type of Janus nanosheet could be used to separate cationic species from water by dispersing them in water and subsequently increasing the temperature.

These results clearly indicate that inorganic Janus nanosheets can be prepared by regioselective surface modification using $K_4Nb_6O_{17}\cdot 3H_2O$ and organophosphonic acids and phosphoric acid with subsequent exfoliation. Furthermore, changing the functional group of the surface modifiers could lead to Janus nanosheets that can be employed as functional materials, such as a two-dimensional surfactant and a cation adsorbent that can be used as an aqueous dispersion. The present strategy for preparing $K_4Nb_6O_{17}\cdot 3H_2O$-based Janus

nanosheets is an important approach to realizing applications for inorganic Janus nanosheets, because it offers significant potential for preparation of various functional Janus nanosheets.

List of Publications

The Publications Related to This Thesis

(1) “Inorganic Janus nanosheets bearing two types of covalently bound organophosphonate groups *via* regioselective surface modification of $K_4Nb_6O_{17}\cdot 3H_2O$”, *Chemical Communications*, **54**, 5756-5759 (2018).
Ryoko Suzuki, Mitsuhito Sudo, Megumi Hirano, Naokazu Idota, Masashi Kunitake, Taisei Nishimi and Yoshiyuki Sugahara.

(2) “Janus Nanosheets Derived from $K_4Nb_6O_{17}\cdot 3H_2O$ *via* Regioselective Interlayer Surface Modification”,
In *Functional Materials*, D. R. Sahuin Ed., Intech Open, London (2019). DOI: 10.5772/intechopen.84228
Ryoko Suzuki, Mitsuhito Sudo, Megumi Hirano, Naokazu Idota, Masashi Kunitake, Taisei Nishimi and Yoshiyuki Sugahara.

(3) “Dual-functional Janus nanosheets with cation exchangeability and thermo-responsiveness prepared via regioselective modification of $K_4Nb_6O_{17}\cdot 3H_2O$”,
Chemistry Letters, *Accepted*.
Ryoko Suzuki, Naokazu Idota, Taisei Nishimi, Yoshiyuki Sugahara.

Other Publication

“Single- and double-layered organically modified nanosheets by selective interlayer grafting and exfoliation of layered potassium hexaniobate”, *Langmuir*, **30**, 1169-1175 (2014).
Nanako Kimura, Yumi Kato, Ryoko Suzuki, Akira Shimada, Sei-ichi Tahara, Teruyuki Nakato, Kimihiro Matsukawa, P. Hubert Mutin and Yoshiyuki Sugahara.

解説
“無機層状物質への有機化合物のグラフト反応による機能性付与”，工業材料, **66(6)**, 69-72 (2018) 鈴木涼子, 菅原義之.

Acknowledgement

First of all, I would like to express my deepest gratitude to my supervisor, Professor Yoshiyuki Sugahara, for his valuable discussions, precious advice and continuous encouragement. I'm also grateful to Professor Kazuyuki Kuroda, Professor (without tenure) Hiroaki Wada, Professor Toshiyuki Momma and Professor Atsuhi Shimojima for their advice.

I would also like to express my gratitude to Dr. Taisei Nishimi of Japan Technological Research Association of Artificial Photosynthetic Chemical Process (ARPChem) for his advice and teaching on surface chemistry. I extend my gratitude to Professor Masahi Kunitake of Kumamoto University for his valuable advice and discussions to evaluate Janus nanosheets. My gratitude also goes to Dr. Naokazu Idota of Tokyo Institute of Technology for giving me precious advice and kindly teaching me synthesis of organophosphonic acids and ATRP technique. I would also like to thank Megumi Hirano and Emika Onitsuka for AFM observation and measurement of surface tension.

Furthermore, I owe many thanks to my seniors, my colleagues and my juniors in the laboratory for their experimental teaching, technical discussions and continuous encouragement. Especially, I thank Mr. Mitsuhito Sudo and Mr. Tomoki Nagai for their experimental contributions and assistance.

Finally, I fully thank my family for their hearty support and continuous

encouragement.

July, 2020

Ryoko Suzuki